Quantitative Geomorphic Analyses of Neotectonic Activity in the Central U.S. and Implications for Current Increased Seismicity

Samia Noor[1], Md Rizwanul Hasan[1], Randy Cox[1]

[1]Department of Earth Sciences, University of Memphis, Memphis, TN 38152, USA

5   *Correspondence to:* Randy Cox (randycox@memphis.edu)

Abstract. This regional reconnaissance compares vector and scalar geomorphic indicators (transverse drainage basin asymmetry (TI), hypsometric integral (HI), and stream sinuosity index (SI)) in Kansas and Oklahoma to assess neotectonic geomorphology and explore the spatial association between geomorphic indices and basement structure. The study is motivated by both an observed increase in seismicity in the area between 2009 and 2019 and the gap in studies of crustal deformation in this region. In Kansas 10   and Oklahoma, 1,697 and 950 4th-order basins, respectively, were analysed to assess TI to generate spatially averaged mean vectors. Geographic 'domains' with the preferred azimuthal direction of mean vectors were defined. In Kansas, six azimuthal domains were defined, whereas in Oklahoma, five azimuthal domains were defined. Most of the basin asymmetry can be attributed to regional climate conditions; however, an azimuthal domain containing increased seismicity in Oklahoma is consistent with neotectonic activity on faults of the Ozark Uplift. HI and SI pattern maps for both Kansas and Oklahoma were generated from 15   hotspot analysis (LISA method) and the Total Sinuosity method combined with Empirical Bayesian Kriging (EBK). The distribution of HI hotspots and SI anomalies suggests ongoing tectonism. In eastern Kansas, active crustal deformation is indicated for an area containing increased seismicity within the Bourbon Arch and Nemaha Ridge fault zones. Another HI hotspot may relate to neotectonism of the Central Kansas Uplift fault zone, while a HI cold spot and low SI anomaly in Gray and Finney counties may indicate a subsiding neotectonic block. In Oklahoma, two possible neotectonic corridors coincide with high earthquake 20   activity. A north-south corridor of high HI and SI values aligns with the Nemaha Ridge, extending into Kansas along the Humboldt Fault Zone. A high SI anomaly across the Cherokee Shelf and Arkoma Basin fault zones corresponds to an area of anomalous drainage basin asymmetry, consistent with neotectonism. These results are consistent with slow active tectonism in Kansas and Oklahoma, suggesting that the significant increase in earthquakes over the past two decades may have a natural source of seismicity.

1   Introduction

Earthquakes remain among the most complex and least predictable natural hazards, especially those occurring within continental interiors far from tectonic plate boundaries. These intraplate earthquakes are especially challenging to predict, primarily due to their rarity, low strain accumulation rates, and lack of well-defined recurrence patterns (Calais et al., 2006). Despite their infrequency, intraplate earthquakes can be highly destructive and are associated with greater stress drops than their interplate 30   counterparts (Kanamori and Anderson, 1975; Scholz et al., 1986). The 1811–1812 New Madrid seismic events, which shook the midcontinent region of North America, exemplify the potential magnitude and impact of such events in stable continental settings (Johnston and Schweig, 1996; Hough et al., 2000; Hough and Page, 2011; Liu and Stein, 2016).

For the past decades (2009-2019), seismic activity has increased dramatically in regions such as Kansas and Oklahoma, which 35   are located within the relatively stable interior of the North American Plate, according to the 2014 National Seismic Hazard Map.

Historically, these states have experienced low levels of seismic activity. However, over the past decade and a half, a surge of low-to-moderate-magnitude earthquakes (generally M2–M4, with occasional events exceeding M5) has emerged unexpectedly, which is anomalous given the less frequent nature of these intraplate earthquakes. This anomaly has prompted considerable scientific investigation, particularly into anthropogenic factors that can induce seismicity, such as underground fluid injection.

40 Figure 1(a) illustrates the earthquake distribution in the study area from 2000 to 2023, including some earthquakes with magnitudes greater than 4.5, and Figure 1(b) shows the earthquakes from 1850 to 1999, which predate the fluid injection. The earthquakes in Figure 1(b) may be occurring due to natural causes, as they cannot be attributed to anthropogenic causes. These facts indicate the existence of unexplored neotectonic elements in the study area.
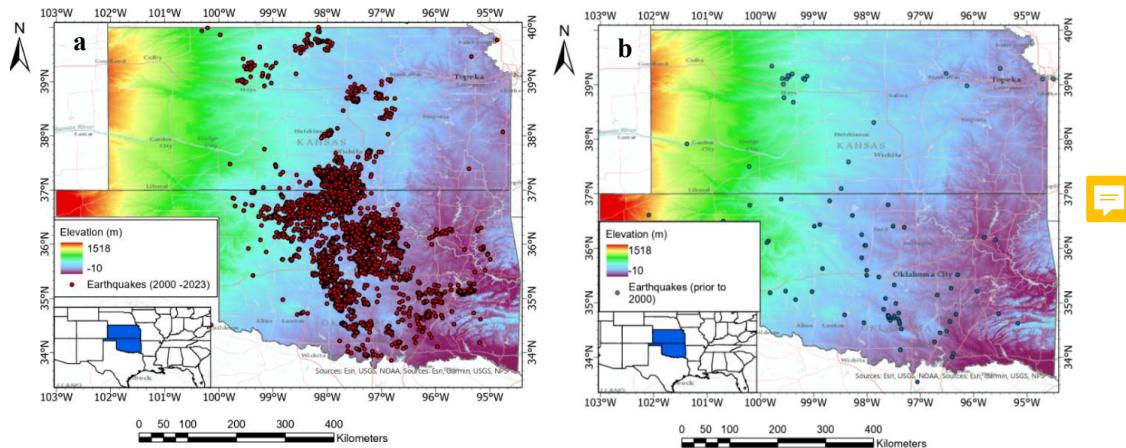

Figure 1: (a) Earthquake Distribution in Oklahoma and Kansas from 2000 to 2023, and (b) Earthquake Distribution in Oklahoma and Kansas (1850 – 1999) before the increased seismicity era (datasource: IRIS).

In Kansas and Oklahoma, these injection-induced earthquakes exhibit a spatial and temporal correlation (Weingarten et al., 50 2015). However, there are anomalous changes in the Quaternary alluvial deposition of the western tributaries of the Mississippi River system over the central plain, which suggest that dynamic geomorphology may account for neotectonics, the sources of natural earthquakes. Despite the growing body of work on induced seismicity, a critical gap remains in research regarding the natural source of earthquakes related to tectonic movements in this region. Quantitative analysis of geomorphic indices is a proven method to study neotectonics, the natural sources of earthquakes.

55

This study addresses this gap by investigating the extent of neotectonic activity in Kansas and Oklahoma through quantitative geomorphic analysis. This investigation employed analyses of geomorphic indices supplying both vector quantities (transverse drainage basin asymmetry) and scalar quantities (hypsometric integral and stream sinuosity index). By assessing geomorphic indices to evaluate Quaternary tectonic activity, the research ultimately contributes to a better understanding of seismic hazard 60 potential in stable continental interiors, where natural and human-increased seismicity may coexist. A critical question remains unanswered: Is there geomorphic evidence of neotectonics in areas of increased seismicity within the basement structures of Kansas and Oklahoma? This study employs quantitative analysis of one vector (Transverse Basin Asymmetry Index) and two scalar (Hypsometric Integral and Stream Sinuosity Index) geomorphic indices to address this question.

1.1 Research Statement

65

The primary objective of this study was to evaluate whether a spatial association exists between basement structures and indicators of geomorphic activity, specifically basin asymmetry, hypsometric integral, and stream sinuosity. Upon identification of such spatial patterns, the relationships were further investigated to explore potential causal attributions. To address this objective, a series of research questions was formulated to guide the application of geomorphic indices in assessing the factors

70

contributing to the observed patterns. The first question seeks to determine whether discernible spatial patterns exist in basin asymmetry, hypsometric integral, and stream sinuosity, or whether the observed variations are random. Following the detection of spatial patterns, the data and geomorphic indices were interrogated to evaluate possible attributions. Specifically, the analysis examined whether the observed patterns could be attributed to surface geology, basement structures, climatic influences, or active tectonism. Finally, the nature of each spatial pattern was described with the geomorphic indices applied.

1.2 Background

75

1.2.1 Surface and Subsurface Structures

It is essential to comprehend the regional geological conditions and tectonic factors before a tectonic-geomorphic analysis. The Central Plains Orogen, formed during the Proterozoic era between 1.63 and 1.80 billion years ago, is an extensive feature in the basement of Nebraska, Kansas, and Missouri. Portions of it are visible as the early Proterozoic fold belt in Colorado and

80

southeastern Wyoming. This orogen extends to the southern edge of the Superior-Archean craton and affects other early Proterozoic orogens like the Penokean (1.83-1.90 Ga) and the Trans-Hudson (1.85-1.95 Ga) (Sims and Peterman, 1986). It is the most ancient crust in southeastern Nebraska and northeastern Kansas and includes both Mazatzal (1.76-1.72 Ga) and Yavapai (1.69-1.65 Ga) orogens (Whitmeyer and Karlstrom, 2007) (Figure 2). In the midcontinent region, the most consistently identified subsurface feature through geophysical and subsurface drilling investigations is the Middle Proterozoic Mid-Continental Rift

85

System (MRS), a failed rift extended from Lake Superior southward into southeastern Nebraska, Central Kansas, and Oklahoma (Baars, 1995; Burberry et al., 2018; Van Schmus and Hinze, 1985; Stein et al., 2018). Extensional-fault systems from the Proterozoic era were reactivated due to tectonic stress during two significant events: the Ancestral Rockies orogeny, occurring from the Pennsylvanian to Permian periods, and the Laramide orogeny in the Cretaceous to Paleogene periods. These reactivation events caused the formation of flat-topped uplifts and outward bordering, monoclinal folds (Marshak et al., 2000).

90

The Central Plains orogen has been intersected by the NE-SW oriented MRS (1100 Ma) and the NNE-SSW trending Nemaha Tectonic Zone (NTZ) (300-250 Ma) (Burberry et al., 2015). Geophysical observations of the rift reveal a distinctive pattern, characterized by a gravitational high surrounded by areas of reduced gravity. This gravitational high results from deep-seated igneous intrusions and contributions from volcanic activity associated with the rift (Burberry et al., 2018). In Oklahoma and

95

southern Kansas, the Precambrian Southern Granite-Rhyolite Province, dating back to around 1.4 billion years ago, overlays the older Yavapai/Mazatzal craton (Denison et al., 1984; Soreghan & Soreghan, 2013) (Figure 2). This granitic basement is the focal point of much of the current seismic activity in the region (Kolawole et al., 2019; Schoenball and Ellsworth, 2017). In Figure 2, the Granite-Rhyolite Province (GRP) is divided by an isotopic boundary known as the "Nd line," which trends southwest to northeast. Rocks northwest of this line have Nd model ages over 1.55 billion years, formed from the melting of the older

100

Paleoproterozoic crust (Van Schmus et al., 1996). In contrast, rocks southeast of the line are younger, with ages between 1.55 and 1.35 billion years, representing a juvenile crust formed in an extended arc system (Bickford et al., 2015; Van Schmus et al., 1996; Whitmeyer and Karlstrom, 2007).
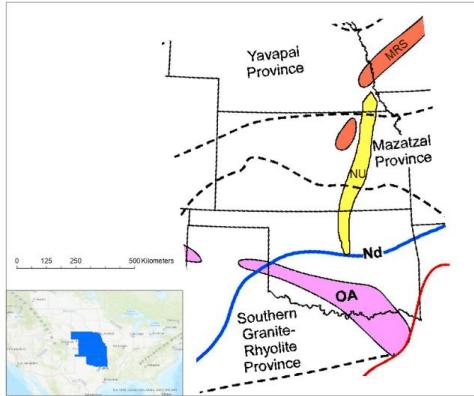
Figure 2: Basement terranes of the Laurentian midcontinent in the study area (modified from Freiburg et al., 2022). The above figure illustrates the Midcontinent Rift System (MRS), the Nemaha Uplift (NU), and the Oklahoma Aulacogen (OA). The red line is the Cambrian Continental Margin. The Dark blue line is the Nd line that separates the crust-yielding Nd model ages greater than 1.55 Ga to the north and less than 1.55 Ga to the south.

The eastern Kansas segment of the MRS exhibits a distinctive trend that diverges from the Nebraska segment, as depicted in Fig. 3. Seismic reflection data reveal that this segment is characterized by lower-angle normal faults, with angles significantly less than 60 degrees, in contrast to the Nebraska segment. The MRS, in conjunction with the Nemaha Tectonic Zone (MRS-NTZ), has experienced significant displacement due to sinistral strike-slip offset within a broader regional NW-striking wrench fault zone during Pennsylvanian reactivation of the basement structures. (Baars, 1995; Berendsen and Blair, 1986). The MRS-NTZ corresponds to either the Central Plains province or the suture zone between this Central Plains province and the older Penokean province (2.0-1.8 Ga) situated to the southeast of the MRS (Burberry et al., 2018).

Similarly, the Nebraska segment of the MRS runs parallel to geological structures within the Penokean crust to the southeast (Burberry et al., 2015). It contains a central horst surrounded by sedimentary basins within Nebraska, a correlation that aligns with data from Iowa (Burberry et al., 2015). Based on seismic reflection data obtained from Iowa, it is suggested that the Southern Boundary fault, known as the Thurman Redfield Fault Zone (shown in Figure 3), may exhibit a westward dip of up to 60 degrees, while the Northern Boundary fault zone displays a gentler dip (Chandler et al., 1989). The Burchard fault acts as the demarcation between the MRS and NTZ, with the Northern Bounding fault and Union fault delineating the boundaries of the MRS within Nebraska and Iowa, and the Kansas Bounding fault serves as the northern boundary of the MRS within the Kansas segment (Figure 3).
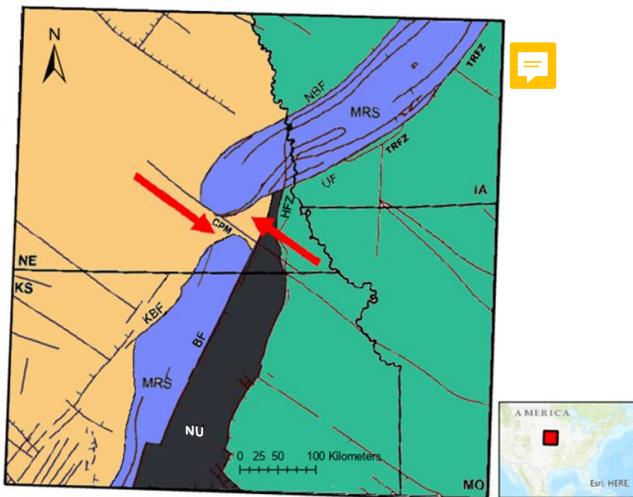
Figure 3: Subsurface Midcontinental Rift System (MRS) Extension from Iowa and Nebraska to Kansas. NU - Nemaha Uplift, HFZ - Humboldt Fault Zone, TRFZ - Thurman Redfield Fault Zone, BF - Burchard fault, KBF - Kansas Bounding fault, NBF - Northern Bounding fault, UF - Union fault. The tan-colored crust denotes Yavapai, and the green-colored crust denotes Mazatzal. Red arrows denote the sinistral shearing of Central Plains Megashear (CPM) (modified after Burberry et al., 2018).

The Nemaha Tectonic Zone (NTZ) extends from southeastern Nebraska and northeastern Kansas, traversing the states of Kansas and northern Oklahoma, and further south into central Oklahoma (McBee, 2003), as illustrated in Figure 4 and **Error! Reference source not found.**. This geological structure is bounded to the north by the Central Plains Megashear (Figure 3) and to the south by the Oklahoma Megashear (Fig. 5) (McBee, 2003). From southeastern Nebraska to Central Oklahoma, the Nemaha Uplift is a concealed, high-relief basement block (McBee, 2003). It is characterized by the nearly vertical Humboldt or Nemaha fault, which truncates it on the eastern side, as shown in Fig. 4.

Seismic data acquired through a deep 2D profile conducted by COCORP reveals the NTZ as a 40-kilometer-wide uplift (Serpa et al., 1989). Within the deep crust, this zone is characterized by a complex network of faulting and folding (Burberry et al., 2018). It's worth noting that the sense of slip direction is observed to be vertically reversed in multiple segments of the Humboldt fault Zone (HFZ) (McBee, 2003).

Baars (1992) and Wilson and Berendsen (1998) propose that the NTZ may have originated as part of the transfer zone within the MRS during the Proterozoic. Over time, it has evolved to exhibit a transpressive sense of relative offset, implying a compressional tectonic regime. A significant tectonic event during the Ordovician period is documented to have reactivated the NTZ and led to the uplifting of the Nemaha uplift (Burberry et al., 2018).

The Central Kansas Uplift (CKU) is a fault zone stretching from northwest to southeast, with its origins dating back to the Precambrian era (Baars, 1995). It covers a significant portion of the west-central region of Kansas, as depicted in Figure 4. This fault zone exhibits a left-lateral, strike-slip displacement and has experienced several episodes of reactivation and erosion throughout the Paleozoic and Mesozoic eras (Baars, 1995).

In addition to the NTZ and CKU, there is another basement fault known as Bourbon Arch Complex (BAC), which runs in a distinctive northwest direction, forming a right angle with the NTZ, as depicted in Figure 4. The BAC stretches from Central Missouri into east-central Kansas and consists of faults oriented in the northwest-southeast direction. This arch disrupts the NTZ faults in east-central Kansas, leading to the division of the basement into suborthogonal crustal blocks (Berendsen and Blair,

160   1986). The intersection of these major fault zones results in forming a conjugate-set in central Kansas.
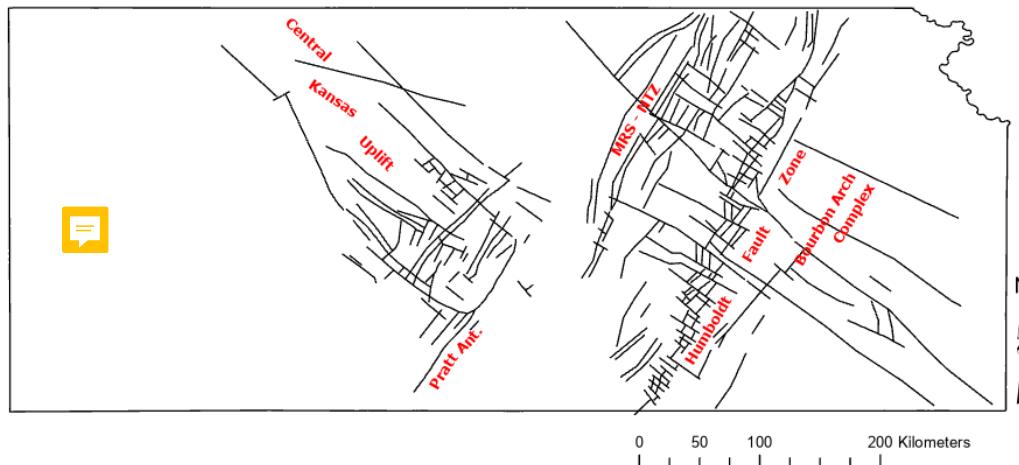

Figure 4: The basement fault map of Kansas showing the major fault systems of the state (modified after Baars, 1992). MRS = Midcontinental Rift System; NTZ = Nemaha Tectonic Zone.

165

The change in the stress field from a strike-slip regime in Oklahoma into an extensional regime in Kansas is observed in the U.S. stress map (Levandowski et al., 2018). The fault database of Oklahoma, compiled by Marsh and Holland (2016), reveals the presence of various fault segments and, notably, the existence of large north-south trending faults exceeding 50 kilometers in length in the north-central region (Figure 5). Recent three-dimensional seismic reflection data (Patel et al., 2021) has also

170   revealed that these substantial north-south faults and their associated secondary splays (red circle in Figure 5), along with northwest and northeast-trending ones, are rooted in the basement, similar to that schematically illustrated in Figure 6 for the Wichita Uplift. These faults are the southward extension of Nemaha Uplift. In the northeastern region of Oklahoma, there is compelling evidence of dextral offsets occurring along the faults within the Nemaha Tectonic Zone (McBee, 2003). This geological setting includes a pop-up block that characterizes a restraining bend known as the Garber uplift (McBee, 2003).

175   Additionally, there is an east-bounding reverse fault of this uplift. In Oklahoma, the NTZ is regarded as a relatively narrow fault zone with a transpressional nature, and its initial activation can be traced back to the Taconian orogeny in the Ordovician period (McBee, 2003).

The Oklahoma Megashear comprises significant faults associated with the Arbuckle and Amarillo-Wichita-Criner Hills uplifts

180   (Figure 5). The Wichita Frontal fault (WFF) system delineates the southern boundary of the Anadarko basin and provides evidence of the Pennsylvanian-era inversion of a Cambrian continental rift, as discussed by McBee (2003). This fault system, which involves the basement, consists of multiple segments along its length, underscoring the capacity of Great Plains basement fault systems to generate substantial earthquakes, including in the Holocene epoch.

185   One notable component of this system is the Meers fault; an oblique reverse fault considered a major tectonic feature capable of
        causing significant seismic events in the region (Chase et al., 2022; Harlton, 1963). It is part of the WFF system and serves as the
        boundary separating the Anadarko-Ardmore basin to the northeast from the Wichita-Amarillo uplift to the southwest (Harlton,
        1963). The Meers fault is included in the Mountain View fault system (Figure 5). The Meers fault ruptured the surface multiple
        times in the mid and late Holocene (Crone and Luza, 1990; Hornsby et al., 2020).

190

        A regional stress map reveals a gradual shift from oblique, normal faulting in western Oklahoma to basement strike-slip faulting
        in central and eastern Oklahoma (Qin et al., 2019). This transition is indicative of the evolving tectonic stress patterns across the
        region. One noteworthy fault near Western Kansas's border is the Cheraw fault, extending approximately 80 kilometers through
        southeastern Colorado (Ostenaa et al., 2022). Similar to the Meers fault, the Cheraw fault is recognized as a distinct source of

195   intraplate seismic activity and has a Quaternary history of surface ruptures to the east of the Rocky Mountains. Along the 45-
        kilometer-long southwestern section of this normal fault, there is compelling evidence of four paleoseismic events involving
        Quaternary surface rupture since 19 Ka (Ostenaa et al., 2022). Furthermore, the slip rate of the Cheraw fault has increased from
        0.03 millimeters per year to 0.16 millimeters per year since ~19 Ka, possibly due to rapid erosional unloading caused by the
        Arkansas River in the late Cenozoic (Ostenaa et al., 2022).

200
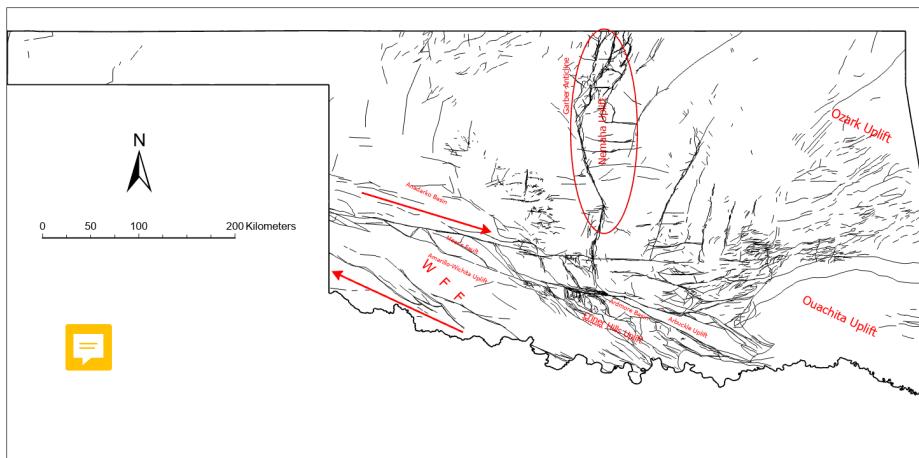
**Figure 5: The basement structures of Oklahoma shows the Wichita Frontal Fault (WFF) system, a complex fault system
associated with the Oklahoma Megashear denoted by red arrows, Ozark Uplift, Ouachita Uplift, Nemaha Uplift, Garber
Uplift, Amarillo-Wichita Uplift, Arbuckle Uplift, Criner Hills Uplift, Meers fault, Anadarko Basin, Ardmore Basin**
205   **(modified after Marsh and Holland, 2016).**
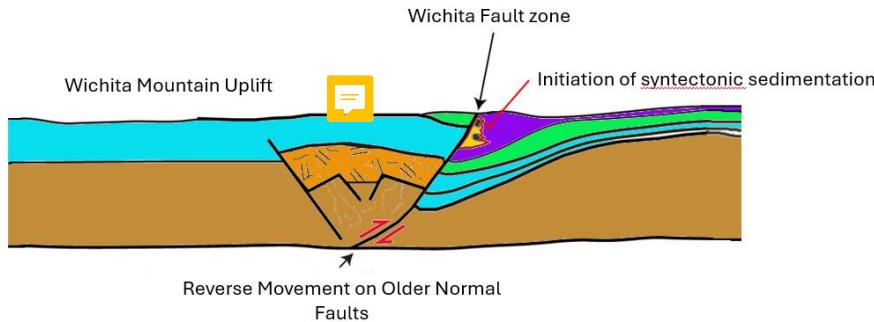
Figure 6: Reverse movement on older normal faults (Modified after Higley, 2014).

1.2.2   Regional Geology

The oldest sedimentary formation in Oklahoma, the Cambrian Reagan Sandstone, can be traced back to a major phase of erosion, where sand and gravel were derived from the ancient Precambrian basement (Johnson and Luza, 2008) (Figure 7). This erosion phenomenon was particularly pronounced in Oklahoma's southern and eastern sectors during the Cambrian period. Notably, similar geological processes in select areas of Kansas and Nebraska led to the creation of the Cambrian Lamotte Sandstone, a correlative rock layer (Lee, 1956). The overlying Arbuckle Group (thickness varies from hundreds of meters to thousands of meters) comprises significant layers of limestone and dolomites deposited during the Late Cambrian and Early Ordovician periods in this region (Franseen et al., 2004) (Figure 7). This formation is the target formation for wastewater injection (Patel et al., 2021).

In the early and middle Paleozoic, the Earth's crust exhibited notable stability, facilitating the deposition of the Ordovician Sycamore Limestone in the southern Oklahoma region (Johnson and Luza, 2008). Simultaneously, the northern sectors of Oklahoma and Kansas accumulated Ordovician sedimentary deposits such as the Simpson Group (a sequence of clastic and sandy carbonate rocks from the Middle Ordovician period, thickness up to 310 meters), Viola Group (an upper Ordovician marine-limestone sequence, thickness up to 213 meters), and Sylvan shale (referred to as the Maquoketa shale in Kansas, thickness up to 125 meters), unconformably followed by deposition of the limestones of the Mississippian sequence (Adkison, 1972; Johnson and Luza, 2008) (Figure 7). A significant basin subsidence event occurred in southern Oklahoma during the Mississippian Period (Bird, 1998; Gries et al., 1992; Willis, 1999). The rapid accumulation of sediments (total thickness ≥ 2 km) deposited formations such as the Caney Shale, Goddard Formation (a mudstone found in the Ardmore and Anadarko Basins of Oklahoma), and Springer Shale (Hobbs et al., 2022; Johnson, 1988).

In Kansas, Pennsylvanian strata consist of alternating cycles of marine shales, limestones, and nonmarine beds, reaching a total thickness of approximately 950 meters. These layers dip gradually westward, with some local changes in direction, and show a noticeable thinning of shale and limestone units as they extend westward. The Pennsylvanian rocks lie conformably beneath Permian strata but unconformably over Mississippian rocks, with geological structures such as the Nemaha anticline and CKU affecting their distribution.

In the early Permian period (Wolfcampian), a shallow sea transgressed a significant expanse encompassing western Oklahoma and the Panhandle of Texas (Johnson and Luza, 2008). Within this sea, shallow marine limestone and gray shales were deposited. Moreover, as the seawater gradually evaporated, it formed substantial salt and gypsum deposits, including prominent ones like

240   the Wellington and Cimarron Evaporites (Johnson and Luza, 2008). Over time, these sedimentary processes led to the late Permian burial of much of the Wichita Mountains in southwestern Oklahoma (Johnson and Luza, 2008).

The Permian rock layers exhibit varying thicknesses, ranging from 300 to 1500 meters on the margins of the Anadarko Basin (Johnson, 1988), while deeper within the basin, the entire Permian sequence can reach a thickness of 1800 to 2000 meters

245   (Johnson, 1988). Notably, the Anadarko Basin is the deepest Phanerozoic basin on the North American continent. Its formation is attributed to thrust loading during the late Mississippian to Early Pennsylvanian periods, involving structural inversion within the core of the southern Oklahoma aulacogen (Perry, 1989). This geological process led to the northward vergence of Wichita thrust-bounded uplift (Perry, 1989) (Figure 7). The rapid subsidence of the basin during the Permian suggests that thrust-loading processes persisted into the Permian period.

250

The upper beds of the Jurassic Morrison Formation unconformably overlie Permian strata and primarily consist of green sandy shale with occasional limestone lenses, while the lower shale beds contain pink chert, anhydrite, and gypsum. In well logs, the Morrison Formation has been recorded at thicknesses ranging from 30 to 100 meters (Merriam, 1963). This formation, present in far western Oklahoma, comprises deposits of mud, silt, sand, and other materials left from a floodplain that existed

255   approximately 150 million years ago. East of the Morrison Formation, Cretaceous marine rock layers are positioned above the Permian sequence, indicating a significant unconformity in the geological record (Johnson and Luza, 2008). The Cretaceous rocks, with a total thickness ranges from approximately 60 to 900 meters, consist of various formations including the Cheyenne Sandstone and Kiowa Shale from the Comanchean Series, the Dakota Formation (a succession of sandstones and mudstones or shaly strata), Graneros Shale, Greenhorn Limestone, Carlile Shale, Niobrara Chalk from the Gulfian Series, and the Pierre

260   Formation (composed of dark gray shale, interspersed with sandstone layers and numerous beds of bentonite) (Lee, 1956) (Figure 7). During the early Cretaceous period, southeastern Oklahoma was submerged under the ancestral Gulf of Mexico, and as the Cretaceous progressed, the inland sea expanded to cover regions in Oklahoma, Kansas, and Nebraska (Roberts and Kirschbaum, 1995).

265   The late Cretaceous and Paleogene uplift of the Rocky Mountains caused a broad uplift of Oklahoma and Kansas to Nebraska, with an eastward tilt that resulted in the last recession of the inland sea (Johnson and Luza, 2008). The Laramide orogeny (late Cretaceous to Paleocene) that overlapped with the time of Sevier orogeny significantly impacted the uplift of the Rocky Mountains belt. The orogenies had different compressional directions, and the Laramide involved the thrusting of deep crustal rocks (Bird, 1998; Condon, 2005; Gries et al., 1992; Tweto, 1975). The Sevier Orogeny started during the Jurassic when the

270   westward movement of the North American plate caused the continental plate to collide with several oceanic microplates in the Pacific (Condon, 2005).

The Ogallala Formation, composed of sandstone and conglomerate, dates to the Neogene (Zeller, 1968) (Figure 7). These sediments were eroded from the Rocky Mountains and subsequently deposited across the High Plains of western and west-

275   central Oklahoma and Kansas (Johnson and Luza, 2008). During the Quaternary period, the runoff from the melting Rocky

Mountains glaciers followed the major rivers, leaving alluvial deposits in terraces (Johnson and Luza, 2008). Glacial till and loess are commonly encountered in the upland areas of Kansas.

Era	System	Series	Stratigraphic Unit (KS)	Lithology	Stratigraphic Unit (OK)
Cenozoic	Neogene	Pliocene	Ogallala Formation		Ogallala Formation
			Pierre Shale		
Mesozoic	Creataceous	Upper	Niobrara Chalk		Eagle Ford
			Carlile Shale		
			Greenhorn Limestone		Woodbine
			Graneros Shale		
			Dakota Formation		
		Lower	Kiowa Formation		Duck Creek Fm. / Kiamichi Clay / Goodland Lst. / Antlers Fm
			Cheyenne Sandstone		
	Jurrasic	Upper	Morrison Formation		Unconformity
Paleozoic	Permian	Upper	Whitehorese Group	El Reno Group	Cloud Chief / Rush Spring / Marlow
			Nippewalla Group		Dog Creek Shale / Blaine Gypsum / Flowerpot Shale
			Sumner Group		Duncan Sst / Hennessey / Garber Sst / Wellington Shale
		Lower	Chase Group		Chase Group
			Council Grove Group		Council Grove Group
			Admire Group		Admire/Post Oak Conglomerate
	Pennsylvanian	Upper	Wabaunsee Group		Vanoss
			Shawnee Group		Ada
			Douglas Group		Vamoosa
			Lansing Group		Hilltop Fm.
			Kansas City Group		Caddo Fm. / Wann and Iola Lst / Chanute Shale
			Pleasanton Group		Nellie Bly Fm. / Checkerboard Lst/Hogshooter / Seminole Fm / Holdenville Shale
		Middle	Marmaton Group	Deese Group	Wewoka / Senora / Boggy
			Cherokee Group		Savanna / McAlester
		Lower			Lynn Fm. / Jackfork Sandstone
	Mississippian	Upper	Chesterian		Caney Shale/Stanley Shale
			Meramecian		Keokuk
		Lower	Osagean		Reed Spring/ Sycamore Lst
					St. Joe
			Kinderhookian		Unconformity
	Devonian	Upper	Unconformity		Woodford Shale
	Ordovician	Upper	Maquoketa Shale		Sylvan Shale
			Viola Limestone		Viola Limestone
		Middle	Simpson Group		Simpson Group/Wichita Granite Group
		Lower	Arbuckle Group		Arbuckle Group
	Cambrian	Upper	Reagan Sandstone		Regan Sandstone
	Precambrian		Granite, Schist		Granite, Schist

Legend:
- ∿ Unconformity
- Sandstone - Conglomerate
- Silty Shale
- Limestone
- Shale
- Clayey Sandstone
- Sandstone
- Silty Redbeds
- Granite, Schist

280 **Figure 7: General Stratigraphy of Kansas and Oklahoma, modified after Carr et al., 2005 and Liner and Liner, 2014.**

The structural attitudes of surficial rocks in Kansas and Oklahoma exhibit distinct regional variations. In Kansas, the bedrock strata of the eastern regions, specifically the Osage Cuestas and Flint Hills, dip gently west-to-northwest, trending away from the Ozark Dome to the east (Figure 8(a)). In contrast, the bedrock strata of western Kansas, encompassing the Smoky Hills, High Plains, and Red Hills, exhibit minimal dip, generally 1° or less (Figure 8(a)).

285

In Oklahoma, the regional dip patterns of surficial rocks are more varied. In the northeastern region, strata dip gently to the west and southwest, away from the Ozark Dome (Figure 8(b)). Southeastern Oklahoma, however, shows more complex structural characteristics, with strata dipping moderately to steeply in multiple directions—north, northwest, southeast, and south—within the fold-and-thrust belt of the Ouachita Mountains and Arkoma Basin (Figure 8(b)). In south-central Oklahoma, including the

290 Arbuckle and Wichita Mountains, stratal dips are locally moderate-to-steep with variable orientations (Figure 8(b)). Central and north-central Oklahoma, situated on the Cherokee Platform, exhibit gentle westward dips (Figure 8(b)). In contrast, in western Oklahoma, including the Anadarko Shelf and Basin, the dip is minimal, generally 1° or less (Figure 8(b)).
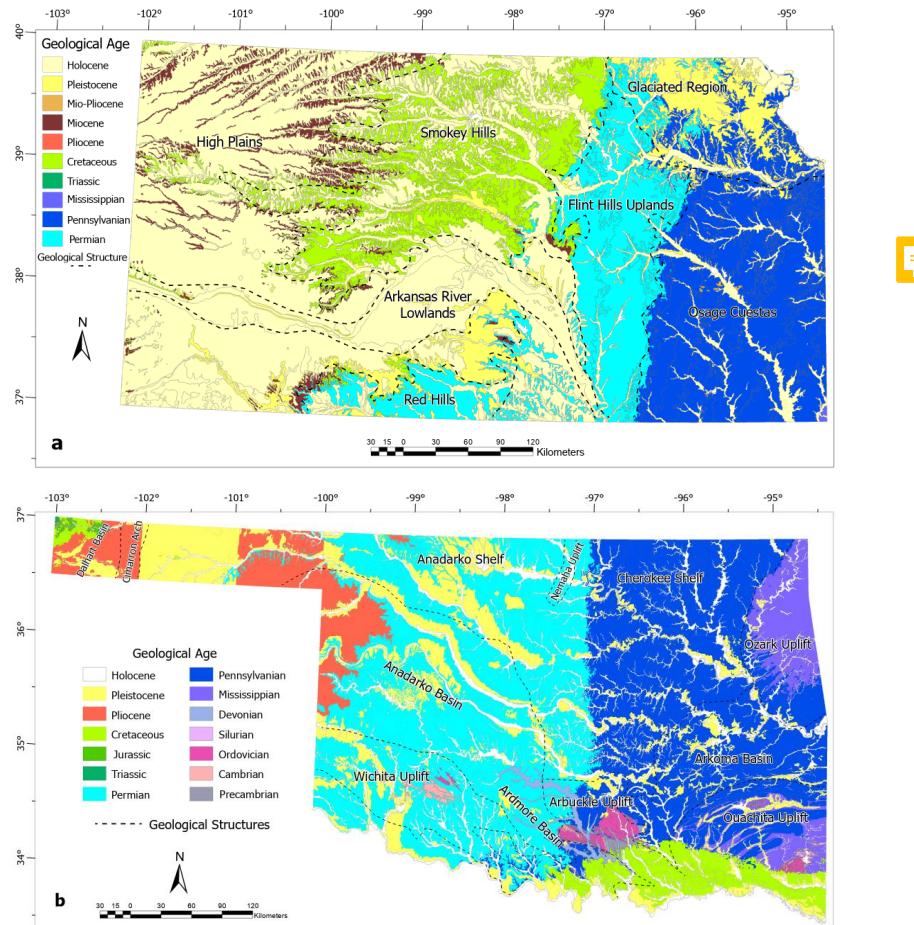
295

Figure 8: (a) Geological Map illustrating the geological ages and geomorphic boundaries within Kansas; (b) Geological Map of Oklahoma illustrating the geological ages and structural boundaries within Oklahoma (data source: Horton, 2017).

300 ### 1.2.3 Seismicity and Stress

Park et al. (2022) conducted a comprehensive study of the southern Kansas and Oklahoma region by applying advanced earthquake relocation algorithms, namely HYPOINVERSE-2000 (Klein, 2002) and hypoDD (Waldhauser, 2001), along with a

11

machine learning-based phase picker known as Phasenet (Zhu and Beroza, 2019). They utilized continuous waveform data spanning from 2010 to 2019, totaling 796 station-years, to compile a detailed regional earthquake catalog. Park et al. (2022) used

305   ridge detection algorithm (Chen et al., 2015) to map epicenters into ridges for better constraints. Their findings revealed that seismicity clusters with a length-scale of an earthquake with a given magnitude of 1.14 kilometers or greater (referred to as LM4) had approximately a 5% probability of hosting one or more earthquakes with a magnitude equal to or exceeding M4 within a year. Importantly, their research indicated that 80% of these earthquakes could have been predicted before they occurred. Furthermore, Park et al. (2022) concluded that the relocated seismicity clusters provide insights into previously unrecognized

310   geological structures. Some known fault lines are also defined by seismicity (Chen et al., 2017; Keranen et al., 2013; Yeck et al., 2016).

Qin et al. (2019) employed a combination of relocated earthquake catalogs and focal mechanisms to construct a stress-state map for the seismogenic faults in the Oklahoma and southern Kansas regions. This mapping effort allowed them to quantify the stress

315   state of these faults using a parameter called "understress." The parameter "understress" serves as a measure to assess the degree of fault criticality, where a value of 0 indicates faults under significant stress and a value of 1 indicates faults experiencing no applied shear stress. This parameter helps gauge the fault's vulnerability and potential for failure. Their findings revealed that 78% of the faults studied were characterized by critically stressed conditions (with understress values less than or equal to 0.2). In contrast, several seismogenic faults exhibited non-optimal orientations and high understress values exceeding 0.4. Importantly,

320   the seismogenic faults were found to be distinct from the known sedimentary faults, although they shared common basement faults. Additionally, these seismogenic faults displayed two prominent sets of strikes, oriented at approximately 055°- 075° and 105°-125°.

In their study, Zhai et al. (2020) developed a comprehensive physics-based model that integrates hydromechanical processes and

325   increased earthquake rates. They applied this model to analyze the impact of remote, large-scale injection wells in Western Oklahoma on the seismic activity in southern Kansas, using seismic data from 2010 to 2018 and information on 668 Class II injection wells. Their model revealed that the fluid diffusion resulting from injection activities in Oklahoma significantly amplifies the total Coulomb stress change and the seismic activity rate in south-central Kansas, increasing them by 1.5 times and threefold, respectively. Zhai et al. (2020) also report that disregarding the extensive fluid diffusion interaction can consistently

330   lead to underestimating the probability of earthquake magnitude exceedance in Kansas.

Various research studies have employed analysis of seismic event spatial distribution to identify Oklahoma fault segments. For instance, Keranen et al. (2013) used data from the 2011 Mw 5.7 Prague earthquake sequence to map the splays of the Wilzetta fault. In another case, Yeck et al. (2016) delineated the extension of a previously mapped fault segment based on data from the

335   2016 Mw 5.1 Fairview earthquake sequence. Additionally, Chen et al. (2017) mapped the Sooner Lake Fault as the conjugate fault of the previously identified Labette Fault using information from the 2016 Mw 5.8 Pawnee earthquake sequence.

Based on the distribution of high-level Neogene alluvial deposits in eastern Kansas, Aber (1997) found that stream captures, valley entrenchment, and inversion of topography are the results of long-term crustal tilting downward to the south and east

340   (neotectonism). However, there is a lack of quantitative analysis of geomorphic indices in the study area.

1.2.4   Climates and Microclimates

Climatically, most of Kansas and Oklahoma are semi-arid, but the easternmost region is semi-humid, with the average annual precipitation ranging from about 40 cm in the far western portion to about 120 cm in the far southeast (Rosenberg, 1987). The topography of Kansas has been characterized as rolling plains topography, but owing to several ranges of hills (the Ouachita Mountains, the Arbuckle Mountains, the Wichita Mountains, and the Ozark Plateau), southern and eastern Oklahoma have local relief up to 350 m (Osterkamp et al., 1987).

The incidence of solar radiation from the south at the latitude of the semi-arid region gives rise to microclimates on south-facing valley slopes that are hotter and drier than on shaded north-facing slopes, causing sparser plant cover on south-facing slopes (Bass, 1929; Dohrenwend, 1978). Thus, south-facing slopes are subject to greater slope wash erosion, resulting in the more pronounced development of south-flowing tributaries. Sediment delivery from these south-flowing tributaries deflects the trunk stream southwards, causing erosion along the foot of north-facing slopes. These processes result in trunk stream basins with south-directed asymmetry vectors (Bass, 1929; Dohrenwend, 1978).

1.2.5   Hydraulic Fracturing

Substantial evidence indicates that the surge in seismicity can be attributed to the increased adoption of hydraulic fracturing, commonly known as fracking (Ellsworth, 2013; Rubinstein and Mahani, 2015). The technique involves injecting fluids into the geologic formations containing petroleum resources to extract them through hydraulically generated fractures. The process itself is not inherently hazardous, but it may introduce additional stress into the subsurface rock formation that may perturb the poroelastic pressure distribution, either reducing the effective stress of a pre-existing fault system or creating a new fault system (Healy et al., 1968; Raleigh et al., 1976). This phenomenon is well-documented and has been observed in multiple regions all over the United States and globally, where hydraulic fracturing (HF) is prevalent (Ake et al., 2005; Block et al., 2015; Frohlich, 2012; Goebel et al., 2017; Haug et al., 2018; Keranen et al., 2014; Porsani et al., 2012; Wilson et al., 2015; Yeck et al., 2016, 2017). Numerous studies have established a connection between the initiation of HF operations and the resulting seismic events, often termed injection-induced earthquakes. In Kansas and Oklahoma, induced earthquakes are attributed to the initiation of HF activities in some areas of the regions (Weingarten et al., 2015). Figure 9 shows the HF activities in Kansas and Oklahoma.
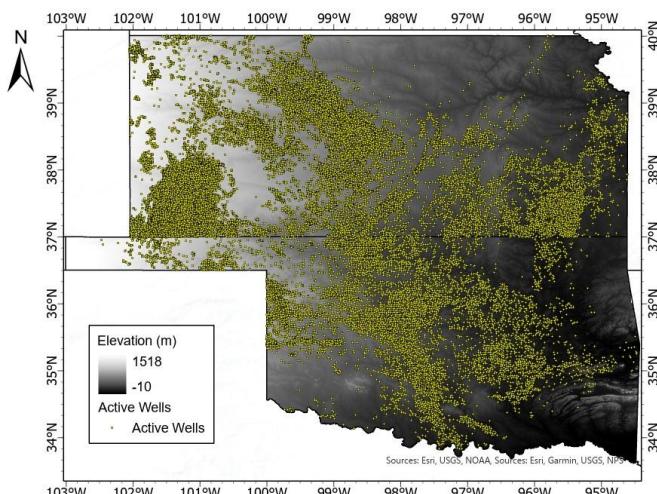

Figure 9: Active hydraulic fracture wells in Oklahoma and Kansas (Data Source: FracTracker)

13

2 Data and Methods

2.1 Data

370 Digital Elevation Models (DEMs) were obtained from the United States Geological Survey (USGS) 3D Elevation Program (3DEP) via the National Map service. These DEMs have a resolution of 1/3 arc-second, corresponding to approximately 10 meters. Data from the National Hydrography Dataset (NHD) prepared by the USGS were obtained and utilized. Basement fault data for Oklahoma were acquired from the Oklahoma Geological Survey (OGS), while for Kansas, basement fault data were digitized from the technical report prepared by the Kansas Geological Survey (KGS) (Baars, 1992). Surficial geological

375 information was sourced from the State Geologic Map Compilation (SGMC) geodatabase of the conterminous United States (Horton, 2017), published by the USGS. Given the distinct nature of basement fault and surficial geological data for Kansas and Oklahoma, the quantitative analyses were conducted separately for each state.

2.2 Methods

Three quantitative geomorphologic methods are described in the following sections to assess the one vector geomorphic index

380 and two scalar indices. The transverse basin asymmetry index (TI) has produced geographic domains containing mean vectors of preferred azimuthal directions. In contrast, two scalar indices (hypsometric integral (HI) and sinuosity index (SI)) are used to produce boxes and corridors of possible neotectonism.

2.2.1 Transverse Basin Asymmetry Index (TI)

The Transverse Basin Asymmetry Index (TI) quantitative analysis of drainage basins' symmetry (T-index) effectively detects

385 areas of neotectonics in regions of high or low seismicity (Baird and Willemin, 1998; Cox, 1988; Cox et al., 2001a; Csontos, 2002; Garrote and Garzón, 2002). Generally, drainage basins within a region of homogeneous and unconsolidated or semi-consolidated sediments have a random pattern of transverse asymmetry for the position of dendritic streams between their drainage-divides (Cox, 1994; Hasbargen and Paola, 2000; Parker, 1977). However, streams flowing near an actively tilting block show a specific asymmetrical orientation, indicating subtle tectonic movements (Cox et al., 2001b).

390

Tectonism is not the only factor influencing basin morphology, additional factors include monoclinal shifting of streams downdip on resistant strata, enhanced erosion on a preferred slope aspect in an arid or cold climate, or uneven development of tributaries due to the initial slope on a dissecting plain need to be assessed as other drivers of basin asymmetry (Cox, 1994), and these factors are considered herein. The T-index is used to identify the asymmetric orientation of streams within a basin (Figure 10)

395 from Cox et al. (2001a). T-index is represented as the magnitude of a drainage basin asymmetry vector in the direction the stream shifted from the center of its basin.

T-index is the ratio between the distance from the channel to the midpoint of the basin (along a straight line perpendicular to the line best fit to the stream for each stream of a given length), Da, and the distance from the drainage divide to the midpoint of the basin (along the same line), Dd. When the basin is symmetrical, and the stream is at the basin's center, Da = 0 and T-index = 0.

400 When streams are closer to the drainage divide, the T-index approaches 1 (See Figure 10).
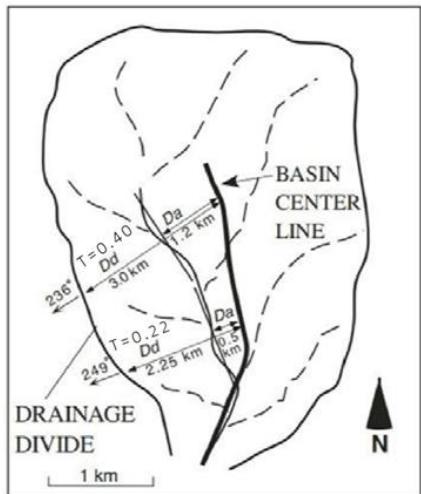
Figure 10: T-index analysis to calculate basin asymmetry for each 1 km stream segment (Cox, 1994). See the text for definitions of D_a and D_d.

405

The generation of stream networks and the assignment of basin orders were carried out following the Strahler method (Strahler, 1952) in ArcGIS Pro using the 10-meter resolution DEM. I worked with fourth-order streams for subsequent analysis. A standard-size sub-basin was chosen for a pilot study to see which order stream has enough data for our basin asymmetry analysis. For this analysis, second-, third-, and fourth-order streams were initially considered. The mean vector of basin asymmetry for

410 second-order streams exhibited only a negligible difference from that of fourth-order streams. Given this minimal variation and considering processing efficiency relative to the total study area, fourth-order streams were selected for the final analysis. Fourth-order stream order provides better-distributed data for analysis than higher-order streams, yet does not overwhelm the analysis with excessive basin data from lower-order streams.

415 Preceding the construction of the stream network, the Fill tool in ArcGIS Pro was applied to rectify errors associated with artificial sinks and peaks resulting from resolution limitations or the rounding of elevation values to the nearest integers. Subsequently, the Flow Direction tool, which creates a raster of flow direction from each cell to its downslope neighbor, or neighbors, was employed to ascertain the directional flow of streams, while the Flow Accumulation tool quantified the accumulated flow for each downslope cell of the flow direction raster.

420

To further refine the analysis, the Raster Calculator was used to generate an output raster that assigned a cell value of zero to cells with a receiving flow from ≤ 2500 other cells and a value of 1 to cells receiving flow from ≥ 2500 other cells, employing the Strahler (D8) method (Strahler, 1952) for flow modeling. The threshold for flow receiving cells < 2500 for stream network comes from the Strahler method to keep the drainage area 0.25 sq. km, as each cell size is 0.0001 sq. km. The cells, classified as

425 numerical value 1, collectively constituted the stream network. Throughout the flow accumulation process, default weights were applied to cells, with the total drainage area for flow-accumulating cells within the stream networks set at 0.25 square kilometers. A drainage area of 0.25 sq. km was selected to best fit the generated stream network with the stream networks in existing stream maps of Kansas and Oklahoma.

430 After completing these steps, the stream order was determined to derive the stream network raster, which was converted into a polyline feature. The stream network feature was divided by Hydrologic Unit Code 8 (HU8) sub-basin boundaries (Appendix A). The highest flow accumulation cell was selected using the Snap Pour Points tool at the mouths of the fourth-order streams, where water pours out of the stream's drainage area. Utilizing the pour points of fourth-order streams, fourth-order basin rasters were generated within each HU8 sub-basin of Kansas and Oklahoma. Subsequently, the basin rasters were converted to polygons, and

435 basin centerlines were established. Due to the irregular shapes of the basins, multiple centerlines were generated.

The centerline exhibiting subparallel alignment with the fourth-order stream was manually chosen for basin asymmetry analysis. Some fourth-order basins lacked subparallel centerlines due to basin capture and were avoided for analysis. Each fourth-order stream was divided into approximately 5 km segments, and a T-index was determined for each 5 km segment. The transverse

440 distance (Dd) between the drainage divides and the centerline was measured using the Calculate Geometry function and recorded in the line feature attribute table. Likewise, the perpendicular distance between the fourth-order stream and the centerline was measured and stored in the corresponding line feature attribute table. A vertical exaggeration of 1000 was applied to enhance visualization. Polar plots were generated to observe the trend and quantity of the basin asymmetry for each HU8 sub-basin (see Appendix B for Polar plots). The flow chart of the method is shown in Figure 11**Error! Reference source not found.**

445
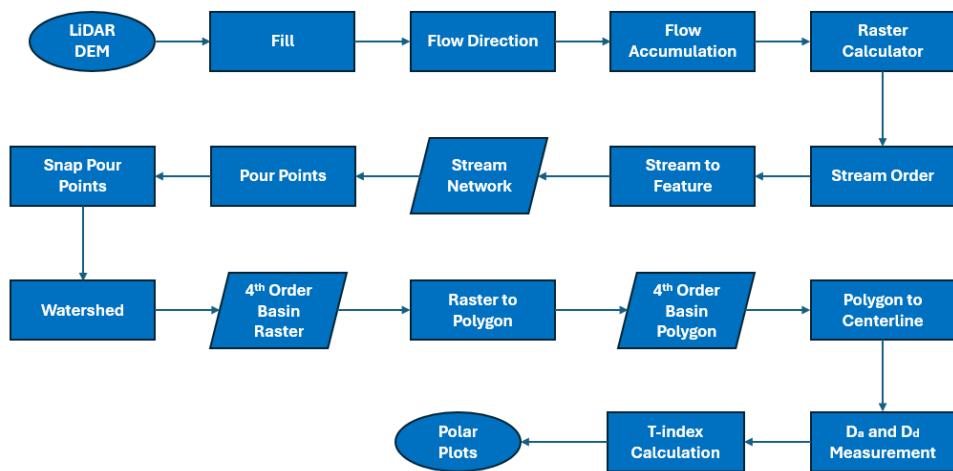
Figure 11: Flow chart for Basin Asymmetry Analysis.

For each sub-basin, the asymmetry vectors were spatially averaged to create smooth fields of mean vectors for better

450 interpretation. Spatial averaging is a statistical method used to represent the average value of a variable across a defined spatial area or volume. It involves calculating the average of multiple measurements taken at different locations within that area or volume. Two classes of spatially averaged asymmetry vector domains were defined visually based on the continuity of mean vectors in neighboring sub-basins. The vector domains are regional polygons that help to define the area with preferred basin asymmetry. The term "preferred azimuthal direction of asymmetry of the mean vectors" means all the asymmetry vectors inside

455 a domain prefer to be oriented in a single, preferred class of direction. The domains were used to present the findings in the results section. To delineate the vector domains as simple polygons, their boundaries were manually drawn along the sub-basin

16

boundaries, ensuring that each domain fell under a single class. The classification criteria for azimuthal vectors, described in this section, were used to delineate the boundaries. One class of domain boundary was restricted where the vector direction changed by more than 30° in azimuth. The classification scheme is adapted from Garrote et al. (2006). The 30° interval was chosen to find

460   the azimuth in terms of NNE (0°–30°), NE (30°–60°), ENE (60°–90°), ESE (90°–120°), SE (120°–150°), SSE (150°–180°), SSW (180°–210°), SW (210°–240°), WSW (240°–270°), WNW (270°–300°), NW (300°–330°), and NNW (330°–360°). This classification allows comparison of azimuth and regional structural dip.

Resultantly, 80 mean-vectors for Oklahoma and 53 for Kansas, derived from a total of 950 fourth-order basins in Oklahoma and

465   1,697 in Kansas, were examined to assess the asymmetry vectors. Using the mean-vector fields generated by analyzing the asymmetry of these fourth-order basins, a detailed process was undertaken to determine the azimuthal-vector fields as fields of random vectors. The mean vectors indicate the average direction and magnitude of the asymmetry in the hydrological sub-basins, offering a broader perspective on regional trends. Therefore, local variations in asymmetry are outside the focus of this study. Sub-basins with fewer than ten basin-asymmetry data points were excluded to minimize the introduction of skewness. This

470   skewed dataset may have introduced a bias in calculating probability with random vectors.

The remaining asymmetry vectors are normalized before calculating the probability of random vectors to compensate for the varying numbers of basin asymmetry data available for each sub-basin due to the varying sub-basin area (Appendix C). The probability (p) of obtaining a mean vector magnitude by pure chance combination of random vectors is calculated from the

475   following equation (Curray, 1956) –

$$(p) = e^{[-(100L)^2 n](10^{-4})} \tag{1}$$

L is the mean vector magnitude, and n is the number of measured basin segments. Before defining the domain boundaries, I excluded those portions of the study area with mean asymmetry vectors exceeding a 0.05 probability (p) threshold, considering them as a field of random vectors (Appendix D). This threshold was crucial to ensure that only the most significant vectors were

480   considered in this analysis, enhancing the reliability of the findings.

Hypsometric Integral (HI) and Pattern Analysis.

Hypsometric analysis, as pioneered by Strahler (1952) and Schumm (1956) and further developed by Hurtrez et al. (1999), focuses on the distribution of surface area with respect to elevation. Key tools in hypsometric analysis include the hypsometric

485   curve and the Hypsometric Integral (HI). The hypsometric curve illustrates the relative proportion of area below or above a given height, while the HI represents the cumulative area below the hypsometric curve. Pike and Wilson (1971), Mayer (1990), and Keller and Pinter (2002) have contributed to understanding the correlation between the HI and the shape of the hypsometric curve. Additionally, Pérez-Peña et al. (2009) emphasize the HI's role in inferring the geomorphic evolution stage of a basin, building upon the work of Strahler (1952), Schumm (1956), Keller and Pinter (2002), Chen et al. (2002), Singh (2009), and

490   Pérez-Peña et al. (2009).

Spatial analysis of HIs within a given area, employing the Local Indices of Spatial Autocorrelation (LISA) technique, has proven effective in identifying neotectonics (Mahmood and Gloaguen, 2011; Pérez-Peña et al., 2009). This method has been used to reveal a clustering pattern of high and low HI values, indicating the influence of tectonics on the topography (Pérez-Peña et al.,

495   2009). Higher HI values (>0.7) suggest a younger landscape less affected by erosion, potentially influenced by active tectonics. For the mature stage, the HI value criteria are >0.3 to <0.7, and for the old stage, the HI value criteria are <0.3, as highlighted by

Mahmood and Gloaguen (2011). However, it is crucial to recognize that the sensitivity of the HI is also contingent on factors such as lithology and climate (Lifton and Chase, 1992; Masek et al., 1994; Pérez-Peña et al., 2009).

500   A shaded relief map of Kansas and Oklahoma was generated using the Sobel (3×3) filter, an image processing filter for edge detection, in the ArcGIS Pro. Previous investigations have underscored the scale-dependent nature of global autocorrelation analyses pertaining to HI values. Although marginal disparities exist with coarser DEMs. Walcott and Summerfield (2008), Pérez-Peña et al. (2009), and Mahmood and Gloaguen (2011) have established that finer resolutions, such as the 10-meter resolution, yield enhanced robustness with a satisfactory high positive Z score in autocorrelation assessments using Moran's I.

505   Moran's I is a spatial autocorrelation measure that informs about data pattern, whether the data are perfectly dispersed or perfectly random.

The study area is discretized based on the USGS's Hydrologic Unit Codes (HUC-8), and the resultant sub-basin areas are further discretized into a 1 km × 1 km grid. The sub-basin boundaries are used to clip the produced grids, avoiding grid cells that contain

510   no value.

For each grid cell, zonal statistics were calculated to derive the mean, maximum, and minimum elevation values, which are then added to a table. The HI is calculated and joined with the attribute tables of 1 km × 1 km grids across all the sub-basins within the geographic regions of Oklahoma and Kansas. The following empirical formula calculates HI-

515    $$HI = \frac{H_{mean} - H_{min}}{H_{max} - H_{min}} \tag{2}$$

Where H denotes the elevation. After being assigned to the grid cells, the HI value distribution appears random and statistically insignificant (Appendix E). To make a statistically significant interpretation, I used the optimized Hot Spot Analysis. Conducting an optimized Hot Spot analysis involves utilizing the Hot Spot Analysis (Getis-Ord Gi*) with parameters specifically derived from the characteristics of the input data. Getis-Ord Gi* is a LISA technique that can distinguish between clusters of high-value

520   (or hot spots) and clusters of low-value (or cold spots) over the study region (Oyana and Margai, 2015). The optimized hotspot analysis automatically identifies an appropriate scale of analysis and corrects for both multiple testing and spatial dependence. This tool analyzes the data to determine settings that produce optimal hotspot analysis results. Cluster maps are generated to facilitate the analysis and discussion of the results. The flow chart of the method is shown in Figure 12.
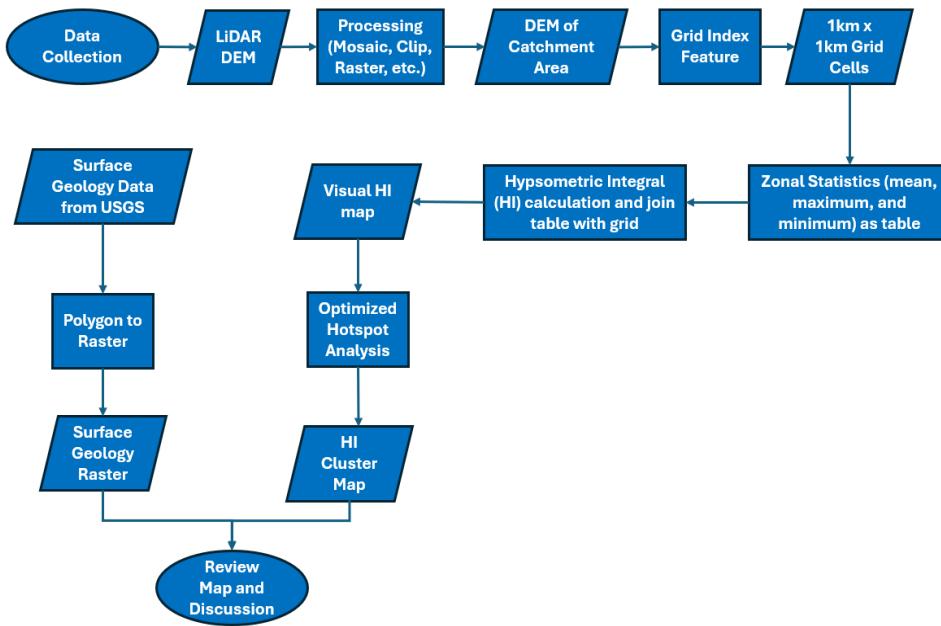
Figure 12: Chart of Hypsometric Integral and Pattern Analysis.

2.2.2   Stream Sinuosity Analysis (SI)

Although the stream sinuosity index (SI) is less commonly applied in neotectonics detection than analyses such as the mountain front sinuosity index, its application is valuable in identifying tectonic activities in comparatively flatland regions (Gomez and Marron, 1991; Petrovszki et al., 2012; Zámolyi et al., 2010). The SI is calculated by dividing the channel length by the valley length. Channels with a sinuosity index greater than 1.5 are considered meandering (Wilzbach and Cummins, 2019). Stream sinuosity is influenced by discharge downstream from confluences, changes in sediment load, and gradient changes due to variations in the geologic substrate (Lazarus and Constantine, 2013; Turowski, 2018), as well as by neotectonic activity (Petrovszki et al., 2012; Timár, 2003). I interpret changes in sinuosity not attributable to changes in stream substrate and discharge as possible evidence of neotectonism.

Several methods are generally used to calculate stream sinuosity index, such as Total Sinuosity, Brice, Inflection Sinuosity, Leopold and Wolman, and the Muller method (Horacio, 2014). For this analysis, the stream length is divided into small sections, and the Total Sinuosity method is employed.

The 4th-order stream network initially generated for Basin Asymmetry analysis was used to conduct a stream sinuosity analysis for the regions of Oklahoma and Kansas. Applying the Unsplit Line tool within ArcGIS Pro, stream flowlines were preserved in an unsplit state, and uneven lengths were removed throughout the stream network. This is necessary to place SI calculation points at evenly spaced intervals of 1 km. Systematically positioning points at 1 km intervals along the flowlines facilitated the subsequent division of the lines into 1 km segments at these designated points. Sinuosity values for these 1 km segments of the 4th-order streams were computed using a self-written Python script, which involved dividing the segment length by its respective

chord distance. The resultant sinuosity values were then linked to the initial points of the corresponding line segments. Empirical
Bayesian Kriging (EBK) was adopted as the chosen method to create an interpolation map reflecting continuous sinuosity values.

550   EBK is an interpolation method commonly used in geology for spatial prediction and mapping. Estimating the unknown values
is based on the known values from nearby locations. The technique addresses the uncertainty associated with estimating the
semivariogram during spatial analysis. Unlike kriging methods, EBK incorporates the concept of error estimation by performing
multiple simulations. This approach accounts for variability in the semivariogram by enhancing the reliability of predictions
across spatial domains. It employs a Bayesian framework to refine semivariogram estimation iteratively, leading to more

555   accurate and robust spatial predictions. However, EBK is very sensitive to outliers, so before using the SI value points, only data
that falls within two standard deviations is used. The SI values follow the normal distribution.

Following the generation of the sinuosity map, a comparative visual interpretation of the surface geology of Kansas and
Oklahoma was conducted to explore the potential association between lithology and sinuosity beyond factors related to

560   neotectonics. The flow chart of the method is shown in Figure 13Error! Reference source not found..
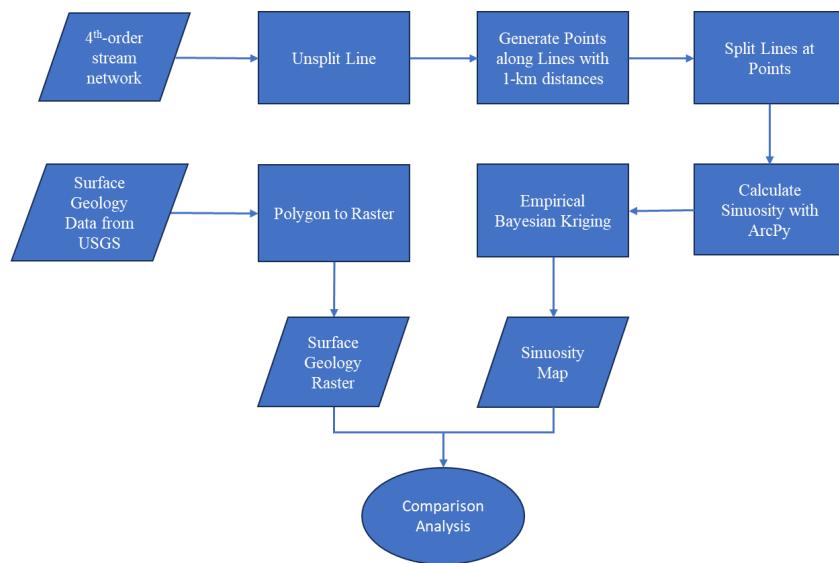

Figure 13: Flow Chart for Stream Sinuosity Analysis

We categorized all HI and SI values into three sample classes for statistical comparison: values from earthquake locations, points

565   above basement structures, and points outside the basement structures, to determine if there is a statistical correlation between
earthquakes and basement structures, and the area outside the basement structure in terms of HI or SI. Descriptive statistics for
HI and SI within each class are presented in Appendix F. Although the z-test is generally more appropriate given the sample size,
We performed both z-tests and t-tests to assess potential significant differences between pairs of classes. In all comparisons, the
hypothesized mean difference between the sample classes was found to be zero, suggesting that neither earthquakes nor

570   basement faults serve as a singular controlling factor influencing HI or SI values.

Additionally, no significant statistical correlation was found between HI and SI in any of the classes (Appendix G). Therefore, We employed spatial pattern analysis to identify clusters of high and low values and investigated the underlying causes when broader spatial patterns emerged. We also calculated the R-squared value to assess the general correlation between SI and HI.

575 First, We created scatter plots and applied the linear correlation formula to find the trend, then computed the R-squared value. The result was very low, indicating minimal correlation. This suggests that lithology alone is not the primary factor controlling the high or low concentrations of HI or SI (Appendix G).

3 Results and Discussion

3.1 Findings

580 This study uses drainage basin asymmetry and the HI and SI scalar values to identify potential long-term neotectonic activity within regions of increased seismicity in Kansas and Oklahoma. We also explored the possibility that observed asymmetry vectors and scalar values arise from alternative geomorphic processes such as microclimate, monoclinal shifting, and alluvial fans. A comprehensive map (Figure 14) with generalized summary tables for the asymmetry vector domains (Table 1 and Table 2) is presented, one for each state, due to the distinct nature of the datasets for Kansas and Oklahoma, to provide a

585 comprehensive overview. These tables provide information on how they are attributed to the basement faults. Another comprehensive map (Figure 15) containing bounded boxes of suspected neotectonic elements, along with a summary table (Table 3) with the findings and characteristics, is presented at the end of Section 3.1. Some suspected regional neotectonic elements extend from Kansas to Oklahoma.

590 In Kansas, the azimuthal mean vector direction are predominantly oriented toward the south-to-southwest or southwest-to-west, and south, southwest, and west in Oklahoma (see supplementary materials)). Only Oklahoma Domain E shows a northward component to its mean basin asymmetry (Figure 14 and Table 1). The southward component in the domains underscores the significant role of solar radiation in shaping hydrological dynamics in these regions. The analysis does not necessarily exclude the presence of fourth-order stream asymmetry vectors oriented northward in any of the domains. However, the frequency of

595 southward-oriented fourth-order stream asymmetry vectors is significantly higher than that of northward-oriented fourth-order stream asymmetry vectors in all domains except Domain E.

Monoclinal shifting of streams down-dip on resistant strata or neotectonism can account for a westward component of basin asymmetry in azimuthal Domains B and E in Kansas and Domains B and C in Oklahoma. The southerly component of the

600 asymmetry of these two domains can be ascribed to microclimate, as discussed above.

In Oklahoma, the azimuthal domains A, B, and C indicate that south-directed asymmetry is influenced by varying degrees of erosion and sediment delivery from south-facing slopes (Figure 14 and Table 2). The azimuthal Domain D, with a trellised stream pattern, indicates structural control. Domain E exhibits an azimuthal direction from northwest (red vectors), indicating

605 that the domain is a suspected area for neotectonic activity. The north and west components of azimuthal Domain E suggest neotectonic activity in that azimuthal domain.
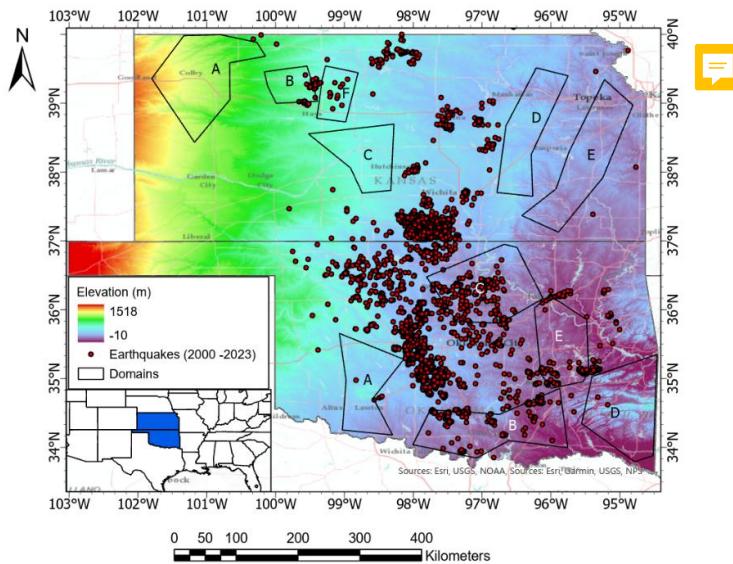
Figure 14: Asymmetry Vector Domains in Kansas and Oklahoma. The domains containing letters have possible causes of asymmetry summarized in Table 1 and Table 2.

Table 1: Characteristics of Drainage Basin Asymmetry Domains in Kansas

Azimuth Domain	Mean Vector Bearing	Bedrock Dip Bearing	Humidity	Remnant Depositional Slope	Seismicity	Mapped Fault Zones	Comments	Cause of Basin Asymmetry
A	SSW	Near horizontal	Semi-arid	Eastward High Plains	None	CKU	Strong southward asymmetry	Microclimate
B	WSW	Near horizontal	Semi-arid	N/A	Present	CKU	West asymmetry component is dominant	Microclimate and/or Neotectonism
C	SSE	Near horizontal	Semi-arid	N/A	None	CKU	Strong southward asymmetry	Microclimate
D	SSW	WNW	Sub-humid	N/A	None	HFZ, BAC	Strong southward asymmetry	Microclimate
E	WSW	WNW	Sub-humid	N/A	None	BAC	Dominant West Asymmetry and W bedrock dip	Microclimate and/or Monoclinal shifting
F	SW	Near horizontal	Semi-arid	N/A	Present	CKU	Strong southward asymmetry	Microclimate

22

Table 2: Characteristics of Drainage Basin Asymmetry Domains in Oklahoma

Azimuth Domain	Mean Vector Bearing	Bedrock Dip Bearing	Humidity	Remnant Depositional Slope	Seismicity	Mapped Fault Zones	Comments	Cause of Basin Asymmetry
A	SW	Variable Moderate to steep	Semi-arid	N/A	Present	WWF, NU	Strong southward asymmetry	Microclimate
B	WSW	Variable Moderate to steep	Semi-arid/ Sub-humid	N/A	Present	WWF	West asymmetry component is dominant	Microclimate and/or Neotectonism
C	WSW	low W	Semi-arid	N/A	Present	Wilzetta FZ	Dominant West asymmetry and west bedrock dip	Microclimate and/or Monoclinal shifting
D	SW	NNW and SSE Moderate to steep	Sub-humid	N/A	Present	Ouachita faults	Strong southward asymmetry	Microclimate
E	NW	low WSW	Sub-humid	N/A	Present	Ozark faults	North component of asymmetry and South component of the bedrock dip	Neotectonism

615

In western Kansas (west of -99°), the hotspots are partly located on top of poorly consolidated silt, siltstones, and shale (see supplementary material for details). The elongated HI hotspots and sinuosity anomalies in the northwest part of Kansas (west of -99° and north of 38°) are likely linked to the lithology of ridge-top conglomerates on the High Plains rather than to neotectonics.

620 In contrast, the coldspots generally correspond to sandy wetlands and active depositional zones, where sediment accumulation is ongoing. The hotspots may be associated with loess and terrace deposits, but in some cases, unexplained anomalies could reflect local or regional uplift or variations in lithology. The SI map indicates that river channel sinuosity tends to increase as the slope decreases.

625 The HI cold spot and low sinuosity anomaly in Gray and Finney counties (between -100.5° and -101°, and 38° to 38.7° and 'A' on Figure 15 and Table 3) are not clearly explained by the local lithology. The area is bordered by linear scarps (seen on the shaded relief map and marked by hotspots in the HI map), suggesting it may be a sinking neotectonic block. The hotspot near the Pratt anticline is situated on top of the sandy wetlands, which are anomalous to the other hotspots present over the terrace deposits.

630

In eastern Kansas, hotspots are present on shale and limestone. Limestone is less erodible than shale, suggesting that the hotspot here does not depend on the rock's resistance. Based on the distribution of high-level alluvial deposits in their study area in Osage Cuestas (from 37.5° to 39° and from -94.9° to -97.8°), the directional changes of east–west-flowing Neogene streams to the south- and southeast-flowing streams resulted from long-term crustal tilting downward to the south and east (Aber, 1997).

635 The HI hotspots and sinuosity anomalies in this area within the Bourbon Arch and the Nemaha Tectonic zone support localized areas of neotectonism. The hotspots in the area have surficial geology consisting of shale and limestone. A group of HI hotspots with moderate seismic activity in the region (between 39° and 40° and between -97.7° and -98.6°, 'B' on Figure 15) has surficial

lithology that is unable to explain their presence. Their association with high sinuosity anomalies suggests they may be the result of localized neotectonic activity. Area 'B' overlies the BAC and a segment of MRS-NTZ. Additionally, the HI hotspots and

640　sinuosity anomalies along this trend, which extend farther toward the NW, may be an extension of the corridor of neotectonism. The corridors here define the collection of hotspots that are spread in a step-like manner on a regional scale. The 4th-order drainage basins have northwestward asymmetry in this area, suggesting tectonic activity. A hotspot in Central Kansas (located approximately at 38.4 ° and -98.4 ° and 'C' on Figure 15) also exhibits a very high sinuosity anomaly, suggesting it could be a neotectonic feature related to the Central Kansas Uplift (CKU).

645

There are HI hotspots in the Wellington-McPherson Lowlands in western Kansas. At the south bank of the Arkansas Lowlands and shared with the High Plains, the hotspot (approximately 37.8°, -98°, and 'D' on Figure 15) has a surficial geology primarily consisting of alluvium sands and wetland sediments. The HI characteristics are anomalous because such lithology manifests coldspots. Although the sinuosity is in the lower range, this hotspot may reflect a local uplift.

650

Amemoutou et al. (2021) analyzed 589 earthquakes in southern Kansas and found that 72% of the events had double-couple (DC) constrained source mechanism (which are characteristic of tectonic earthquakes), and 28% of the events had non-DC source mechanisms with isotropic volumetric components. They concluded that the increased earthquakes were generated from optimally oriented fault planes aligned with the regional stress field, which was sensitive to small perturbations. The HI hotspot

655　in their study area, along with increased sinuosity value (from 37° to 37.5° and from -97.5° to -98.1°, and 'E' on Figure 15), could be a sign of the underlying crustal deformation due to neotectonics.

In western Oklahoma (west of 98°), the HI hotspots in the Anadarko Basin and farther west on the Anadarko Shelf may be related to ridge-top conglomerates located near deeply incised streams, as evident from the lithologic patterns. The hotspots in

660　the Ozark Plateau, Ouachita Mountains, and Arbuckle Mountains correspond to areas of resistant bedrock, including sandstone and limestone. The high sinuosity anomalies in this region are likely related to the presence of incised meanders in this resistant bedrock as well.

A possible neotectonic element in Oklahoma is a north-south HI hotspot corridor located between 35° and 37°N and -97.5° to -

665　98° ('E' on Figure 15). The high earthquake numbers mark this corridor. The northern section of the north-south corridor lies above Nemaha Ridge basement faulting. The HI hotspots corresponding to this corridor appear to coincide with high sinuosity anomalies, consistent with the corridor being a neotectonic feature characterized by a high sinuosity trend that extends into Kansas along the HFZ.

670　A large, high-sinuosity anomaly spanning both the Cherokee Shelf and Arkoma Basin (approximately from 35° to 36°, and from -95.5° to -96.5°, and 'F' on Figure 15) is observed within the Azimuthal vector domain E. Earthquakes near these anomalies reinforce the idea of neotectonism in the area.
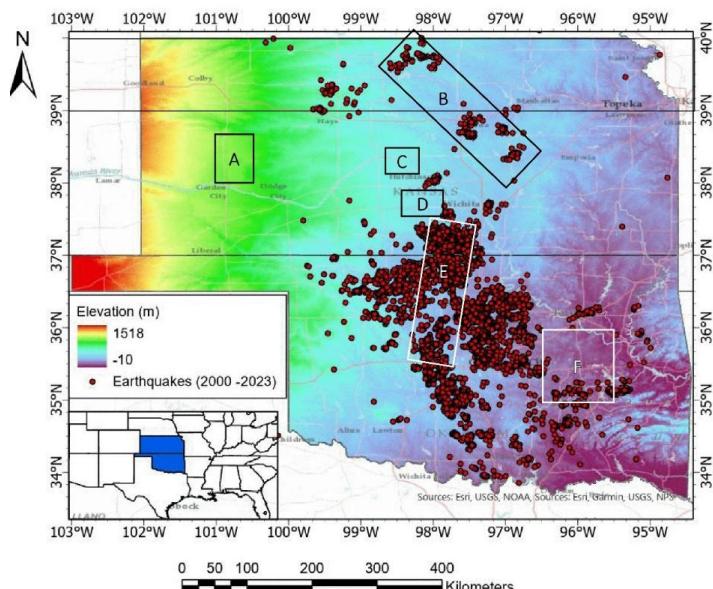
Figure 15: Possible neotectonic elements in Kansas and Oklahoma. The boxes containing letters indicate the possible area of neotectonics discussed in the text.

Table 3: Summary of possible neotectonic elements and characteristics

Box	HI Hotspot or Coldspot	SI Value	Basement Structures	Lithology	Topography	Scale	Possible Neotectonic element	Seismicity
A	Coldspot	No	Unknown	Silt	Subsidence surrounded by scarps	Local	Sinking block	Absent
B	Multiple hotspots	High	MRS-NTZ and BAC	Shale, Silt, Limestone	Basin and Ridges	Regional	Slow crustal deformation	Present
C	Hotspot	High	CKU	Terrace deposits	Ridge	Local	Local uplift	Absent
D	Hotspot	Low	Pratt Anticline	Alluvial deposits	Ridge	Local	Local uplift	Absent
E	Multiple hotspots	High	NU and HFZ	Sand and Shale	Basin and Ridge	Regional	Fault movement	Present
F	Several smaller hotspots	High	Arkoma Basin faults	Ridge top Sandstone	Basin	Local	Fault movement	Present

680

25

3.2 Contributions

Basin asymmetry vectors are beneficial in providing the direction of stream shifting, possibly indicating ongoing neotectonic deformation. The analysis of basin asymmetry of fourth-order streams in the study area reveals the microclimatic influence on

685 trunk stream basins producing south-directed asymmetry vectors. The azimuthal domains that exhibit combined west and south asymmetry components in the drainage basins reflect the combined influence of structural and microclimatic controls, as well as neotectonism. However, areas that have a vector component other than the structural dip direction without a southerly component, generally attributed to microclimatic conditions, may be attributed to neotectonic activity. The characteristics of HI hotspots and river channel sinuosity anomalies across Kansas and Oklahoma suggest lithological controls, active sedimentation,

690 and neotectonic activity influence their occurrence and patterns. Geomorphic indices, such as HI and SI, which provide scalar values rather than vector data, are also effective in delivering a comparatively smaller area of investigation for a neotectonic element. This study found that the spatial distribution of HI hotspots and stream sinuosity anomalies indicates that their occurrence depends on a complex interplay of lithological controls, active sedimentation, and neotectonic activity. In many regions, such as the High Plains and the Anadarko Basin, elongated hotspots and sinuosity anomalies are likely controlled by

695 lithologic features, including ridge-top conglomerates and resistant bedrock. However, several HI hotspots and sinuosity anomalies, particularly those occurring over alluvium, wetlands, or areas lacking clear lithologic explanations, suggest possible neotectonic activity. The presence of HI hotspots and high-sinuosity anomalies within the Bourbon Arch supports ongoing crustal deformation. Central Kansas and parts of southern Kansas show anomalous features potentially linked to structures such as the Central Kansas Uplift and areas sensitive to stress perturbation. The alignment of hotspots with known tectonic elements, such as

700 the Nemaha Ridge and HFZ, reinforces the possibility of neotectonic control. The high-sinuosity corridor coincides with zones of elevated seismicity, supporting the idea of natural fault movements in these structurally sensitive areas. Overall, while lithologic and geomorphic influences can explain some anomalies, the presence of unexplained HI hotspots and high-sinuosity zones, particularly in seismically active and tectonically complex regions, suggests the likelihood of ongoing neotectonic deformation.

3.3 Limitations

705 A key limitation of the basin asymmetry analysis is that the presence of a neotectonic signal may be obscured by the dominant southern asymmetry component, which is commonly attributed to microclimatic factors. In that case, the HI and SI analyses have become an effective tool to avoid falsely excluding any area for neotectonic investigation. However, the limitation of SI is that it may miss the signal of a very new and subtle neotectonic element by showing a possible neotectonic area with a low SI value. Therefore, it is always recommended to use the HI hotspot analysis map in combination with the SI analysis. As this is a

710 reconnaissance study in a regional area, some local potential areas may escape observation. A more local reconnaissance study with lower-order streams is recommended for these areas.

4 Conclusion

This research presents a reconnaissance of potential neotectonic elements in Kansas and Oklahoma by applying a suite of geomorphic indices. The findings of this study offer insights into the dynamics of neotectonic processes within the study area.

715 The possible regional-scale vector domains and corridors of neotectonism delineate areas where fluid injection could perturb the stress field of pre-existing faults, potentially influencing fault reactivation and seismicity. Overall, this study provides a

foundation for more detailed investigations into neotectonic activity in the region and demonstrates the utility of geomorphic analysis as a preliminary tool for tectonic investigations in intraplate settings.

720   Both vector and scalar studies demonstrate that quantitative geomorphic analysis is a valuable tool for identifying areas of neotectonic activity within increased seismicity. In this study, the Hypsometric Integral (HI) and Stream Sinuosity Index (SI) scalar values proved more effective in delineating neotectonic zones compared to fourth-order basin asymmetry vectors. Nonetheless, the latter also showed utility in detecting potential neotectonic signals, particularly when integrated with structural dip. These findings can inform decision-making processes regarding selecting suitable areas for controlled high-volume fluid

725   injection activities.

730

735

740

Appendices

Appendix A
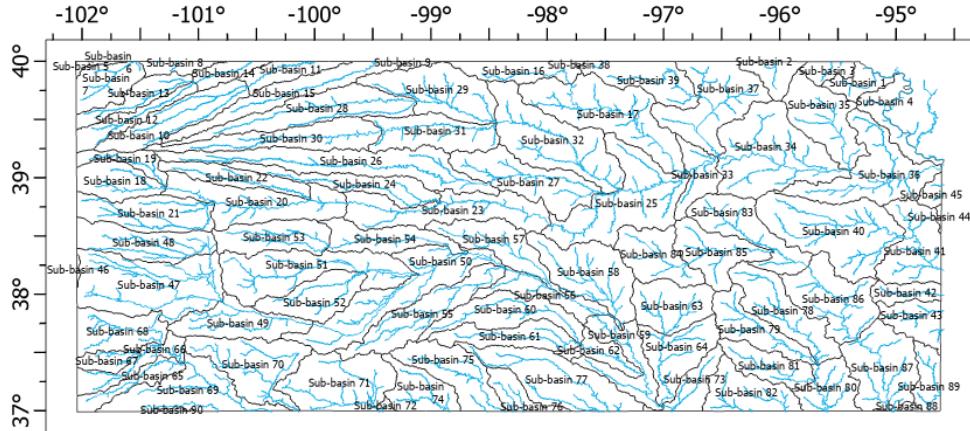


Fig. A1: Map of Sub-basins of Kansas

745
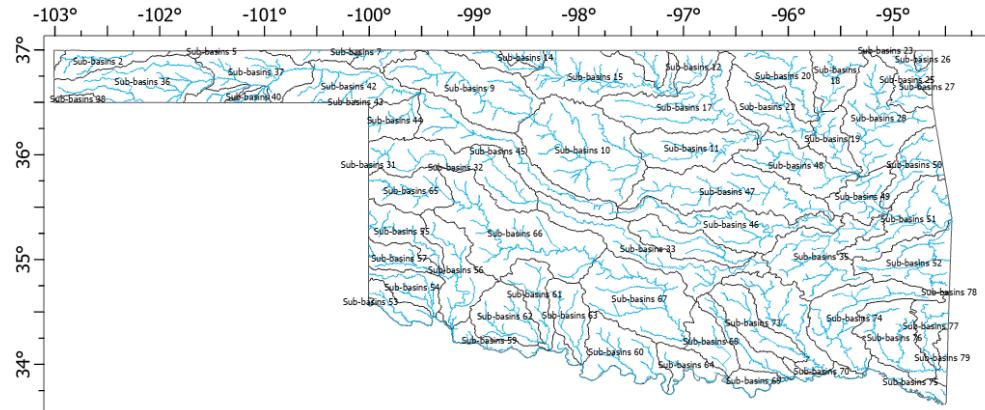
Fig. A2: Map of Sub-basins of Oklahoma

750

Appendix B
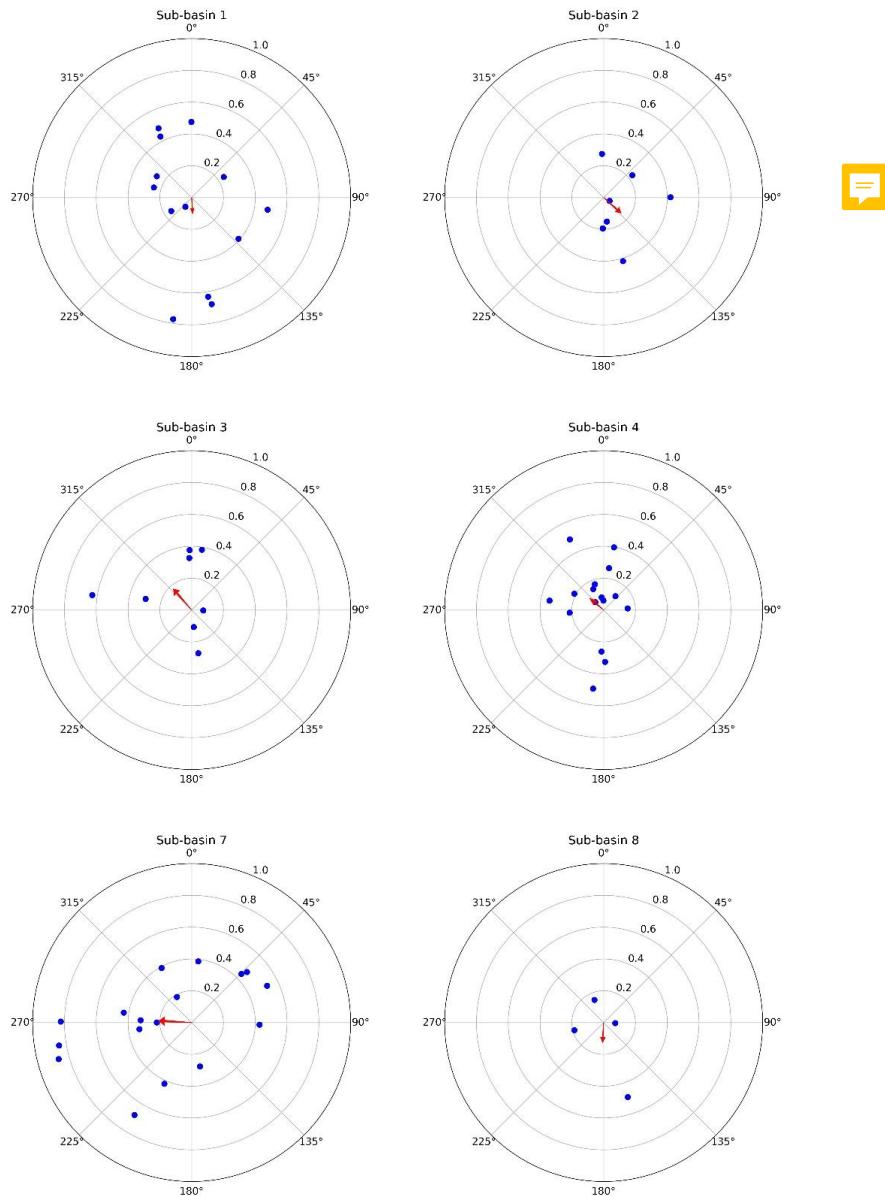
755

Fig. B1: Polar plots of asymmetry vectors of HU8 subbasins in Kansas (sub-basins 1-4, 7, 8)
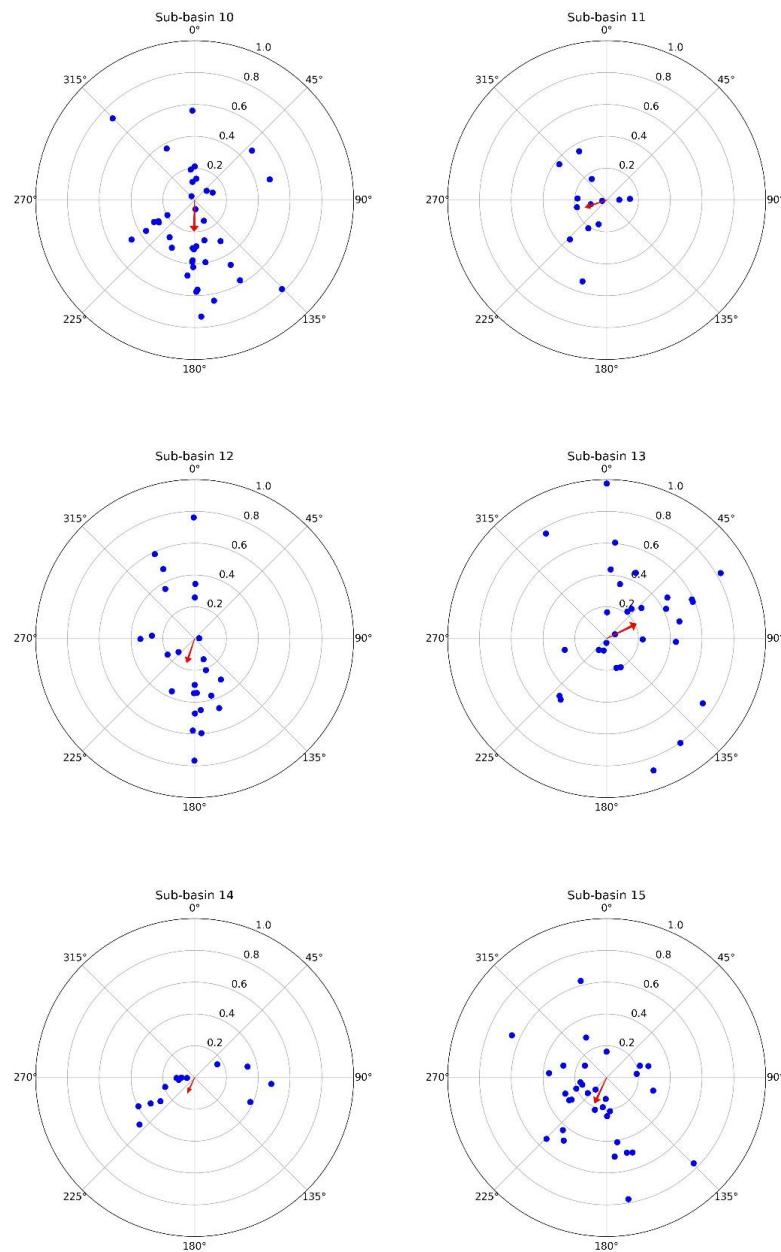
Fig. B2: Polar plots of asymmetry vectors of HU8 subbasins in Kansas (Sub-basins 10-15)
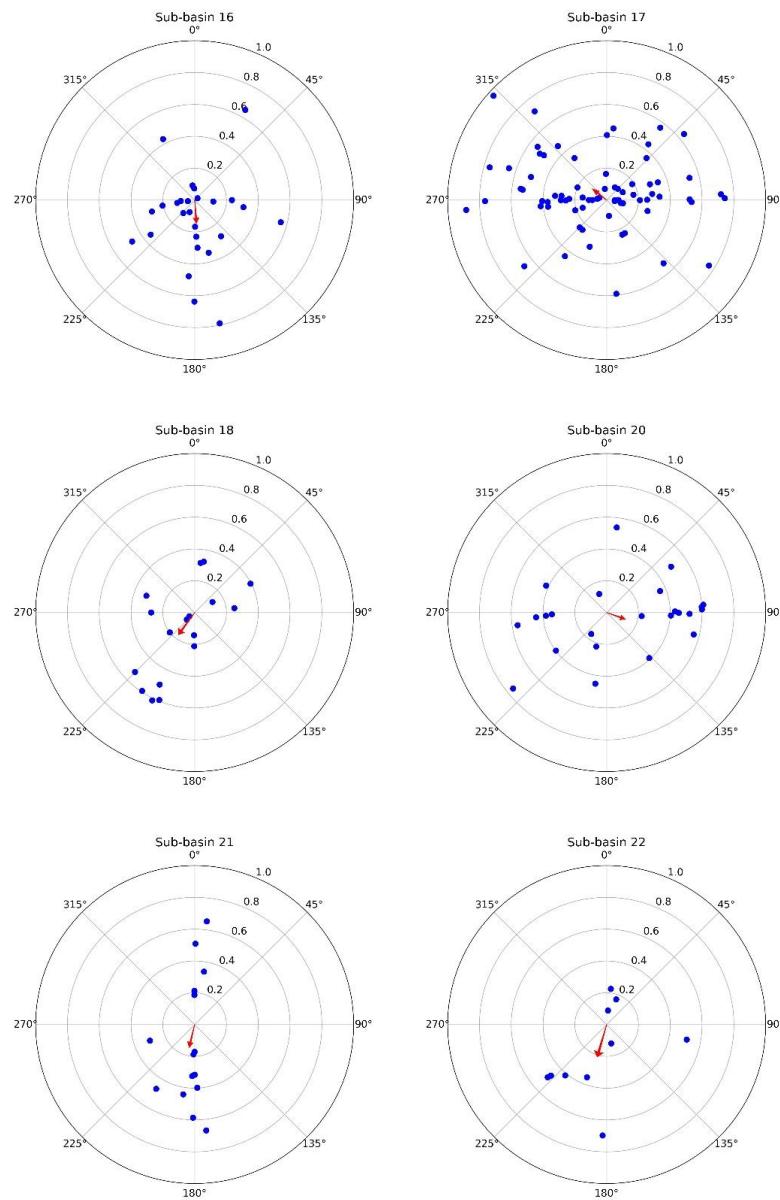
Fig. B3: Polar plots of asymmetry vectors of HU8 subbasins in Kansas (Sub-basins 16-18, 20-22)
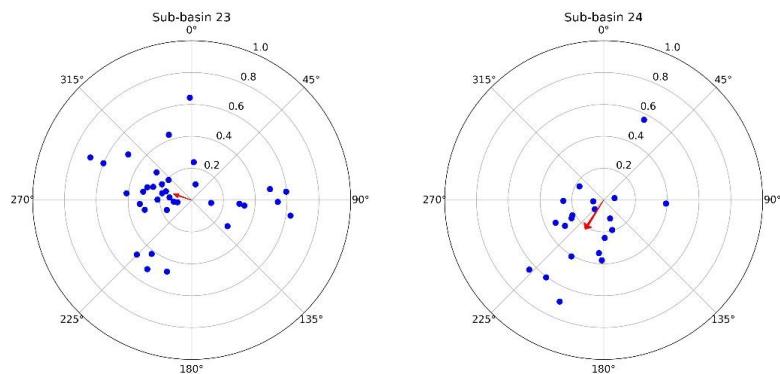
765
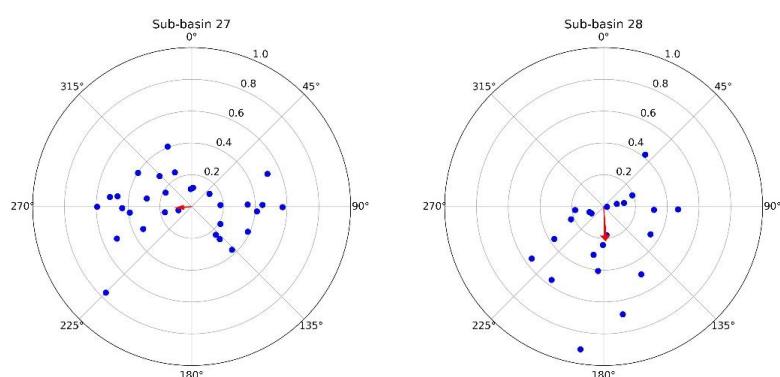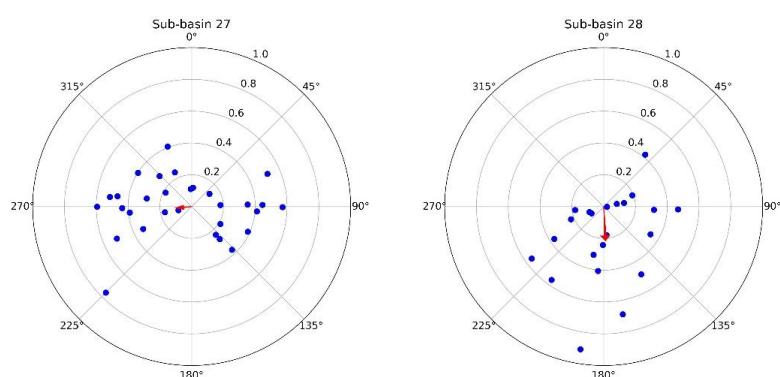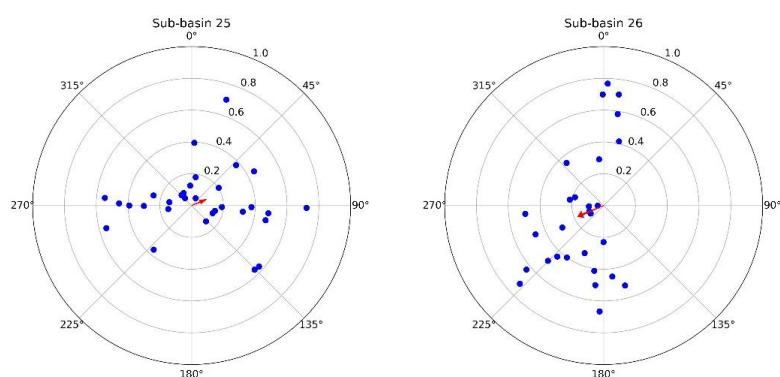
Fig. B4: Polar plots of asymmetry vectors of HU8 subbasins in Kansas (Sub-basins 23-28)
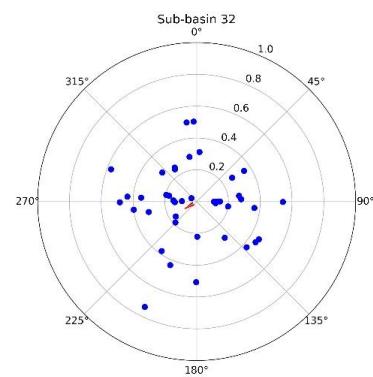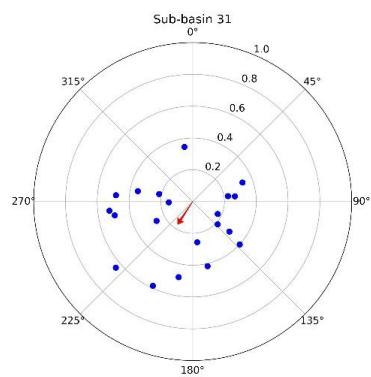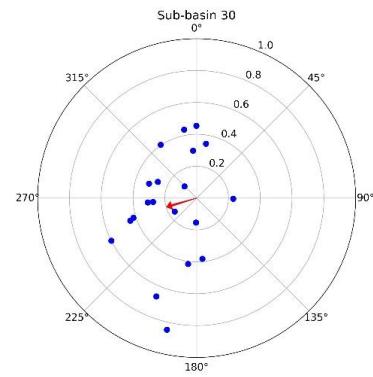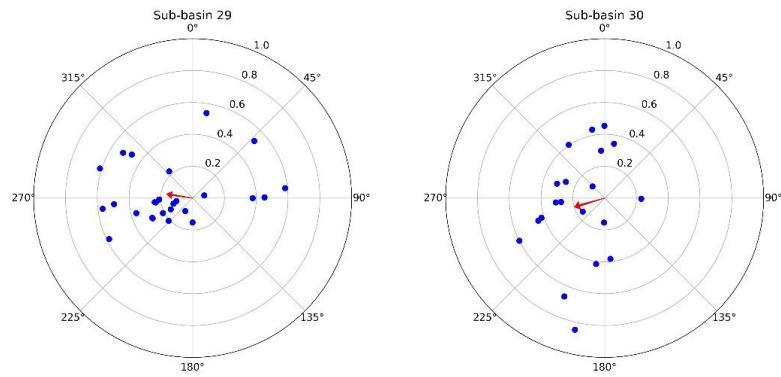
770
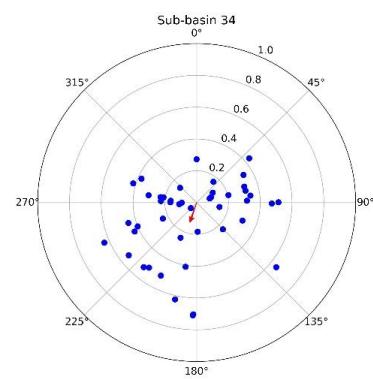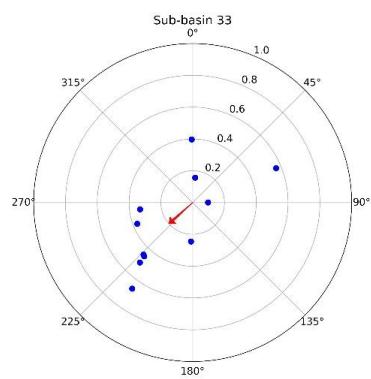
Fig. B5: Polar plots of asymmetry vectors of HU8 subbasins in Kansas (Sub-basins 29-34)
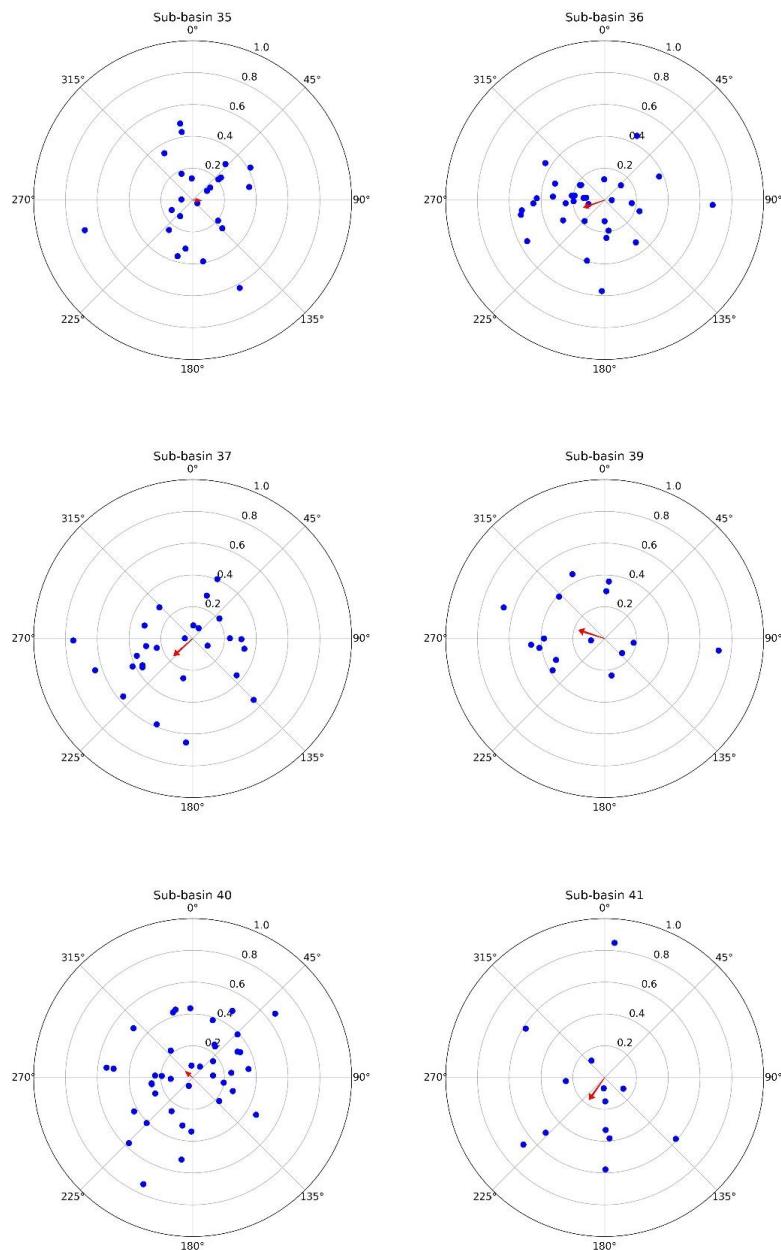
775

Fig. B6: Polar plots of asymmetry vectors of HU8 subbasins in Kansas (Sub-basins 35-37, 39-41)
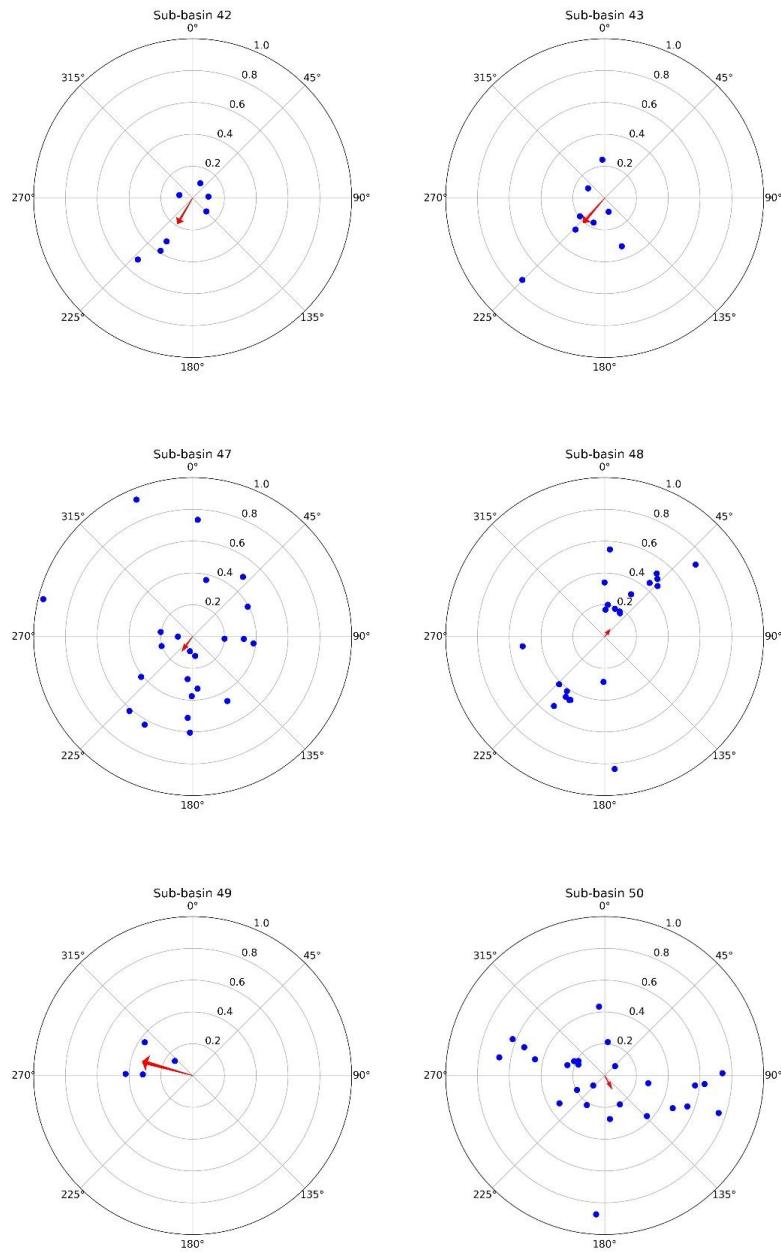
Fig. B7: Polar plots of asymmetry vectors of HU8 subbasins in Kansas (Sub-basins 42, 43, 47-50)
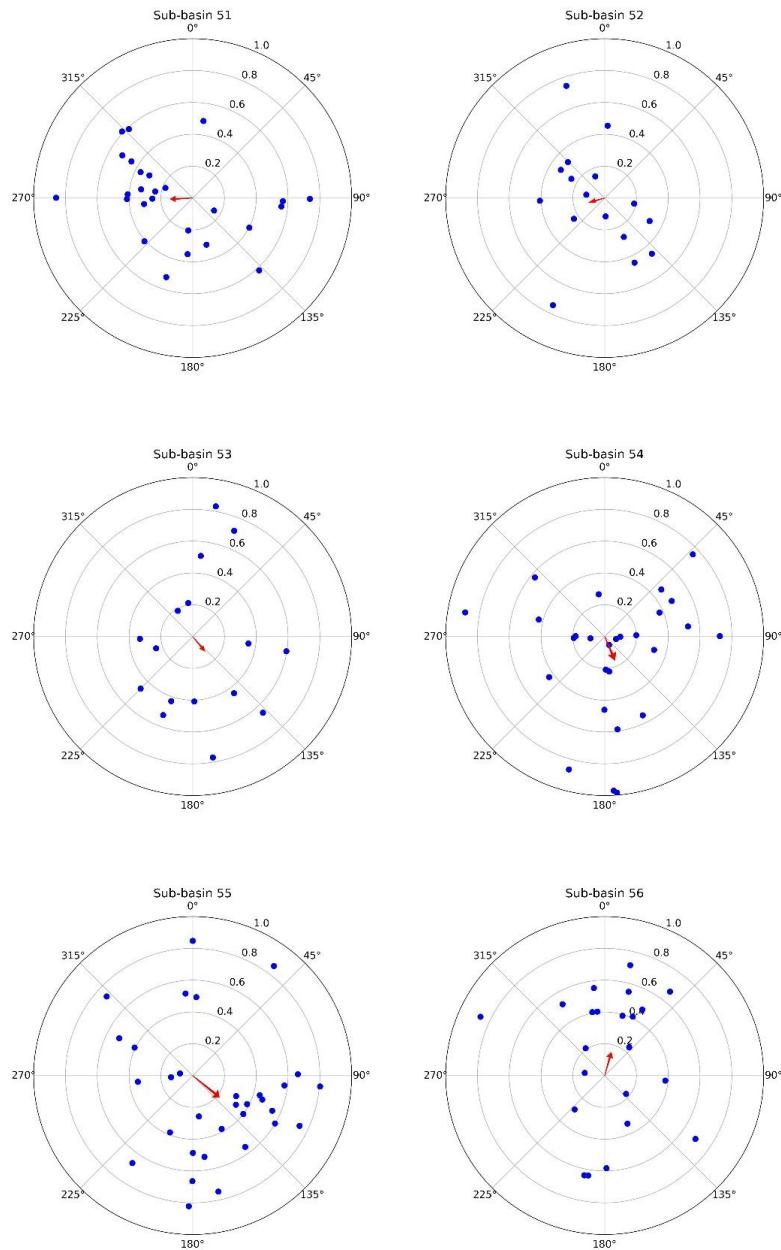
Fig. B8: Polar plots of asymmetry vectors of HU8 subbasins in Kansas (Sub-basins 51-56)
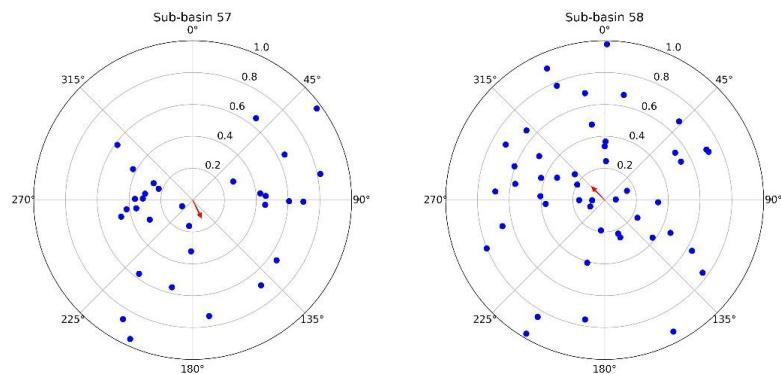
785
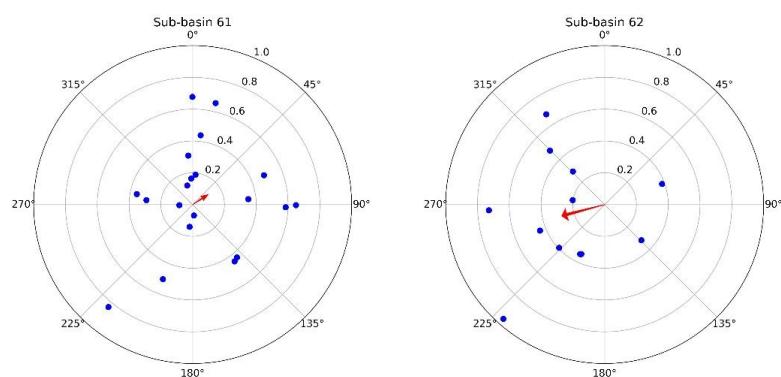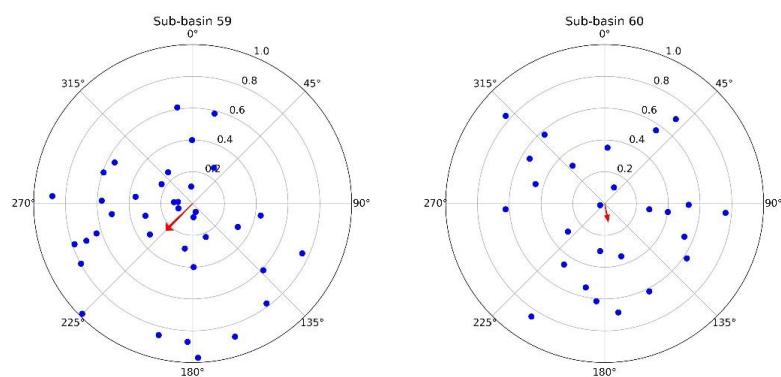
Fig. B9: Polar plots of asymmetry vectors of HU8 subbasins in Kansas (Sub-basins 57-62)

790
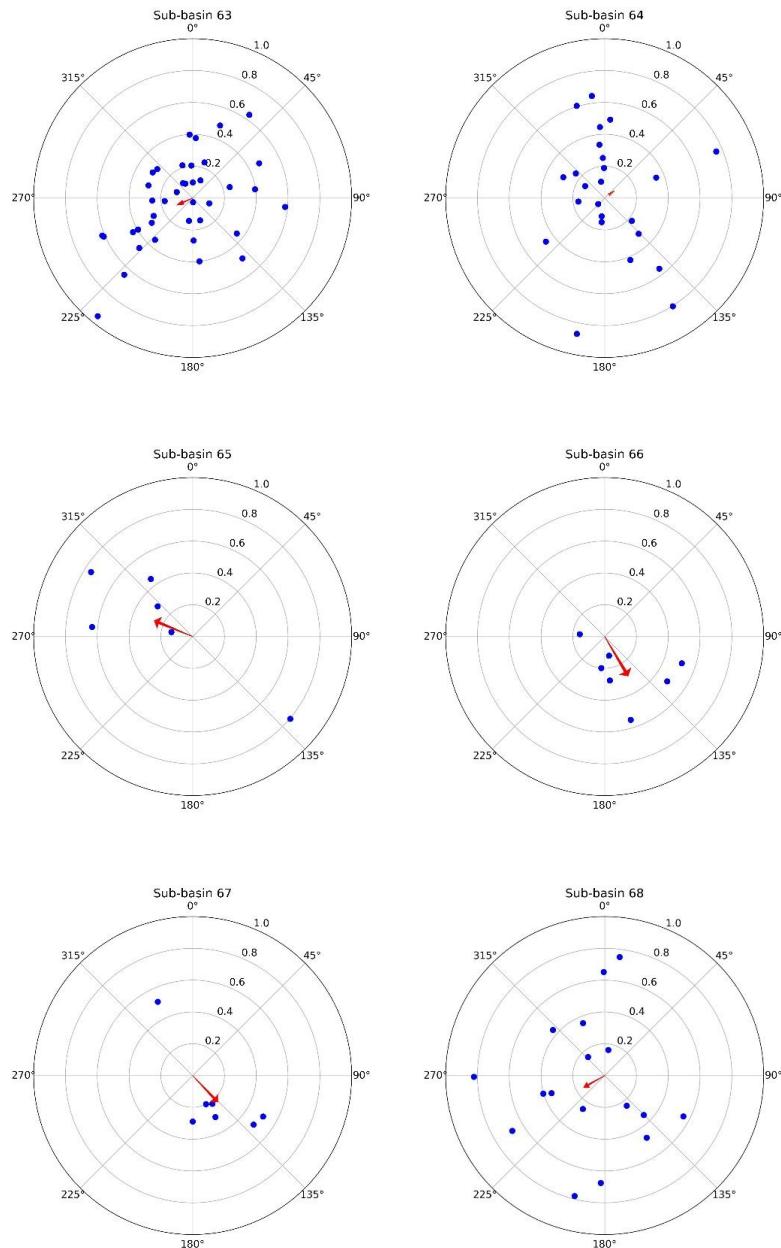
Fig. B10: Polar plots of asymmetry vectors of HU8 subbasins in Kansas (Sub-basins 63-68)
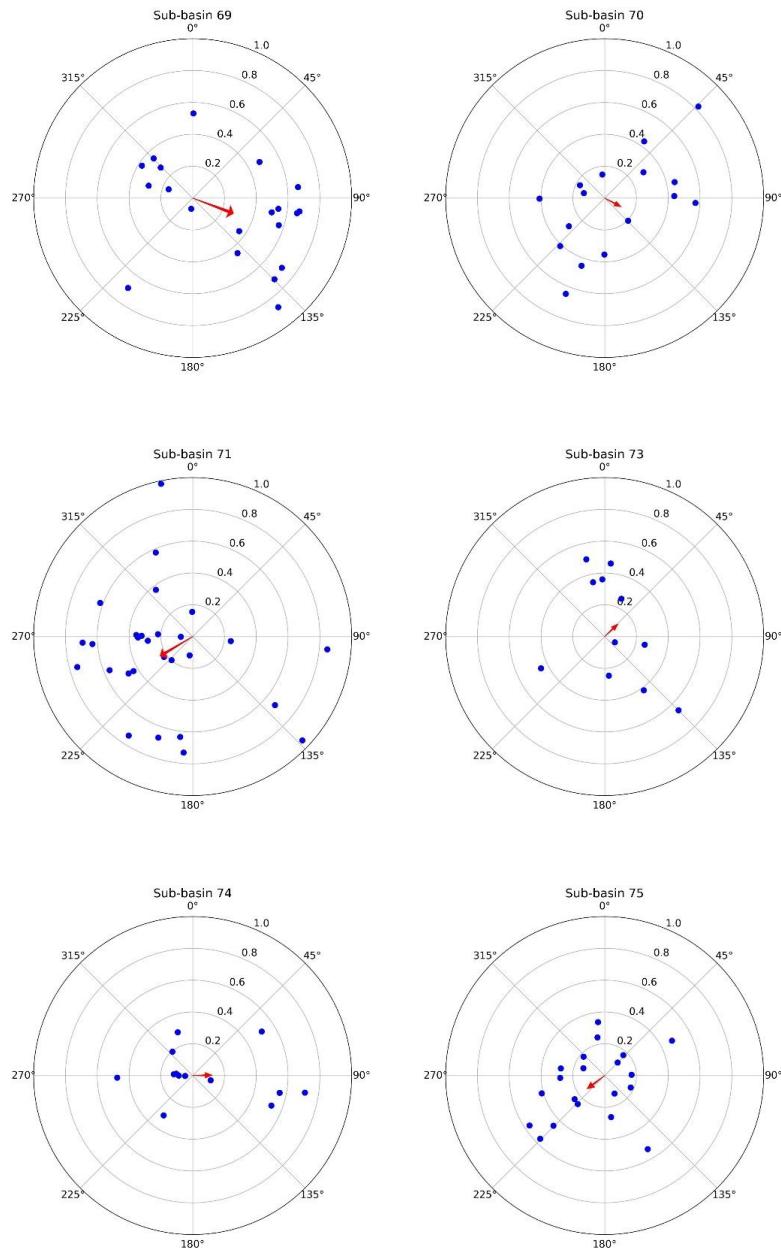
795

**Fig. B11: Polar plots of asymmetry vectors of HU8 subbasins in Kansas (Sub-basins 69-71, 73-75)**
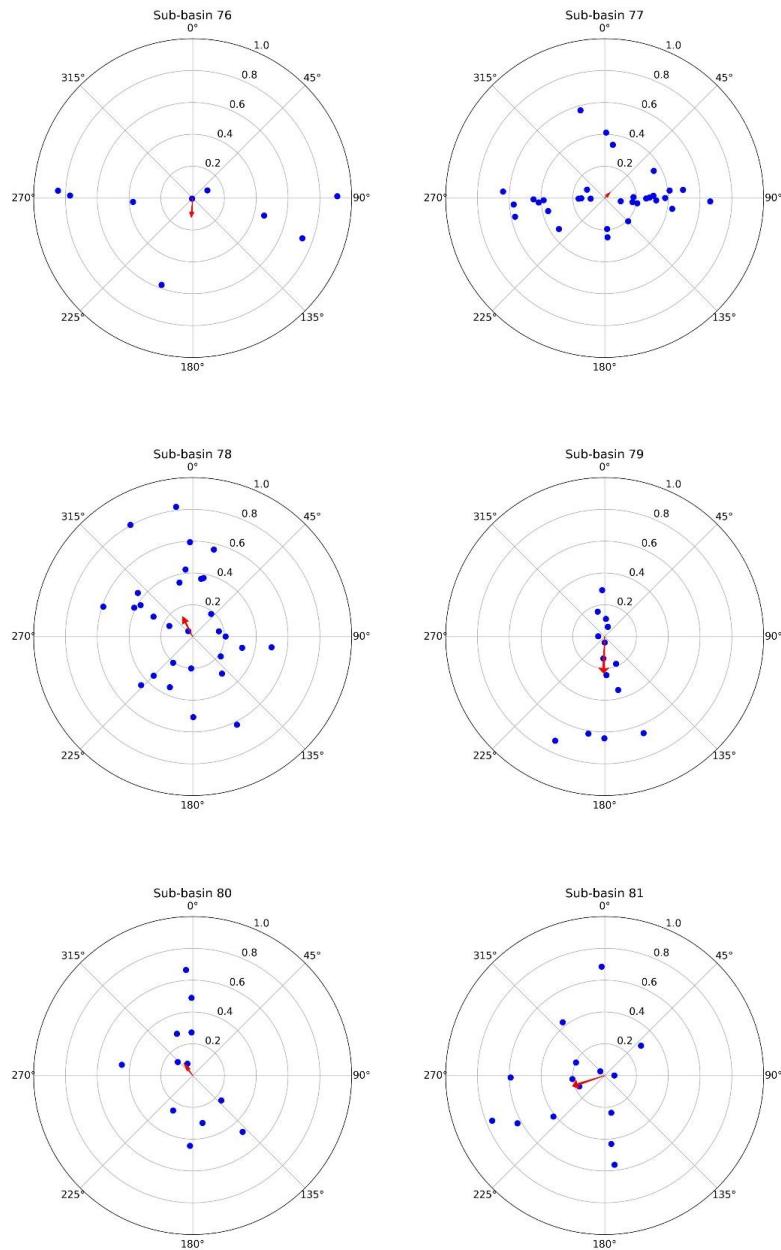
Fig. B12: Polar plots of asymmetry vectors of HU8 subbasins in Kansas (Sub-basins 76-81)
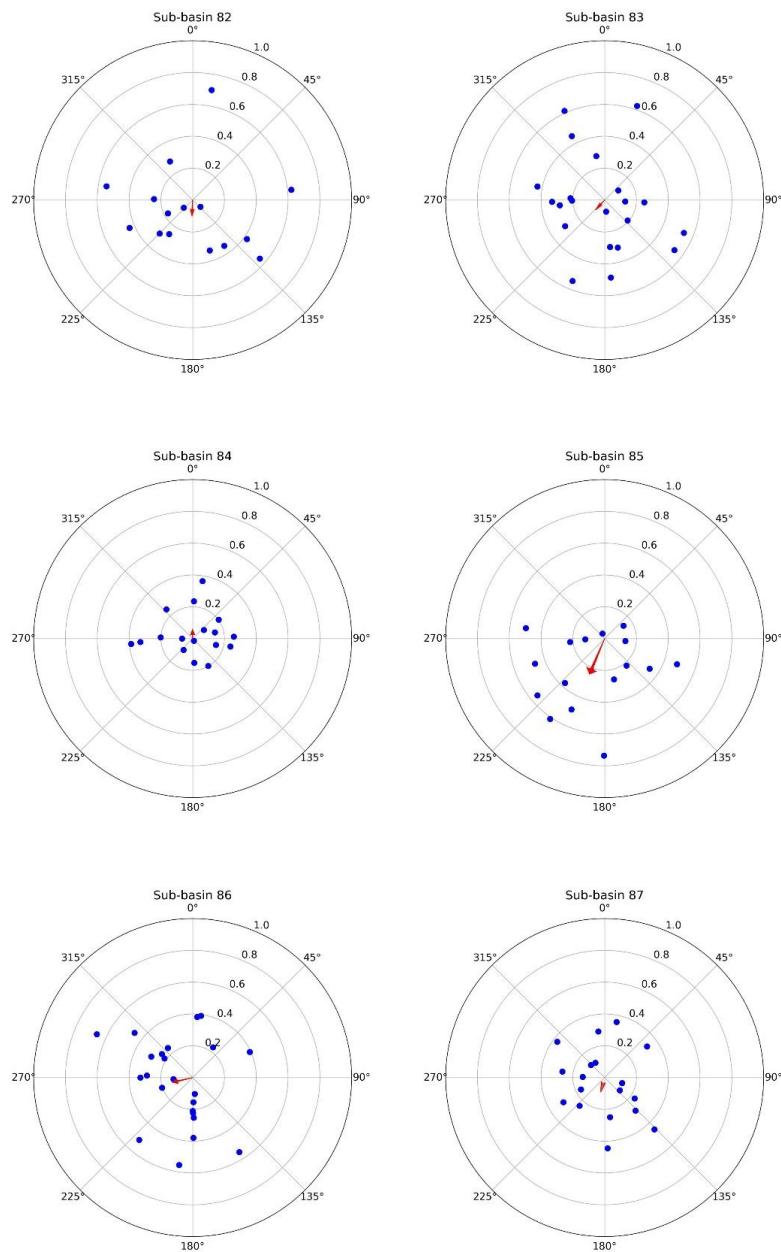
**Fig. B13: Polar plots of asymmetry vectors of HU8 subbasins in Kansas (Sub-basins 82-87)**

805   **Appendix C**
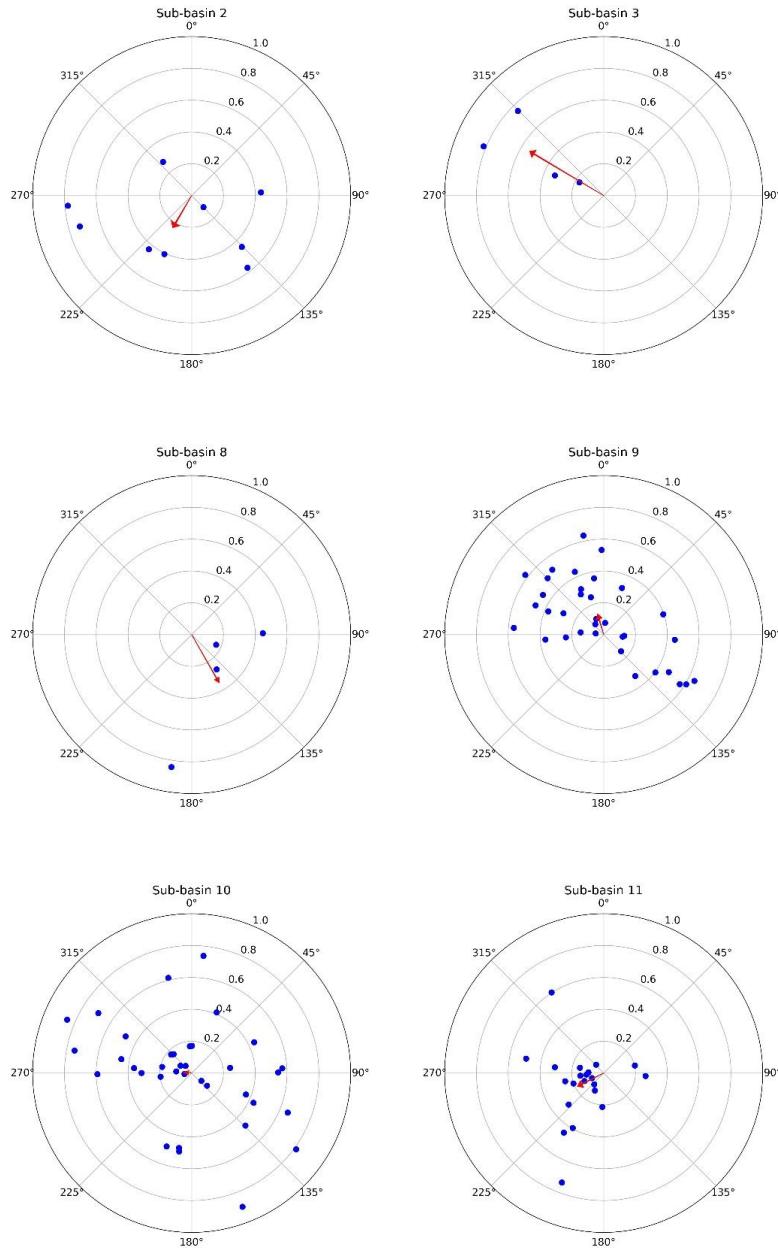
Fig. C1: Polar plots of asymmetry vectors of HU8 subbasins in Oklahoma (Sub-basins 2, 3, 8-11)
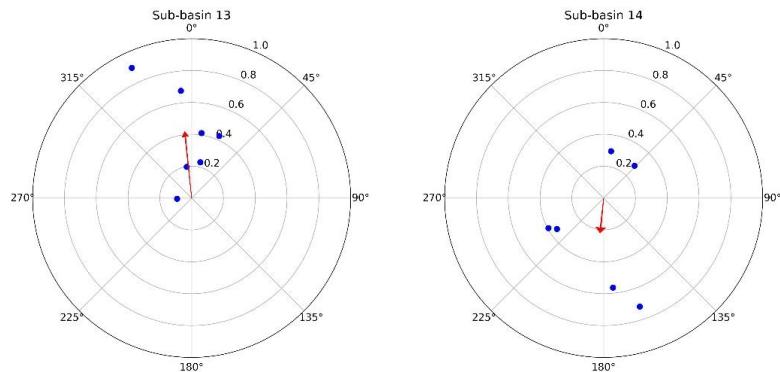
810
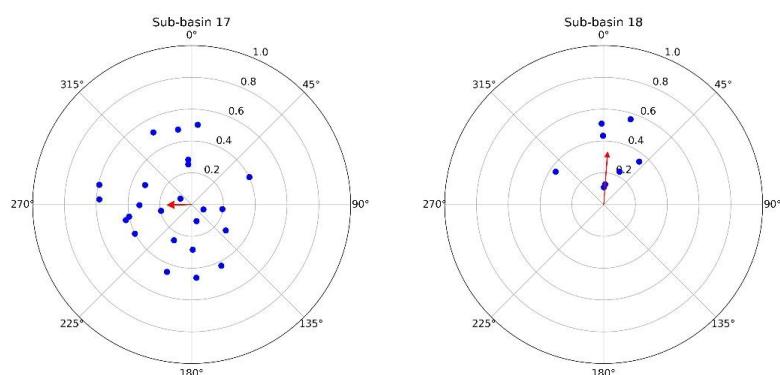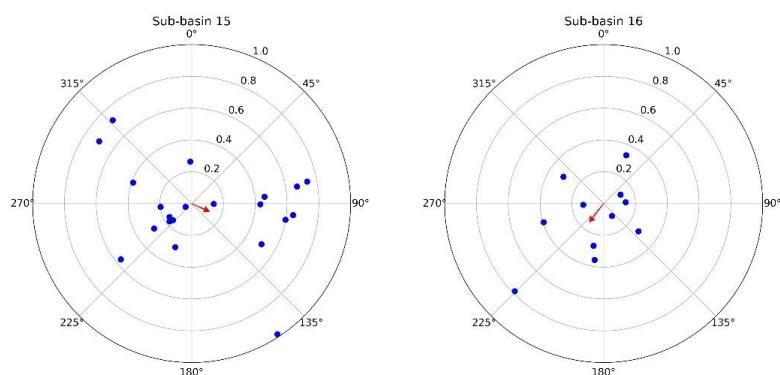
Fig. C2: Polar plots of asymmetry vectors of HU8 subbasins in Oklahoma (Sub-basins 13-18)
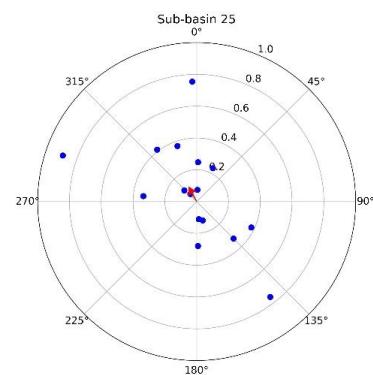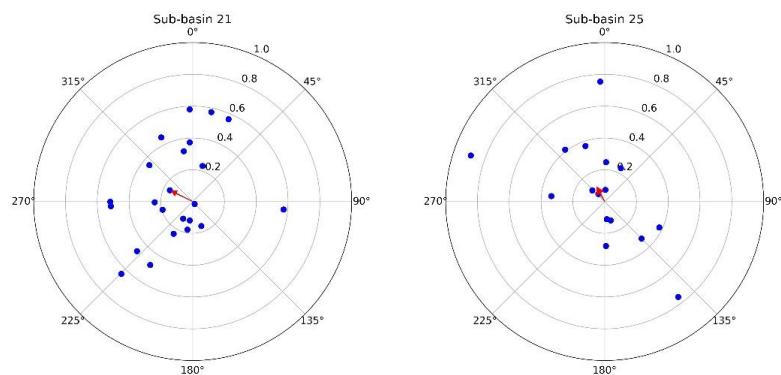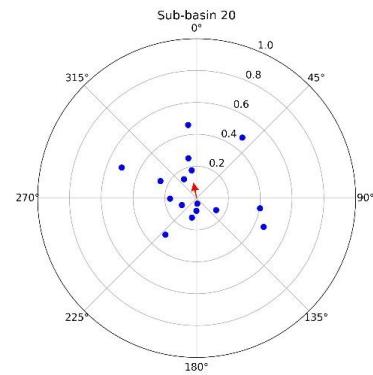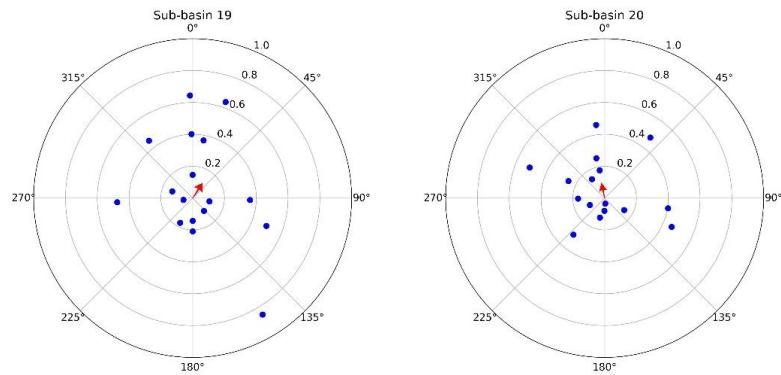
815
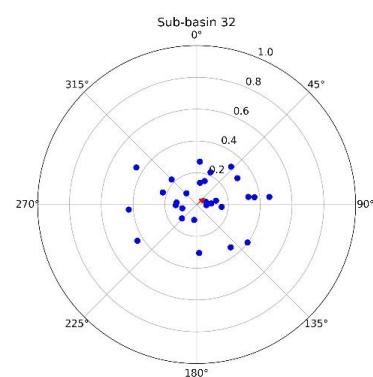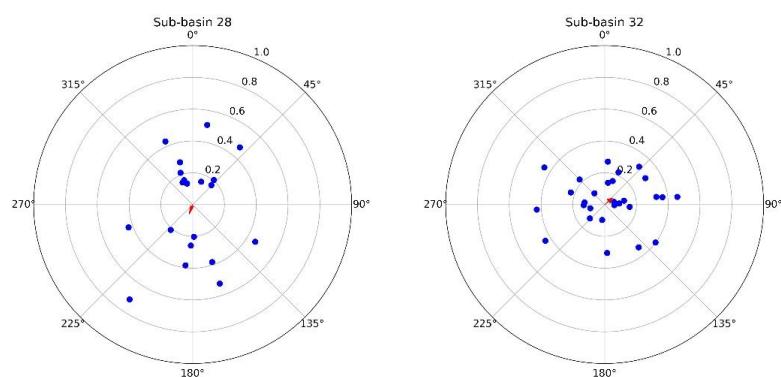
Fig. C3: Polar plots of asymmetry vectors of HU8 subbasins in Oklahoma (Sub-basins 19-21, 25, 28, 32)
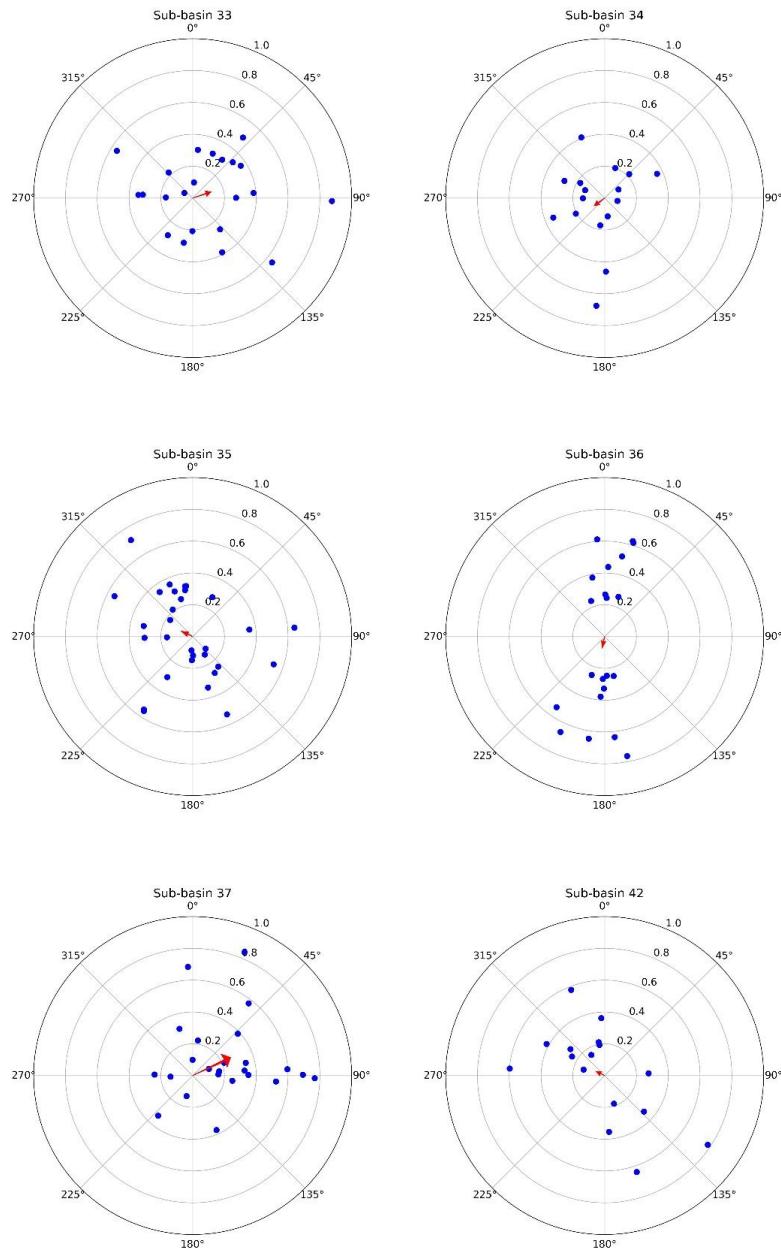
Fig. C4: Polar plots of asymmetry vectors of HU8 subbasins in Oklahoma (Sub-basins 33-37, 42)

820
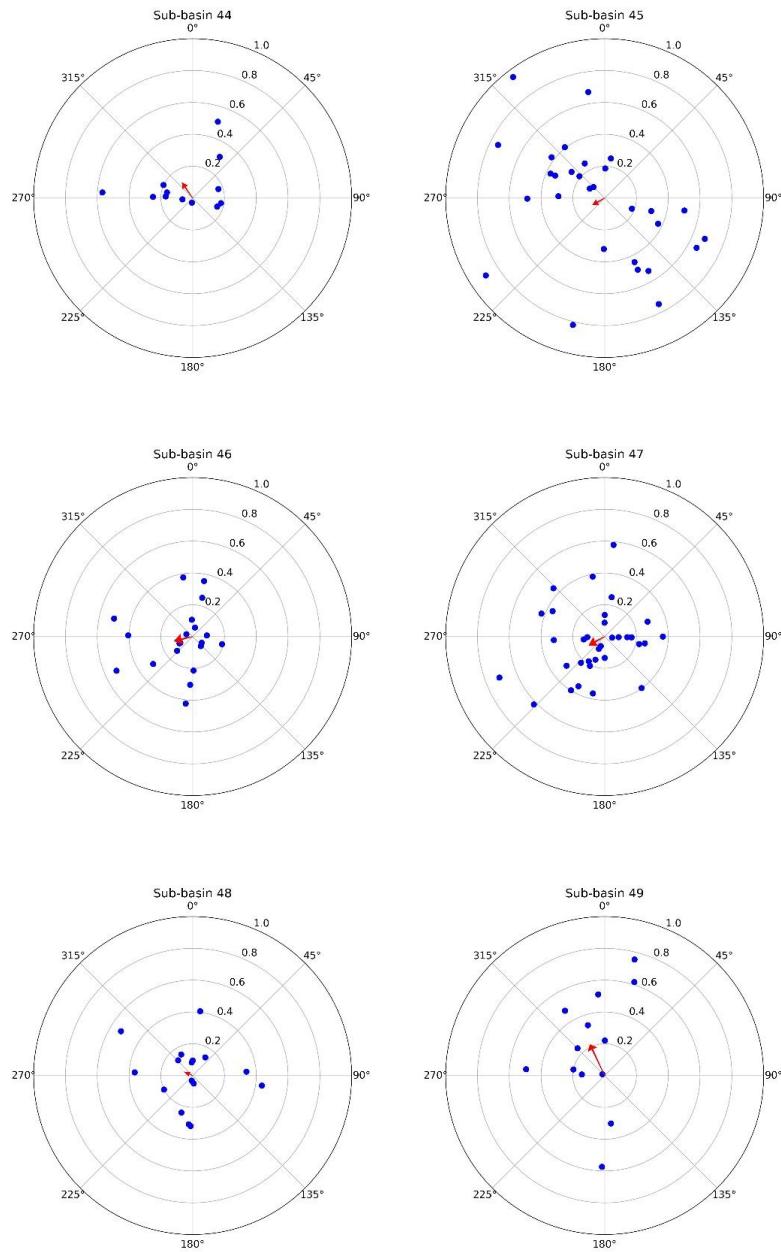
825   **Fig. C5: Polar plots of asymmetry vectors of HU8 subbasins in Oklahoma (Sub-basins 44-49)**
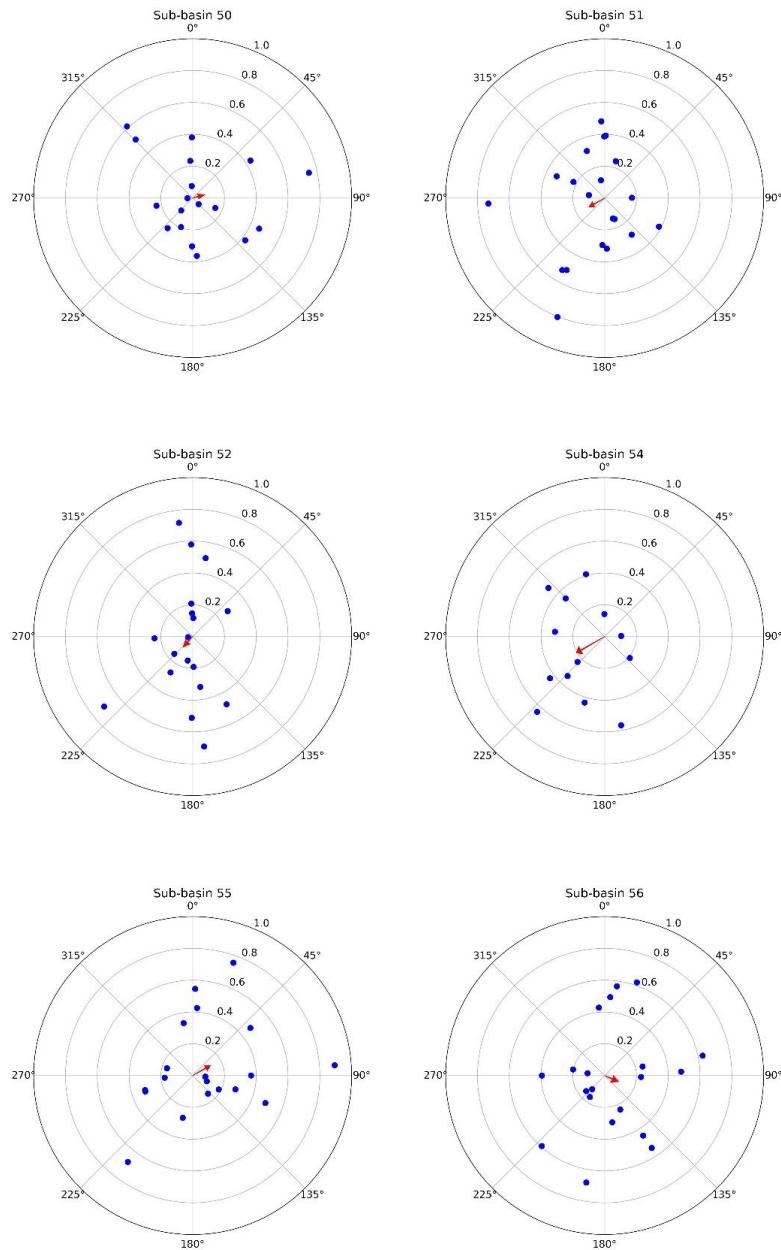
Fig. C6: Polar plots of asymmetry vectors of HU8 subbasins in Oklahoma (Sub-basins 50-52, 54-56)
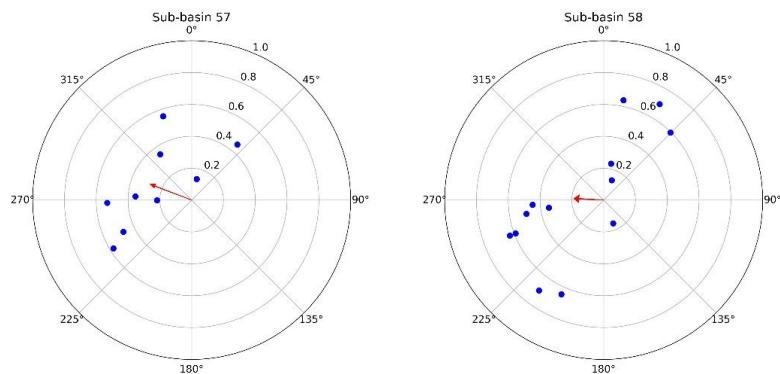
830
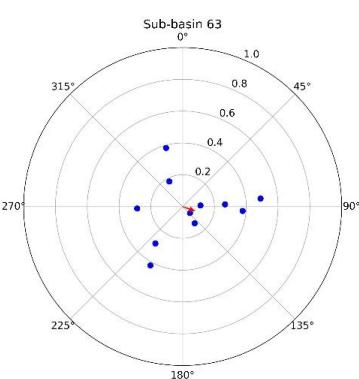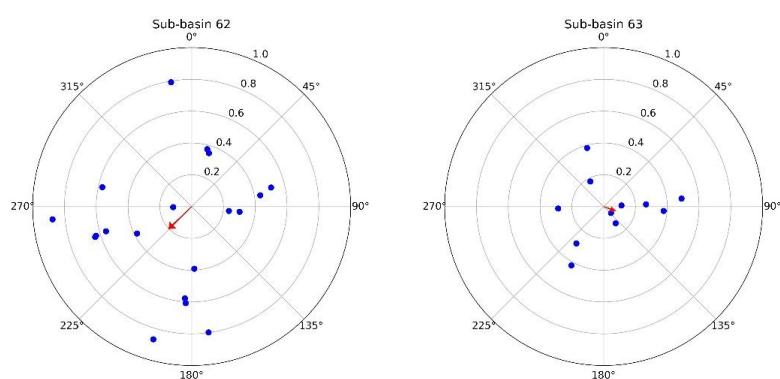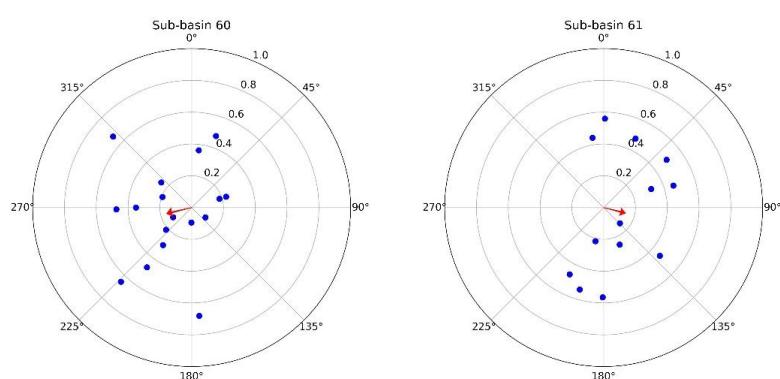
Fig. C7: Polar plots of asymmetry vectors of HU8 subbasins in Oklahoma (Sub-basins 57, 58, 60-63)
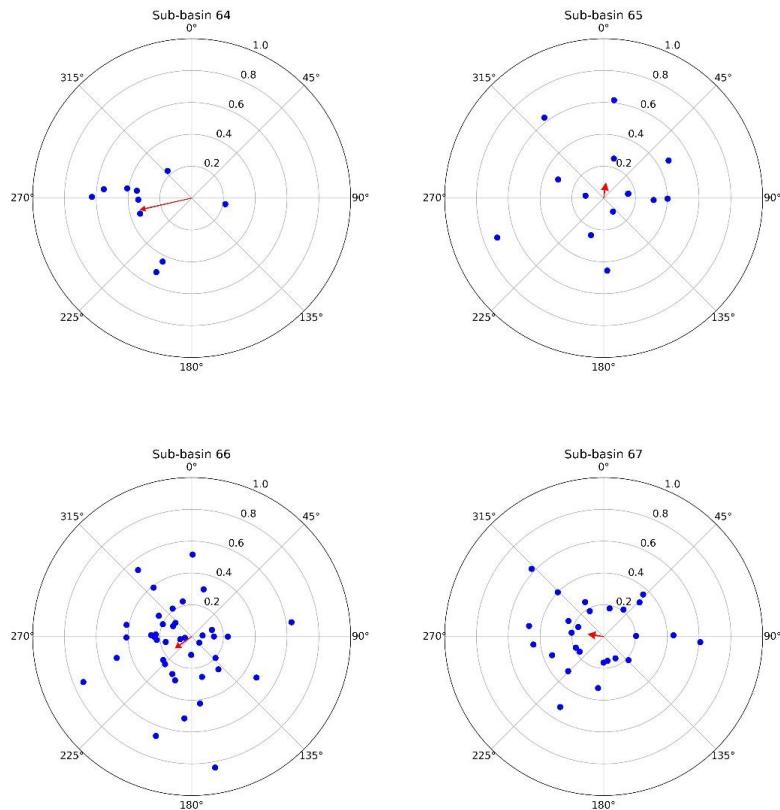
835
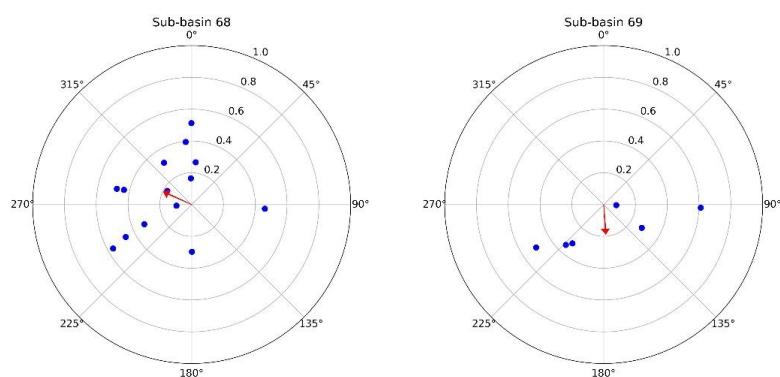
Fig. C8: Polar plots of asymmetry vectors of HU8 subbasins in Oklahoma (Sub-basins 64-69)

840
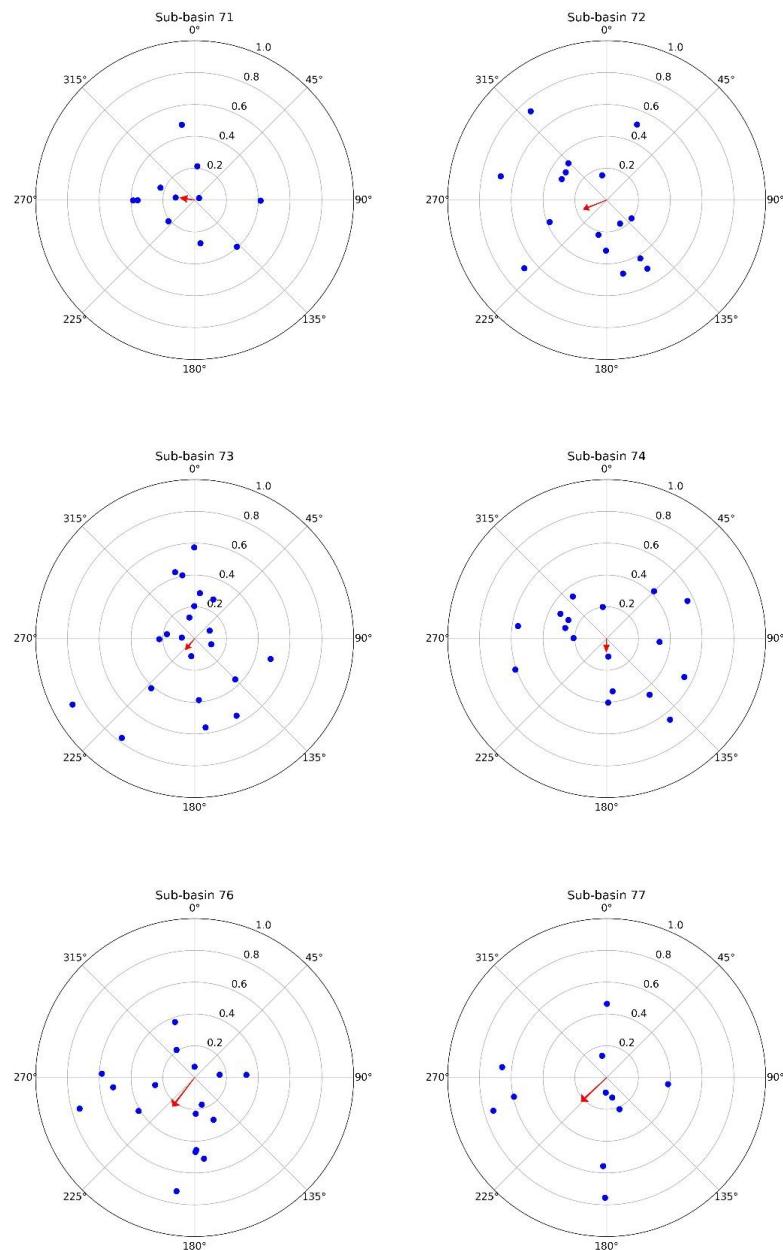
**Fig. C9: Polar plots of asymmetry vectors of HU8 subbasins in Oklahoma (Sub-basins 71-74, 76, 77)**

Appendix D

Table D1: Table of Kansas Sub-basins with assigned numbers and area.

Kansas		
Numbers assigned	**Sub-basins**	**Area (in Sq. Kms)**
1	Arikaree	933.85
2	Arkansas-Dodge City	936.75
3	Bear	630.15
4	Beaver	1338.09
5	Big	88.95
6	Big Nemaha	73.07
7	Buckner	1730.54
8	Caney	590.86
9	Chikaskia	6.47
10	Coon-Pickerel	2747.69
11	Cow	1115.37
12	Crooked	1385.25
13	Delaware	1434.05
14	Elk	810.33
15	Fall	2701.10
16	Gar-Peace	1740.08
17	Hackberry	5125.40
18	Harlan County Reservoir	1867.55
19	Independence-Sugar	930.12
20	Kaw Lake	3828.82
21	Ladder	2965.13
22	Lake O' The Cherokees	1680.03
23	Little Arkansas	4089.90
24	Little Beaver	2231.71
25	Little Osage	5174.08
26	Lower Big Blue	4976.13
27	Lower Cimarron-Eagle Chief	3524.75
28	Lower Cottonwood	3634.57
29	Lower Kansas, Kansas	3479.94
30	Lower Little Blue	2996.56
31	Lower Marais Des Cygnes	2754.80
32	Lower Missouri-Crooked	4912.87
33	Lower North Fork Solomon	1389.65
34	Lower Republican	5647.84
35	Lower Saline	2996.50
36	Lower Salt Fork Arkansas	4269.24
37	Lower Sappa	4027.22
38	Lower Smoky Hill	23.72

Kansas		
Numbers assigned	**Sub-basins**	**Area (in Sq. Kms)**
39	Lower South Fork Solomon	2278.14
40	Lower Walnut Creek	5636.77
41	Lower Walnut River	2913.66
42	Marmaton	943.22
43	Medicine Lodge	1570.13
44	Middle Arkansas-Lake McKinney	75.70
45	Middle Arkansas-Slate	410.67
46	Middle Beaver	54.19
47	Middle Kansas	5841.23
48	Middle Neosho	2813.86
49	Middle Republican	2639.17
50	Middle Smoky Hill	4853.50
51	Middle Verdigris	4630.69
52	Neosho Headwaters	2352.95
53	Ninnescah	2403.40
54	North Fork Cimarron	2095.49
55	North Fork Ninnescah	3226.67
56	North Fork Republican	1654.53
57	North Fork Smoky Hill	2479.92
58	Pawnee	3684.47
59	Prairie Dog	2350.49
60	Rattlesnake	2754.91
61	Sand Arroyo	2099.43
62	Smoky Hill Headwaters	1058.93
63	Solomon	2513.03
64	South Fork Beaver	2658.33
65	South Fork Big Nemaha	1243.30
66	South Fork Ninnescah	1502.85
67	South Fork Republican	738.67
68	South Grand	2378.95
69	Spring	3555.77
70	Tarkio-Wolf	3713.51
71	Upper Arkansas-John Martin Reservoir	4001.86
72	Upper Cimarron	114.81
73	Upper Cimarron-Bluff	1292.42
74	Upper Cimarron-Liberal	1888.68
75	Upper Cottonwood	2802.48
76	Upper Kansas	1067.03
77	Upper Little Blue	4274.15
78	Upper Marais Des Cygnes	3102.09

Kansas		
Numbers assigned	**Sub-basins**	**Area (in Sq. Kms)**
79	Upper Neosho	2226.79
80	Upper North Fork Solomon	1800.66
81	Upper Republican	1815.81
82	Upper Saline	2376.99
83	Upper Salt Fork Arkansas	2927.99
84	Upper Sappa	2433.20
85	Upper Smoky Hill	2493.69
86	Upper South Fork Solomon	3526.33
87	Upper Verdigris	3677.95
88	Upper Walnut Creek	126.33
89	Upper Walnut River	1154.59
90	Whitewoman	76.78

845

850

855

860

865

Table D2: Table of Oklahoma Sub-basins with assigned numbers and area.

Oklahoma		
Numbers assigned	**Sub-basins**	**Area (in Sq. Kms)**
1	Cimarron Headwaters	5208.4
2	Upper Cimarron	526.82
3	Upper Cimarron-Liberal	1104.88
4	Upper Cimarron-Liberal	2309.59
5	Upper Cimarron-Liberal	1613.93
6	Upper Cimarron-Liberal	2932.24
7	Crooked	317.28
8	Upper Cimarron-Bluff	351.61
9	Lower Cimarron-Eagle Chief	3218.7
10	Lower Cimarron-Eagle Chief	2949.8
11	Lower Cimarron	0.03
12	Kaw Lake	5.91
13	Upper Salt Fork, Arkansas	2260.6
14	Medicine Lodge	3009.22
15	Lower Salt Fork Arkansas	366
16	Chikaskia	3826.05
17	Black Bear-Red Rock	1057.85
18	Middle Verdigris	1393.48
19	Lowr Verdigris	2990.85
20	Caney	506.56
21	Bird	65.82
22	Middle Neosho	1443.1
23	Middle Neosho	2305.29
24	Middle Neosho	2170.44
25	Lake O' The Cherokees	1.71
26	Spring	4036.32
27	Elk	3437.14
28	Lower Neosho	3188.27
29	Rita Blanca	1650.74
30	Middle Canadian-Spring	2128.08
31	Middle Canadian-Spring	1282.15
32	Lower Canadian-Deer	4.88
33	Lower Canadian-Walnut	0.63
34	Little	160.34
35	Lower Canadian	3350.73
36	Upper Beaver	1176.66
37	Middle Beaver	4082.2

Oklahoma		
Numbers assigned	**Sub-basins**	**Area (in Sq. Kms)**
38	Coldwater	730.43
39	Coldwater	563.06
40	Palo Duro	1286.94
41	Lower Beaver	83.72
43	Lower Wolf	2.86
44	Lower Wolf	1049.49
45	Middle North Canadian	19.49
46	Lower North Canadian	2926.99
47	Deep Fork	3095.25
48	Polecat-Snake	1390.46
49	Dirty-Greenleaf	599.24
50	Illinois	1830.52
51	Robert S. Kerr Reservoir	5164.06
52	Poteau	914.62
53	Lower Prairie Dog Town Fork Red	175.85
54	Lower Salt Fork Red	232.94
55	Middle North Fork Red	1138.22
56	Lower North Fork Red	2130.56
57	Elm Fork Red	1323.3
58	Groesbeck-Sandy	1894.02
59	Blue-China	3.22
60	Farmers-Mud	1149.28
61	Cache	18.09
62	West Cache	315.13
63	Northern Beaver	2390.99
64	Lake Texoma	1167.37
65	Washita Headwaters	0.21
66	Upper Washita	964.93
67	Middle Washita	2227.81
68	Lower Washita	0.29
69	Bois D'Arc-Island	1.66
70	Bois D'Arc-Island	100.62
71	Blue	473.07
72	Muddy Boggy	632.57
73	Clear Boggy	2228.35
74	Kiamichi	0.64
75	Pecan-Waterhole	1770.15
76	Upper Little	667.81

Oklahoma		
Numbers assigned	**Sub-basins**	**Area (in Sq. Kms)**
77	Mountain Fork	906.54
78	Mountain Fork	824.11
79	Lower Little	1572.59

870

875

880

885

890

Appendix E

895   **Table E1: Kansas Sub-basins with Probability that Asymmetry Vectors are Random**

Sub-basin	Probability	Sub-basin	Probability
Cells highlighted in red = Non-random vectors (p≤0.05)			
1	3.34E-14	48	5.82E-15
2	0.49998141	49	1.25E-04
3	2.00E-04	50	4.27E-13
4	3.40E-01	51	7.14E-17
7	8.81E-24	52	2.32E-07
8	0.561592182	53	1.04E-24
10	1.23E-08	54	5.12E-19
11	7.20E-01	55	2.34E-32
12	1.52E-10	56	1.41E-22
13	1.74E-16	57	4.77E-29
14	0.089452451	58	2.02E-29
15	3.01E-06	59	2.16E-27
16	0.004536441	60	5.24E-28
17	5.37E-09	61	8.62E-12
18	1.80E-05	62	3.38E-22
20	6.78E-18	63	2.24E-06
21	3.34E-11	64	3.78E-10
22	3.42E-08	65	1.30E-30
23	3.22E-07	66	7.00E-06
24	8.44E-05	67	1.32E-08
25	1.98E-05	68	4.39E-24
26	2.07E-13	69	6.35E-28
27	2.15E-07	70	8.42E-12
28	5.17E-06	71	1.49E-27
29	2.35E-06	73	2.93E-09
30	2.57E-10	74	0.000120508
31	2.88E-08	75	0.000799809
32	0.000138472	76	1.33E-34
33	2.44E-11	77	1.28E-06
34	4.27E-06	78	2.50E-11
35	6.23E-03	79	0.000413619
36	0.001819025	80	9.33E-07
37	1.21E-07	81	8.57E-11
39	2.05E-09	82	2.10E-08
40	3.71E-06	83	4.75E-07
41	3.02E-13	84	1
42	4.36E-01	85	1.92E-07
43	4.01E-02	86	2.47E-05
47	6.09E-16	87	0.106484525

Table E2: Oklahoma Sub-basins with Probability that Asymmetry Vectors are Random

Sub-basin	Probability	Sub-basin	Probability
Cells highlighted in red = Non-random vectors (p≤0.05)			
2	2.30E-15	47	0.3372092
3	6.42E-23	48	0.95082
8	2.23E-11	49	2.32E-06
9	3.28E-05	50	0.0230585
10	4.10E-09	51	0.0003573
11	0.640742077	52	0.0001812
13	3.43E-10	54	6.56E-05
14	9.38E-12	55	9.71E-06
15	8.58E-12	56	9.09E-07
16	0.100249857	57	8.34E-09
17	0.000327932	58	6.11E-18
18	0.001170661	60	0.0004885
19	0.000746442	61	8.18E-10
20	0.677381131	62	3.53E-24
21	0.000134416	63	0.3456663
25	0.000552028	64	1.88E-08
28	0.005953577	65	0.0001054
32	0.994395701	66	0.0311052
33	0.000705992	67	0.0431556
34	0.702496984	68	9.53E-05
35	0.002948868	69	6.98E-05
36	5.11E-12	71	0.186939
37	9.31E-06	72	2.57E-08
42	4.57E-05	73	4.05E-05
44	0.99949643	74	3.08E-07
45	2.31E-13	76	8.01E-07
46	1	77	2.26E-11

900

905

910

915

Appendix F
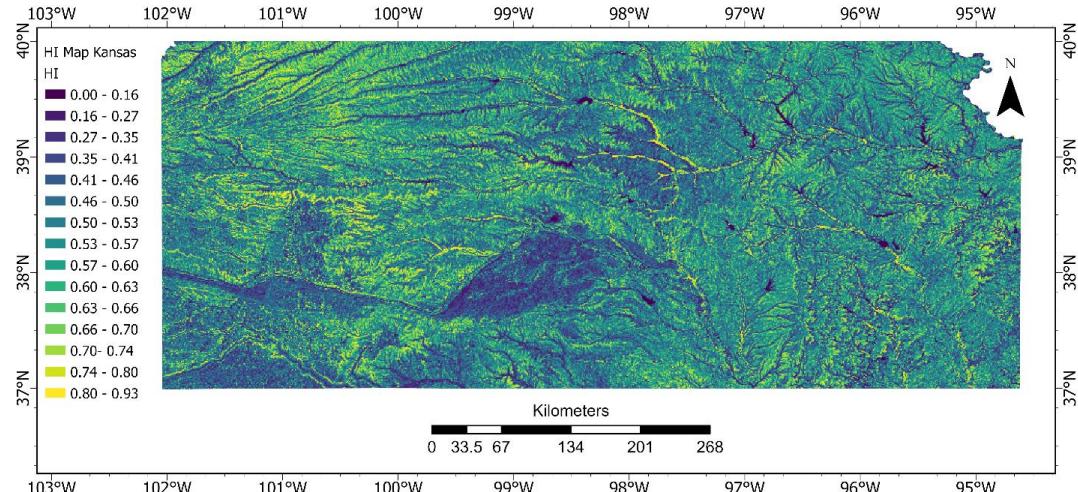

920

Fig. F1: HI Map of Kansas
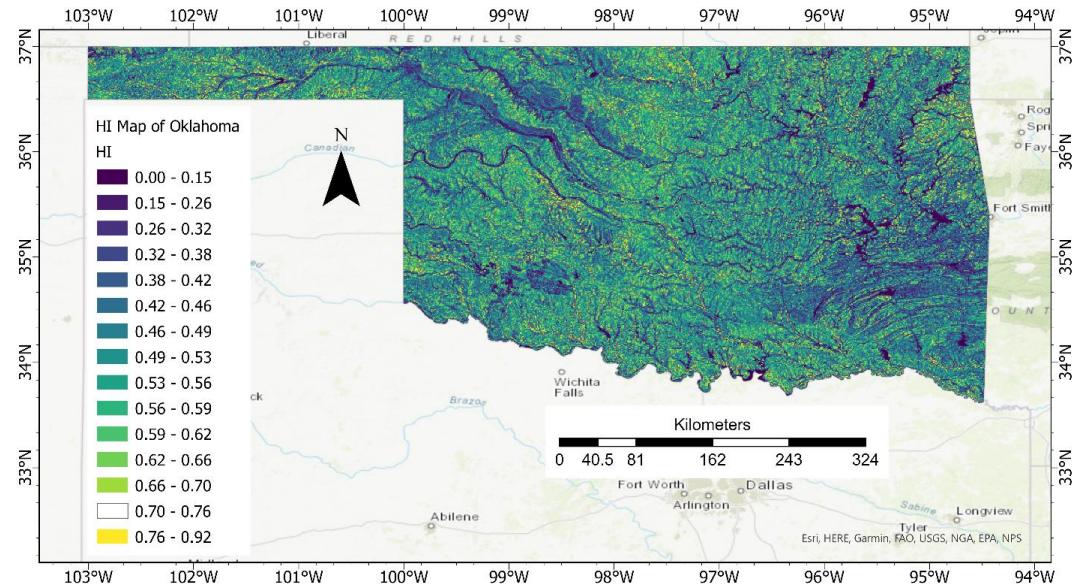
Fig. F2: HI Map of Oklahoma

925

Appendix G

Table G1: Statistical Analysis of HI and SI in Kansas

Descriptive Statistics - Hypsometric Integral (HI)

HI with Seismicity	
Mean	0.57
Standard Error	0.00
Median	0.57
Mode	0.74
Standard Deviation	0.09
Sample Variance	0.01
Kurtosis	0.86
Skewness	-0.15
Range	0.68
Minimum	0.17
Maximum	0.85
Sum	2424
Count	4237
Confidence Level(95.0%)	0.00

HI with Basement Structures	
Mean	0.52
Standard Error	0.00
Median	0.52
Mode	0.53
Standard Deviation	0.12
Sample Variance	0.01
Kurtosis	0.67
Skewness	-0.42
Range	0.83
Minimum	0.00
Maximum	0.83
Sum	616
Count	1186
Confidence Level (95.0%)	0.01

HI outside Basement Structures	
Mean	0.53
Standard Error	0.00
Median	0.54
Mode	-
Standard Deviation	0.12
Sample Variance	0.02
Kurtosis	0.48
Skewness	-0.30
Range	0.86
Minimum	0.04
Maximum	0.89
Sum	756
Count	1423
Confidence Level (95.0%)	0.01

t-Test: Two-Sample Assuming Equal Variances

	HI (earthquakes)	HI (Basement Structures)
Mean	0.57	0.52
Variance	0.01	0.01
Observations	4237	1186
Pooled Variance	0.01	
Hypothesized Mea	0.00	
df	5421	
t Stat	16.1	
P(T<=t) one-tail	0.00	
t Critical one-tail	1.65	
P(T<=t) two-tail	0.00	
t Critical two-tail	1.96	

	HI (earthquakes)	HI (Outside Basement Structures)
Mean	0.57	0.53
Variance	0.01	0.02
Observations	4237	1423
Pooled Variance	0.01	
Hypothesized Mea	0.00	
df	5658	
t Stat	13.0	
P(T<=t) one-tail	0.00	
t Critical one-tail	1.65	
P(T<=t) two-tail	0.00	
t Critical two-tail	1.96	

	HI (Basement Structures)	HI (Outside Basement Structures)
Mean	0.52	0.53
Variance	0.01	0.02
Observations	1186	1423
Pooled Variance	0.01	
Hypothesized Mea	0.00	
df	2607	
t Stat	-2.57	
P(T<=t) one-tail	0.01	
t Critical one-tail	1.65	
P(T<=t) two-tail	0.01	
t Critical two-tail	1.96	

930

z-Test: Two Sample for Means

	HI (earthquakes)	HI (Basement Structures)
Mean	0.57	0.52
Known Variance	0.01	0.01
Observations	4237	1186
Hypothesized Mea	0.00	
z	14.0	
P(Z<=z) one-tail	0.00	
z Critical one-tail	1.64	
P(Z<=z) two-tail	0.00	
z Critical two-tail	1.96	

	HI (earthquakes)	HI (Outside Basement Structures)
Mean	0.57	0.53
Known Variance	0.01	0.02
Observations	4237	1423
Hypothesized Mea	0.00	
z	11.4	
P(Z<=z) one-tail	0.00	
z Critical one-tail	1.64	
P(Z<=z) two-tail	0.00	
z Critical two-tail	1.96	

	HI (Basement Structures)	HI (Outside Basement Structures)
Mean	0.52	0.53
Known Variance	0.01	0.02
Observations	1186	1423
Hypothesized Mea	0.00	
z	-2.58	
P(Z<=z) one-tail	0.00	
z Critical one-tail	1.64	
P(Z<=z) two-tail	0.01	
z Critical two-tail	1.96	

Descriptive Statistics - Sinuosity Index (SI)

SI (earthquakes)	
Mean	1.51
Standard Error	0.00
Median	1.52
Mode	1.45
Standard Deviation	0.17
Sample Variance	0.03
Kurtosis	2.00
Skewness	0.63
Range	1.44
Minimum	1.09
Maximum	2.53
Sum	6400
Count	4237
Confidence Level (95.0%)	0.01

SI (Basement Structures)	
Mean	1.60
Standard Error	0.01
Median	1.57
Mode	2.05
Standard Deviation	0.27
Sample Variance	0.07
Kurtosis	-0.01
Skewness	0.54
Range	1.58
Minimum	1.01
Maximum	2.59
Sum	1894
Count	1186
Confidence Level (95.0%)	0.02

SI (outside Basement Structures)	
Mean	1.52
Standard Error	0.01
Median	1.48
Mode	-
Standard Deviation	0.27
Sample	0.07
Kurtosis	1.37
Skewness	0.94
Range	2.28
Minimum	1.08
Maximum	3.36
Sum	2168
Count	1423
Confidence Level (95.0%)	0.01

t-Test: Two-Sample Assuming Equal Variances

	SI (earthquakes)	SI (Basement Structures)
Mean	1.51	1.60
Variance	0.03	0.07
Observations	4237	1186
Pooled Variance	0.04	
Hypothesized Mean Difference	0.00	
df	5421	
t Stat	-13.3	
P(T<=t) one-tail	0.00	
t Critical one-tail	1.65	
P(T<=t) two-tail	0.00	
t Critical two-tail	1.96	

	SI (earthquakes)	SI (outside Basement Structures)
Mean	1.51	1.52
Variance	0.03	0.07
Observations	4237	1423
Pooled Variance	0.04	
Hypothesized Mean Difference	0.00	
df	5658	
t Stat	-2.07	
P(T<=t) one-tail	0.02	
t Critical one-tail	1.65	
P(T<=t) two-tail	0.04	
t Critical two-tail	1.96	

	SI (Basement Structures)	SI (outside Basement Structures)
Mean	1.60	1.52
Variance	0.07	0.07
Observations	1186	1423
Pooled Variance	0.07	
Hypothesized Mean Difference	0.00	
df	2607	
t Stat	6.90	
P(T<=t) one-tail	0.00	
t Critical one-tail	1.65	
P(T<=t) two-tail	0.00	
t Critical two-tail	1.96	

z-Test: Two Sample for Means

	SI (earthquakes)	SI (Basement Structures)
Mean	1.51	1.60
Known Variance	0.03	0.07
Observations	4237	1186
Hypothesized Mean Difference	0.00	
z	-10.4	
P(Z<=z) one-tail	0.00	
z Critical one-tail	1.64	
P(Z<=z) two-tail	0.00	
z Critical two-tail	1.96	

	SI (earthquakes)	SI (outside Basement Structures)
Mean	1.51	1.52
Known Variance	0.03	0.07
Observations	4237	1423
Hypothesized Mean Difference	0.00	
z	-1.67	
P(Z<=z) one-tail	0.05	
z Critical one-tail	1.64	
P(Z<=z) two-tail	0.09	
z Critical two-tail	1.96	

	SI (Basement Structures)	SI (outside Basement Structures)
Mean	1.60	1.52
Known Variance	0.07	0.07
Observations	1186	1423
Hypothesized Mean Difference	0.00	
z	6.90	
P(Z<=z) one-tail	0.00	
z Critical one-tail	1.64	
P(Z<=z) two-tail	0.00	
z Critical two-tail	1.96	

935

Table G2: Statistical Analysis of HI and SI in Oklahoma

Descriptive Statistics - Hypsometric Integral (HI) in Oklahoma

HI (earthquakes)	
Mean	0.50
Standard Error	0.00
Median	0.51
Mode	0.34
Standard Deviation	0.13
Sample Variance	0.02
Kurtosis	0.12
Skewness	-0.32
Range	0.84
Minimum	0.00
Maximum	0.85
Sum	2481
Count	4978
Confidence Level (95.0%)	0.00

HI (Basement Structures)	
Mean	0.50
Standard Error	0.00
Median	0.51
Mode	0.49
Standard Deviation	0.13
Sample Variance	0.02
Kurtosis	0.38
Skewness	-0.49
Range	0.85
Minimum	0.00
Maximum	0.85
Sum	502
Count	1006
Confidence Level (95.0%)	0.01

HI (Outside Basement Structures)	
Mean	0.49
Standard Error	0.00
Median	0.50
Mode	0.00
Standard Deviation	0.13
Sample Variance	0.02
Kurtosis	0.81
Skewness	-0.60
Range	0.81
Minimum	0.00
Maximum	0.81
Sum	519
Count	1064
Confidence Level (95.0%)	0.01

940

t-Test: Two-Sample Assuming Equal Variances

	HI (earthquakes)	HI (Basement Structures)
Mean	0.50	0.50
Variance	0.02	0.02
Observations	4978	1006
Pooled Variance	0.02	
Hypothesized Mean Difference	0.00	
df	5982	
t Stat	-0.13	
P(T<=t) one-tail	0.45	
t Critical one-tail	1.65	
P(T<=t) two-tail	0.90	
t Critical two-tail	1.96	

	HI (earthquakes)	HI (Outside Basement Structures)
Mean	0.50	0.49
Variance	0.02	0.02
Observations	4978	1064
Pooled Variance	0.02	
Hypothesized Mean Difference	0.00	
df	6040	
t Stat	2.52	
P(T<=t) one-tail	0.01	
t Critical one-tail	1.65	
P(T<=t) two-tail	0.01	
t Critical two-tail	1.96	

	HI (Basement Structures)	HI (Outside Basement Structures)
Mean	0.50	0.49
Variance	0.02	0.02
Observations	1006	1064
Pooled Variance	0.02	
Hypothesized Mean Difference	0.00	
df	2068	
t Stat	1.98	
P(T<=t) one-tail	0.02	
t Critical one-tail	1.65	
P(T<=t) two-tail	0.05	
t Critical two-tail	1.96	

z-Test: Two Sample for Means

	HI (earthquakes)	HI (Basement Structures)
Mean	0.50	0.50
Known Variance	0.02	0.02
Observations	4978	1006
Hypothesized Mean Difference	0.00	
z	-0.13	
P(Z<=z) one-tail	0.45	
z Critical one-tail	1.64	
P(Z<=z) two-tail	0.90	
z Critical two-tail	1.96	

	HI (earthquakes)	HI (Outside Basement Structures)
Mean	0.50	0.49
Known Variance	0.02	0.02
Observations	4978	1064
Hypothesized Mean Difference	0.00	
z	2.47	
P(Z<=z) one-tail	0.01	
z Critical one-tail	1.64	
P(Z<=z) two-tail	0.01	
z Critical two-tail	1.96	

	HI (Basement Structures)	HI (Outside Basement Structures)
Mean	0.50	0.49
Known Variance	0.02	0.02
Observations	1006	1064
Hypothesized Mean Difference	0.00	
z	1.98	
P(Z<=z) one-tail	0.02	
z Critical one-tail	1.64	
P(Z<=z) two-tail	0.05	
z Critical two-tail	1.96	

Descriptive Statistics - Sinuosity Index (SI)

SI (earthquakes)	
Mean	1.41
Standard Error	0.00
Median	1.40
Mode	1.40
Standard Deviation	0.21
Sample Variance	0.04
Kurtosis	0.19
Skewness	0.54
Range	1.27
Minimum	1.01
Maximum	2.29
Sum	7034
Count	4977
Confidence Level (95.0%)	0.01

SI (Basement Structures)	
Mean	1.37
Standard Error	0.01
Median	1.33
Mode	1.26
Standard Deviation	0.19
Sample Variance	0.04
Kurtosis	1.35
Skewness	1.05
Range	1.21
Minimum	1.01
Maximum	2.21
Sum	1376
Count	1006
Confidence Level(95.0%)	0.01

SI (Outside Basement Structures)	
Mean	1.41
Standard Error	0.01
Median	1.38
Mode	-
Standard Deviation	0.21
Sample Variance	0.04
Kurtosis	7.38
Skewness	1.38
Range	2.40
Minimum	1.01
Maximum	3.41
Sum	1503
Count	1063
Confidence Level(95.0%)	0.01

t-Test: Two-Sample Assuming Equal Variances

	SI (earthquakes)	SI (Basement Structures)
Mean	1.41	1.37
Variance	0.04	0.04
Observations	4977	1006
Pooled Variance	0.04	
Hypothesized Mean Difference	0.00	
df	5981	
t Stat	6.49	
P(T<=t) one-tail	0.00	
t Critical one-tail	1.65	
P(T<=t) two-tail	0.00	
t Critical two-tail	1.96	

	SI (earthquakes)	SI (Outside Basement Structures)
Mean	1.41	1.41
Variance	0.04	0.04
Observations	4977	1063
Pooled Variance	0.04	
Hypothesized Mean Difference	0.00	
df	6038	
t Stat	-0.08	
P(T<=t) one-tail	0.47	
t Critical one-tail	1.65	
P(T<=t) two-tail	0.94	
t Critical two-tail	1.96	

	SI (Basement Structures)	SI (Outside Basement Structures)
Mean	1.37	1.41
Variance	0.04	0.04
Observations	1006	1063
Pooled Variance	0.04	
Hypothesized Mean Difference	0.00	
df	2067	
t Stat	-5.17	
P(T<=t) one-tail	0.00	
t Critical one-tail	1.65	
P(T<=t) two-tail	0.00	
t Critical two-tail	1.96	

z-Test: Two Sample for Means

	SI (earthquakes)	SI (Basement Structures)
Mean	1.41	1.37
Known Variance	0.04	0.04
Observations	4977	1006
Hypothesized Mean Difference	0.00	
z	6.77	
P(Z<=z) one-tail	0.00	
z Critical one-tail	1.64	
P(Z<=z) two-tail	0.00	
z Critical two-tail	1.96	

	SI (earthquakes)	SI (Outside Basement Structures)
Mean	1.41	1.41
Known Variance	0.04	0.04
Observations	4977	1063
Hypothesized Mean Difference	0.00	
z	-0.08	
P(Z<=z) one-tail	0.47	
z Critical one-tail	1.64	
P(Z<=z) two-tail	0.94	
z Critical two-tail	1.96	

|	SI (Basement Structures)	SI (Outside Basement Structures)
Mean	1.37	1.41
Known Variance	0.04	0.04
Observations	1006	1063
Hypothesized Mean Difference	0.00	
z	-5.03	
P(Z<=z) one-tail	0.00	
z Critical one-tail	1.64	
P(Z<=z) two-tail	0.00	
z Critical two-tail	1.96	

945

Appendix H

950

**Fig. H1: HI Vs. SI Correlation, Kansas**

955
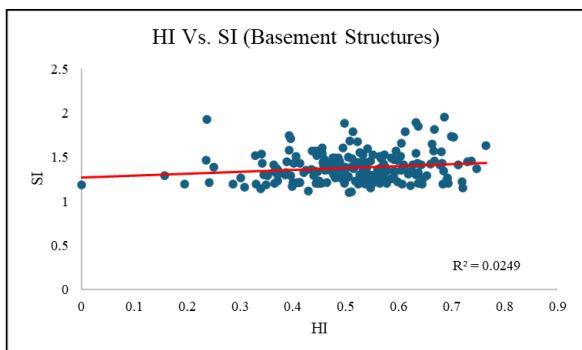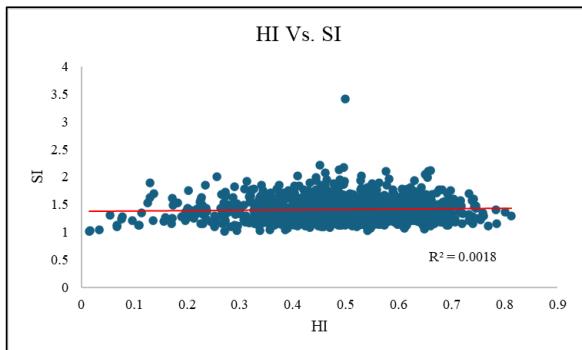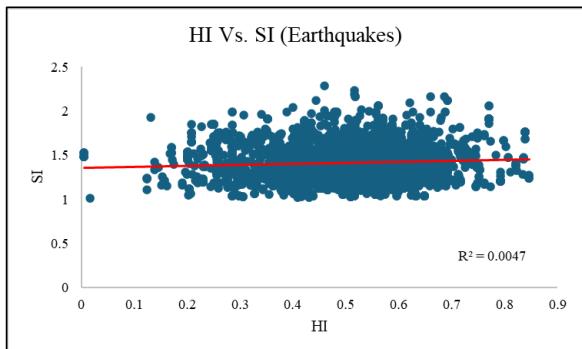
Fig. H2: HI Vs. SI Correlation, Oklahoma

960

965

Appendix I
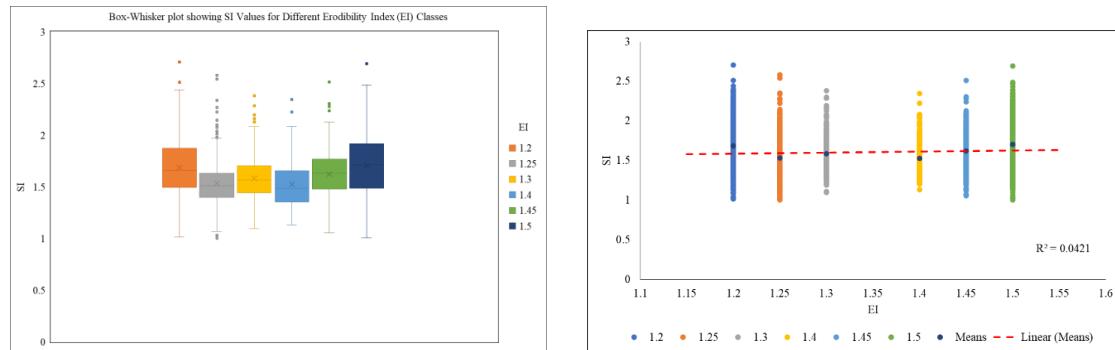
970 **Fig. I1: SI Vs Erodibility Index (EI), Kansas**
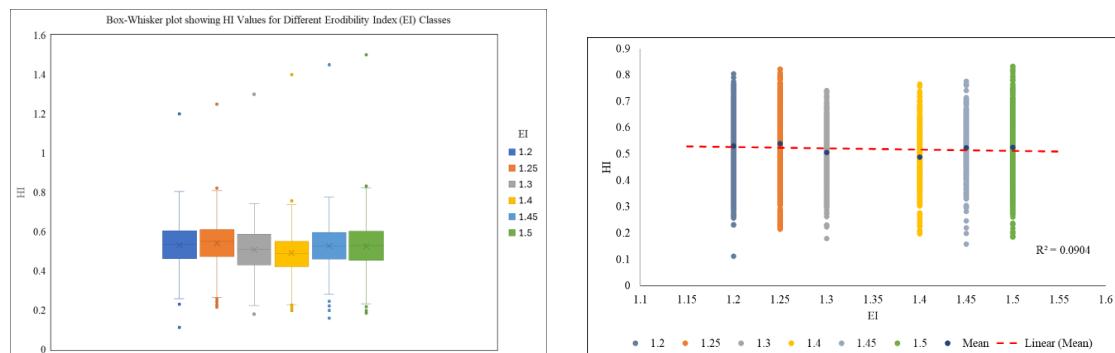
Fig. I2: HI Vs Erodibility Index (EI), Kansas

Code Availability

All codes can be provided by the corresponding authors upon request.

975 **Data Availability**

All raw data can be provided by the corresponding authors upon request.

Interactive Computing Environment

ArcGIS Pro and Jupyter Notebook.

Supplement Link

980 Link

Author Contribution

SN and RC conceptualized the research; SN performed data curation, formal analysis, methodology, and project administration; SN analyzed and visualized the data; SN developed and conceptualized the codes; SN and MRH modified the codes. SN prepared the original draft. RC supervised the project. MRH and RC reviewed and edited the manuscript.

985 **Competing interests**

The authors declare that they have no conflict of interest.

Financial support

No Financial support

Review statement

990

References

Aber, J. S.: Chert Gravel and Neogene Drainage in East-Central Kansas, https://doi.org/https://doi.org/10.17161/cres.v0i240.11776, 1997.

995 Adkison, W. L.: Stratigraphy and structure of Middle and Upper Ordovician rocks in the Sedgwick Basin and adjacent areas, south-central Kansas, Professional Paper, 33 pp., https://doi.org/10.3133/pp702, 1972.

Ake, J., Mahrer, K., O'Connell, D., and Block, L.: Deep-Injection and Closely Monitored Induced Seismicity at Paradox Valley, Colorado, Bull. Seismol. Soc. Am., 95, 664–683, https://doi.org/10.1785/0120040072, 2005.

1000

Amemoutou, A., Martínez-Garzón, P., Kwiatek, G., Rubinstein, J. L., and Bohnhoff, M.: Earthquake Source Mechanisms and Stress Field Variations Associated With Wastewater-Induced Seismicity in Southern Kansas, USA, J. Geophys. Res. Solid Earth, 126, e2020JB021625, https://doi.org/10.1029/2020JB021625, 2021.

1005 Baars, D. L.: Conjugate Basement Rift Zones in Kansas, Midcontinent, USA, in: Basement Tectonics 9, Proceedings of the International Conferences on Basement Tectonics, Canberra, Australia, 201–210, 1992.

Baars, D. L.: Basement Tectonic Configuration in Kansas, in: Geophysical Atlas of Selected Oil and Gas Fields in Kansas, vol. Bull. 237, edited by: Anderson, N. L. and Hedke, D. E., Kansas Geological Survey, Lawrence, KS, 3, 1995.

1010

Baird, G. and Willemin, J. H.: Off-center rivers and tectonic tilting on the Oregon coast; testing an improved measurement method for drainage basin asymmetry, in: Geological Society of America Abstracts with Programs, 142, 1998.

Bass, N. W.: The Geology of Cowley County, Kansas, with Special Reference to the Occurrence of Oil and Gas, Bull. (Kansas
1015 Geol. Surv., 1–203, 1929.

Berendsen, P. and Blair, K. P.: Subsurface structural maps over the Central North American rift system (CNARS), Central
Kansas, with discussion, Kansas Geological Survey, Lawrence, KS, United States, 23 pp., 1986.

1020 Bickford, M. E., Van Schmus, W. R., Karlstrom, K. E., Mueller, P. A., and Kamenov, G. D.: Mesoproterozoic-trans-Laurentian
magmatism: A synthesis of continent-wide age distributions, new SIMS U–Pb ages, zircon saturation temperatures, and Hf and
Nd isotopic compositions, Precambrian Res., 265, 286–312, https://doi.org/https://doi.org/10.1016/j.precamres.2014.11.024,
2015.

1025 Bird, P.: Kinematic history of the Laramide orogeny in latitudes 35°–49°N, western United States, Tectonics, 17, 780–801,
https://doi.org/https://doi.org/10.1029/98TC02698, 1998.

Block, L. V, Wood, C. K., Yeck, W. L., and King, V. M.: Induced seismicity constraints on subsurface geological structure,
Paradox Valley, Colorado, Geophys. J. Int., 200, 1172–1195, https://doi.org/10.1093/gji/ggu459, 2015.

1030

Burberry, C. M., Joeckel, R. M., and Korus, J. T.: Post-Mississippian Tectonic Evolution of the Nemaha Tectonic Zone and
Midcontinent Rift System, SE Nebraska and N Kansas, Mt. Geol., DigitalCom, 46–73, 2015.

Burberry, C. M., Swiatlowski, J. L., Searls, M. L., and Filina, I.: Joint and Lineament Patterns across the Midcontinent Indicate
1035 Repeated Reactivation of Basement-Involved Faults, Geosciences, 8, 215, https://doi.org/10.3390/geosciences8060215, 2018.

Carr, T. R., Merriam, D. F., and Bartley, J. D.: Use of relational databases to evaluate regional petroleum accumulation,
groundwater flow, and CO2 sequestration in Kansas, Am. Assoc. Pet. Geol. Bull., 89, 1607–1627,
https://doi.org/10.1306/07190504086, 2005.

1040

Chandler, V. W., McSwiggen, P. L., Morey, G. B., Hinze, W. J., and Anderson, R. R.: Interpretation of Seismic Reflection,
Gravity, and Magnetic Data Across Middle Proterozoic Mid-Continent Rift System, Northwestern Wisconsin, Eastern
Minnesota, and Central Iowa1, Am. Assoc. Pet. Geol. Bull., 73, 261–275, https://doi.org/10.1306/703C9B68-1707-11D7-
8645000102C1865D, 1989.

1045

Chase, B. F., Kolawole, F., Atekwana, E. A., Carpenter, B. M., Turko, M., Abdelsalam, M., and Finn, C.: The 180-km-long
Meers-Willow fault system in the Southern Oklahoma Aulacogen: A potential U.S. mid-continent seismic hazard, GSA Bull.,
135, 663–677, https://doi.org/10.1130/B36363.1, 2022.

1050 Chen, X., Nakata, N., Pennington, C., Haffener, J., Chang, J. C., He, X., Zhan, Z., Ni, S., and Walter, J. I.: The Pawnee
earthquake as a result of the interplay among injection, faults and foreshocks, Sci. Rep., 7, 4945, https://doi.org/10.1038/s41598-
017-04992-z, 2017.

Chen, Y.-C., Sung, Q., and Cheng, K.-Y.: Along-strike variations of morphotectonic features in the Western Foothills of Taiwan:
1055   Tectonic implications based on stream-gradient and hypsometric analysis, Geomorphology, 56, 109–137,
https://doi.org/10.1016/S0169-555X(03)00059-X, 2002.

Chen, Y.-C., Genovese, C. R., and Wasserman, L.: Asymptotic Theory for Density Ridges, Ann. Stat., 43, 1896–1928, 2015.

Condon, S.: Geologic Studies of the Platte River, South-Central Nebraska and Adjacent Areas—Geologic Maps, Subsurface
1060   Study, and Geologic History, U. S. Geological Survey Professional Paper, U.S. Geological Survey, 2005.

Cox, R.: Evidence of quaternary ground tilting associated with the Reelfoot Rift Zone, Northeast Arkansas, SE Geol., 28, 211–
224, 1988.

1065   Cox, R. T.: Analysis of drainage-basin symmetry as a rapid technique to identify areas of possible Quaternary tilt-block
tectonics: An example from the Mississippi Embayment, GSA Bull., 106, 571–581, https://doi.org/10.1130/0016-
7606(1994)106<0571:AODBSA>2.3.CO;2, 1994.

Cox, R. T., Van Arsdale, R., and Harris, J.: Identification of possible Quaternary deformation in the northeastern Mississippi
1070   Embayment using quantitative geomorphic analysis of drainage-basin asymmetry, Geol. Soc. Am. Bull., 113, 615–624,
https://doi.org/10.1130/0016-7606(2001)113<0615:IOPQDI>2.0.CO;2, 2001a.

Cox, R. T., Van Arsdale, R. B., Harris, J. B., and Larsen, D.: Neotectonics of the southeastern Reelfoot rift zone margin, central
United States, and implications for regional strain accommodation, Geology, 29, 419–422, https://doi.org/10.1130/0091-
1075   7613(2001)029<0419:NOTSRR>2.0.CO;2, 2001b.

Crone, A. J. and Luza, K. V: Style and timing of Holocene surface faulting on the Meers fault, southwestern Oklahoma, GSA
Bull., 102, 1–17, https://doi.org/10.1130/0016-7606(1990)102<0001:SATOHS>2.3.CO;2, 1990.

Csontos, R. M.: Evaluation of neotectonism in South Carolina by transverse topographic basin asymmetry analysis, The
1080   University of Memphis, 113 pp., 2002.

Curray, J. R.: The Analysis of Two-Dimensional Orientation Data, J. Geol., 64, 117–131, https://doi.org/10.1086/626329, 1956.

Denison, R. E., Lidiak, E. G., Bickford, M. E., and Kisvarsanyi, E. B.: Geology and geochronology of Precambrian rocks in the
1085   Central Interior region of the United States, Professional Paper, 1–20 pp., https://doi.org/10.3133/pp1241C, 1984.

Dohrenwend, J. C.: Systematic valley asymmetry in the central California Coast Ranges, GSA Bull., 89, 891–900,
1090   https://doi.org/10.1130/0016-7606(1978)89<891:SVAITC>2.0.CO;2, 1978.

Ellsworth, W. L.: Injection-Induced Earthquakes, Science (80-.)., 341, 1225942, https://doi.org/10.1126/science.1225942, 2013.

FracTracker Data Library: https://www.fractracker.org/data/.

1095   Franseen, E., Byrnes, A. P., Cansler, J., Steinhauff, D., and Carr, T.: The Geology of Kansas Arbuckle Group, Curr. Res. Earth Sci., 250, 1–43, https://doi.org/10.17161/cres.v0i250.11789, 2004.

Freiburg, J. T., Malone, D., and Huisman, M.: Geochronology of Cambrian Sedimentary and Volcanic Rocks in the Illinois Basin: Defining the Illinois Aulacogen, Sediment. Rec., 20, 1–11, https://doi.org/10.2110/001c.37650, 2022.

1100

Frohlich, C.: Two-year survey comparing earthquake activity and injection-well locations in the Barnett Shale, Texas, Proc. Natl. Acad. Sci., 109, 13934–13938, https://doi.org/10.1073/pnas.1207728109, 2012.

Garrote, J. and Garzón, G.: La asimetría de la cuenca de drenaje Jarama– Henares, análisis morfométricos y tectónica reciente, 1105   in: Geomorphology. Heritage, Mountain and territorial dynamics, 513–526, 2002.

Garrote, J., Cox, R. T., Swann, C., and Ellis, M.: Tectonic geomorphology of the southeastern Mississippi Embayment in northern Mississippi, USA, Geol. Soc. Am. Bull., 118, 1160–1170, https://doi.org/10.1130/B25721.1, 2006.

1110   Goebel, T. H. W., Weingarten, M., Chen, X., Haffener, J., and Brodsky, E. E.: The 2016 Mw5.1 Fairview, Oklahoma earthquakes: Evidence for long-range poroelastic triggering at >40 km from fluid disposal wells, Earth Planet. Sci. Lett., 472, 50–61, https://doi.org/https://doi.org/10.1016/j.epsl.2017.05.011, 2017.

Gomez, B. and Marron, D. C.: Neotectonic effects on sinuosity and channel migration, Belle Fourche River, Western South 1115   Dakota, Earth Surf. Process. Landforms, 16, 227–235, https://doi.org/https://doi.org/10.1002/esp.3290160304, 1991.

Gries, R., Dolson, J. C., and Raynolds, R. G. H.: Structural and Stratigraphic Evolution and Hydrocarbon Distribution, Rocky Mountain Foreland, in: Foreland Basins and Fold Belts, vol. 55, edited by: Macqueen, R. W. and Leckie, D. A., American Association of Petroleum Geologists, 0, https://doi.org/10.1306/M55563C16, 1992.

1120

Harlton, B. H.: Frontal Wichita Fault System of Southwestern Oklahoma1, Am. Assoc. Pet. Geol. Bull., 47, 1552–1580, https://doi.org/10.1306/BC743AF7-16BE-11D7-8645000102C1865D, 1963.

Hasbargen, L. and Paola, C.: Landscape instability in a model drainage basin, Geology, 28, 1067–1070, 1125   https://doi.org/10.1130/0091-7613(2000)28<1067:LIIAED>2.0.CO;2, 2000.

Haug, C., Nüchter, J.-A., and Henk, A.: Assessment of geological factors potentially affecting production-induced seismicity in North German gas fields, Geomech. Energy Environ., 16, 15–31, https://doi.org/https://doi.org/10.1016/j.gete.2018.04.002, 2018.

1130

Healy, J. H., Rubey, W. W., Griggs, D. T., and Raleigh, C. B.: The Denver Earthquakes, Science (80-.)., 161, 1301–1310, https://doi.org/10.1126/science.161.3848.1301, 1968.

Higley, D. K.: Petroleum systems and assessment of undiscovered oil and gas in the Anadarko Basin Province, Colorado,

1135 Kansas, Oklahoma, and Texas: USGS Province 58, USGS Numbered Series, Reston, VA, 409 pp., https://doi.org/10.3133/ds69EE, 2014.

Hobbs, N. F., van Wijk, J. W., Leary, R., and Axen, G. J.: Late Paleozoic Evolution of the Anadarko Basin: Implications for Laurentian Tectonics and the Assembly of Pangea, Tectonics, 41, e2021TC007197,

1140 https://doi.org/https://doi.org/10.1029/2021TC007197, 2022.

Horacio, J.: River Sinuosity Index: geomorphological characterisation, 6 pp., 2014.

Hornsby, K. T., Streig, A. R., Bennett, S. E. K., Chang, J. C., and Mahan, S.: Neotectonic and Paleoseismic Analysis of the

1145 Northwest Extent of Holocene Surface Deformation along the Meers Fault, Oklahoma, Bull. Seismol. Soc. Am., 110, 49–66, https://doi.org/10.1785/0120180148, 2020.

Horton, J. D.: The State Geologic Map Compilation (SGMC) geodatabase of the conterminous United States (ver. 1.1, August 2017), https://doi.org/10.5066/F7WH2N65, 2017.

1150

Hurtrez J.-E, Sol, C., and Lucazeau F.: Effect of drainage area on hypsometry from an analysis of small-scale basins in the Siwalik Hills (Central Nepal), Earth Surf. Process. Landforms, 24, 799–808, https://doi.org/10.1002/(SICI)1096-9837(199908)24:9<799::AID-ESP12>3.0.CO;2-4, 1999.

1155 Interactive Earthquake Browser - DS IRIS: https://ds.iris.edu/ieb/index.html?format=text&nodata=404&starttime=1970-01-01&endtime=2025-01-01&minmag=0&maxmag=10&mindepth=0&maxdepth=900&orderby=time-desc&src=usgs&limit=1000&maxlat=56.80&minlat=-56.80&maxlon=110.65&minlon=-110.65&zm=3&mt=ter.

Johnson, K. S.: Geologic evolution of the Anadarko Basin, Circ. - Oklahoma Geol. Surv., 90, 3–12, 1988.

1160

Johnson, K. S. and Luza, K. V.: Earth sciences and Mineral resources of Oklahoma, Oklahoma Geological Survey, 1–24 pp., 2008.

Keller, E. A. and Pinter, N.: Active Tectonics, Earthquakes, Uplift and Landscape, 2nd Editio., edited by: Lynch, P., Prentice

1165 Hall, Upper Saddle River, NJ, 362 pp., 2002.

Keranen, K. M., Savage, H. M., Abers, G. A., and Cochran, E. S.: Potentially induced earthquakes in Oklahoma, USA: Links between wastewater injection and the 2011 Mw 5.7 earthquake sequence, Geology, 41, 699–702, https://doi.org/10.1130/G34045.1, 2013.

1170

Keranen, K. M., Weingarten, M., Abers, G. A., Bekins, B. A., and Ge, S.: Sharp increase in central Oklahoma seismicity since 2008 induced by massive wastewater injection, Science (80-.)., 345, 448–451, https://doi.org/10.1126/science.1255802, 2014.

Klein, F. W.: User's guide to HYPOINVERSE-2000, a Fortran program to solve for earthquake locations and magnitudes, U.S.
1175   Geological Survey Open-File Report, 123 pp., https://doi.org/10.3133/ofr02171, 2002.

Kolawole, F., Johnston, C., Morgan, B., Chang, J., Marfurt, K., Lockner, D., Reches, Z., and Carpenter, B.: The susceptibility of Oklahoma's basement to seismic reactivation, Nat. Geosci., 12, 839–844, https://doi.org/10.1038/s41561-019-0440-5, 2019.

1180   Lee, W.: Stratigraphy and Structural Development of the Salina Basin Area, Kansas Geol. Surv. Bull., 121, 173, 1956.

Levandowski, W., Herrmann, R. B., Briggs, R., Boyd, O., and Gold, R.: An updated stress map of the continental United States reveals heterogeneous intraplate stress, Nat. Geosci., 11, 433–437, https://doi.org/10.1038/s41561-018-0120-x, 2018.

1185   Lifton, N. A. and Chase, C. G.: Tectonic, climatic and lithologic influences on landscape fractal dimension and hypsometry: implications for landscape evolution in the San Gabriel Mountains, California, Geomorphology, 5, 77–114, https://doi.org/https://doi.org/10.1016/0169-555X(92)90059-W, 1992.

Liner, K. and Liner, C.: Study of basement rocks in Northeastern Oklahoma with 3D seismic and well logs, in: SEG Technical
1190   Program Expanded Abstracts 2014, 1694–1698, https://doi.org/doi:10.1190/segam2014-0093.1, 2014.

Mahmood, S. A. and Gloaguen, R.: Analyzing Spatial Autocorrelation for the Hypsometric Integral to Discriminate Neotectonics and Lithologies Using DEMs and GIS, GIScience Remote Sens., 48, 541–565, https://doi.org/10.2747/1548-1603.48.4.541, 2011.
1195
Marsh, S. H. and Holland, A. A.: Comprehensive Fault Database and Interpretive Fault Map of Oklahoma, 15 pp., 2016.

Marshak, S., Karlstrom, K., and Timmons, J.: Inversion of Proterozoic extensional faults: An explanation for the pattern of Laramide and Ancestral Rockies intracratonic deformation, United States, Geology, 28, 735–738, https://doi.org/10.1130/0091-
1200   7613(2000)28<735:IOPEFA>2.0.CO;2, 2000.

Masek, J. G., Isacks, B. L., Gubbels, T. L., and Fielding, E. J.: Erosion and tectonics at the margins of continental plateaus, J. Geophys. Res. Solid Earth, 99, 13941–13956, https://doi.org/https://doi.org/10.1029/94JB00461, 1994.

1205   Mayer, L.: Introduction to quantitative geomorphology : an exercise manual , Prentice Hall, Englewood Cliffs, N.J, 1990.

McBee, W.: Nemaha Strike-Slip Fault Zone, in: AAPG Mid-Continent Section Meeting, 14, 2003.

Merriam, D. F.: Triassic rocks of Kansas, The Compass, 40, 122–127, 1963.

1210

Ostenaa, D. A., Zellman, M. S., Morgan, M. L., DuRoss, C. B., Briggs, R. W., Gold, R. D., Mahan, S. A., Gray, H. J., Broes, L., and Lindsey, K.: Mid- to Late-Quaternary Geomorphic and Paleoseismic Event History, Cheraw Fault, Southeastern Colorado, Bull. Seismol. Soc. Am., 112, 1742–1772, https://doi.org/10.1785/0120210285, 2022.

1215 Osterkamp, T. E., Gosink, J. P., Kawasaki, K., of Transportation, A. D., Facilities, P., and of Alaska Fairbanks. Geophysical Institute, U.: Measurements of Permafrost Temperatures to Evaluate the Consequences of Recent Climate Warmings, Alaska Department of Transportation and Public Facilities, 16P pp., 1987.

Oyana, T. and Margai, F. M.: Spatial Analysis: Statistics, Visualization, and Computational Methods, First Edit., CRC Press, 1–
1220 296 pp., https://doi.org/10.1201/b18808, 2015.

Park, Y., Beroza, G. C., and Ellsworth, W. L.: Basement Fault Activation before Larger Earthquakes in Oklahoma and Kansas, Seism. Rec., 2, 197–206, https://doi.org/10.1785/0320220020, 2022.

1225 Parker, R. S.: Experimental study of drainage basin evolution and its hydrologic implications, Colorado State University, Fort Collins, 69 pp., 1977.

Patel, S., Kolawole, F., Walter, J., Chen, X., and Marfurt, K.: Seismic illumination of small-throw seismogenic faults, Anadarko Basin, Oklahoma, Interpretation, 9, 1–50, https://doi.org/10.1190/int-2020-0135.1, 2021.

1230

Pérez-Peña, J. V., Azañón, J. M., Booth-Rea, G., Azor, A., and Delgado, J.: Differentiating geology and tectonics using a spatial autocorrelation technique for the hypsometric integral, J. Geophys. Res. Earth Surf., 114, 15, https://doi.org/10.1029/2008JF001092, 2009.

1235 Perry, W. J.: Tectonic evolution of the Anadarko Basin region, Oklahoma, Bulletin, 19 pp., https://doi.org/10.3133/b1866A, 1989.

Petrovszki, J., Székely, B., and Timár, G.: A systematic overview of the coincidences of river sinuosity changes and tectonically active structures in the Pannonian Basin, Glob. Planet. Change, 98–99, 109–121,
1240 https://doi.org/https://doi.org/10.1016/j.gloplacha.2012.08.005, 2012.

Pike, R. and Wilson, S.: Elevation-Relief Ratio, Hypsometric Integral, and Geomorphic Area-Altitude Analysis, Geol. Soc. Am. Bull., 82, 1079–1084, https://doi.org/10.1130/0016-7606(1971)82[1079:ERHIAG]2.0.CO;2, 1971.
Porsani, J. L., Almeida, E. R., Bortolozo, C. A., and Santos, F. A. M. dos: TDEM survey in an area of seismicity induced by
1245 water wells in Paraná sedimentary basin, Northern São Paulo State, Brazil, J. Appl. Geophys., 82, 75–83, https://doi.org/https://doi.org/10.1016/j.jappgeo.2012.02.005, 2012.

Qin, Y., Chen, X., Walter, J. I., Haffener, J., Trugman, D. T., Carpenter, B. M., Weingarten, M., and Kolawole, F.: Deciphering the Stress State of Seismogenic Faults in Oklahoma and Southern Kansas Based on an Improved Stress Map, J. Geophys. Res.
1250   Solid Earth, 124, 12920–12934, https://doi.org/https://doi.org/10.1029/2019JB018377, 2019.

Raleigh, C. B., Healy, J. H., and Bredehoeft, J. D.: An Experiment in Earthquake Control at Rangely, Colorado, Science (80-.)., 191, 1230–1237, https://doi.org/10.1126/science.191.4233.1230, 1976.

1255   Roberts, L. N. R. and Kirschbaum, M. A.: Paleogeography and the Late Cretaceous of the Western Interior of middle North America; coal distribution and sediment accumulation, Professional Paper, 115 pp., https://doi.org/10.3133/pp1561, 1995.

Rosenberg, N. J.: Climate of the Great Plains region of the United States, Gt. Plains Q., 7, 22–32, 1987.

1260   Rubinstein, J. and Mahani, A.: Myths and Facts on Wastewater Injection, Hydraulic Fracturing, Enhanced Oil Recovery, and Induced Seismicity, Seismol. Res. Lett., 86, 1060–1067, https://doi.org/10.1785/0220150067, 2015.

Van Schmus, W. R., Bickford, M. E., and Turek, A.: Proterozoic geology of the east-central Midcontinent basement, in: Basement and basins of eastern North America, vol. 308, edited by: van der Pluijm, B. A. and Catacosinos, P. A., Geological
1265   Society of America, 7–32., https://doi.org/10.1130/0-8137-2308-6.7, 1996.

Van Schmus, W. and Hinze, W.: The Midcontinent Rift System, Ann. Rev. Earth Planet. Sci., 13, 345–83, https://doi.org/10.1146/annurev.ea.13.050185.002021, 1985.

1270   Schoenball, M. and Ellsworth, W.: A Systematic Assessment of the Spatio-Temporal Evolution of Fault Activation Through Induced Seismicity in Oklahoma and Southern Kansas, J. Geophys. Res. Solid Earth, 122, 10189–10206, https://doi.org/10.1002/2017jb014850, 2017.

Schumm, S.: The evolution of drainage systems and slopes in bad-lands at Perth Amboy, Bull. Geol. Soc. Am., 63, 923–938,
1275   1956.

Serpa, L., Setzer, T., and Brown, L.: COCORP seismic-reflection profiling in northeastern Kansas, Geophys. Kansas Kansas Geol. Surv. Bull., 226, 165–176, 1989.

1280   Sims, P. K. and Petermar, Z. E.: Early Proterozoic Central Plains orogen: A major buried structure in the north-central United States, Geology, 14, 488–491, https://doi.org/10.1130/0091-7613(1986)14<488:EPCPOA>2.0.CO;2, 1986.

Singh, O.: Hypsometry and Erosion Proneness: A Case Study in the Lesser Himalayan Watersheds, J. Soil Water Conserv., 8, 53–59, 2009.
1285

Soreghan, G. and Soreghan, M.: Tracing Clastic Delivery To the Permian Delaware Basin, U.S.A.: Implications For

Paleogeography and Circulation In Westernmost Equatorial Pangea, J. Sediment. Res., 83, 786–802, https://doi.org/10.2110/jsr.2013.63, 2013.

Stein, S., Stein, C. A., Elling, R., Kley, J., Keller, G. R., Wysession, M., Rooney, T., Frederiksen, A., and Moucha, R.: Insights from North America's failed Midcontinent Rift into the evolution of continental rifts and passive continental margins, Tectonophysics, 744, 403–421, https://doi.org/https://doi.org/10.1016/j.tecto.2018.07.021, 2018.

Strahler, A. N.: Hypsometric (Area-Altitude) Analysis of Erosional Topography, GSA Bull., 63, 1117–1142, https://doi.org/10.1130/0016-7606(1952)63[1117:HAAOET]2.0.CO;2, 1952.

Timár, G.: Controls on channel sinuosity changes: a case study of the Tisza River, the Great Hungarian Plain, Quat. Sci. Rev., 22, 2199–2207, https://doi.org/https://doi.org/10.1016/S0277-3791(03)00145-8, 2003.

Tweto, O.: Laramide (Late Cretaceous-Early Tertiary) Orogeny in the Southern Rocky Mountains, in: Cenozoic History of the Southern Rocky Mountains, vol. 144, edited by: Curtis, B. F., Geological Society of America, 1–44, https://doi.org/10.1130/MEM144-p1, 1975.

Walcott, R. and Summerfield, M.: Scale dependence of hypsometric integrals: An analysis of southeast African basins, Geomorphology, 96, 174–186, https://doi.org/10.1016/j.geomorph.2007.08.001, 2008.

Waldhauser, F.: hypoDD -- A Program to Compute Double-Difference Hypocenter Locations, https://doi.org/https://doi.org/10.7916/D8SN072H, 2001.

Weingarten, M., Ge, S., Godt, J. W., Bekins, B. A., and Rubinstein, J. L.: High-rate injection is associated with the increase in U.S. mid-continent seismicity, Science (80-.)., 348, 1336–1340, https://doi.org/10.1126/science.aab1345, 2015.

Whitmeyer, S. J. and Karlstrom, K. E.: Tectonic model for the Proterozoic growth of North America, Geosphere, 3, 220–259, https://doi.org/10.1130/GES00055.1, 2007.

Willis, G. C.: The Utah thrust system -- an overview, in: Geology Of Northern Utah And Vicinity, vol. 27, edited by: Spangler, L. W. and Allen, C. J., Utah Geological Association Publication, 1–9, 1999.

Wilson, F. W. and Berendsen, P.: The Role of Recurrent Tectonics in the Formation of the Nemaha Uplift and Cherokee-Forest City Basins and Adjacent Structural Features in Eastern Kansas and Contiguous States, USA, in: Basement Tectonics 12. Proceedings of the International Conferences on Basement Tectonics, vol. 6, edited by: Hogan, J. P. and Gilbert, M. C., Springer, 301–303, https://doi.org/10.1007/978-94-011-5098-9_49, 1998.

Wilson, M. P., Davies, R. J., Foulger, G. R., Julian, B. R., Styles, P., Gluyas, J. G., and Almond, S.: Anthropogenic earthquakes in the UK: A national baseline prior to shale exploitation, Mar. Pet. Geol., 68, 1–17, https://doi.org/https://doi.org/10.1016/j.marpetgeo.2015.08.023, 2015.

1330

Wilzbach, M. A. and Cummins, K. W.: Rivers and Streams: Physical Setting and Adapted Biota☆, in: Encyclopedia of Ecology, vol. 2, edited by: Fath, B. B. T.-E. of E. (Second E., Elsevier, Oxford, 594–606, https://doi.org/https://doi.org/10.1016/B978-0-12-409548-9.11093-0, 2019.

1335   Yeck, W. L., Weingarten, M., Benz, H. M., McNamara, D. E., Bergman, E. A., Herrmann, R. B., Rubinstein, J. L., and Earle, P. S.: Far-field pressurization likely caused one of the largest injection induced earthquakes by reactivating a large preexisting basement fault structure, Geophys. Res. Lett., 43, 10198–10207, https://doi.org/https://doi.org/10.1002/2016GL070861, 2016.

Yeck, W. L., Hayes, G. P., McNamara, D. E., Rubinstein, J. L., Barnhart, W. D., Earle, P. S., and Benz, H. M.: Oklahoma
1340   experiences largest earthquake during ongoing regional wastewater injection hazard mitigation efforts, Geophys. Res. Lett., 44, 711–717, https://doi.org/https://doi.org/10.1002/2016GL071685, 2017.

Zámolyi, A., Székely, B., Draganits, E., and Timár, G.: Neotectonic control on river sinuosity at the western margin of the Little Hungarian Plain, Geomorphology, 122, 231–243, https://doi.org/https://doi.org/10.1016/j.geomorph.2009.06.028, 2010.

1345

Zeller, D. E.: The stratigraphic succession in Kansas: Kansas Geological Survey, in: Kansas Geological Survey, Bulletin, vol. 189, Kansas Geological Survey, 81, 1968.

Zhai, G., Shirzaei, M., and Manga, M.: Elevated Seismic Hazard in Kansas Due to High-Volume Injections in Oklahoma,
1350   Geophys. Res. Lett., 47, e2019GL085705, https://doi.org/10.1029/2019GL085705, 2020.

Zhu, W. and Beroza, G. C.: PhaseNet: a deep-neural-network-based seismic arrival-time picking method, Geophys. J. Int., 216, 261–273, https://doi.org/10.1093/gji/ggy423, 2019.